Politecnico di Torino

ScuDo
Scuola di Dottorato ~ Doctoral School
WHAT YOU ARE, TAKES YOU FAR

UNIVERSITÀ DEGLI STUDI DI TORINO

Doctoral Thesis

Doctoral Program in Pure and Applied Mathematics (37.th cycle)

Network effects and behavioral feedback in epidemic models

Author:

Martina Alutto

Supervisors:

Prof. Fabio Fagnani

Prof. Giacomo Como

Politecnico di Torino

Department of Mathematical Sciences "G. L. Lagrange"

Università di Torino

Department of Mathematics "G. Peano"

August 17, 2025

Declaration of Authorship

I, hereby declare that, the contents and organization of this dissertation constitute my own original work and does not compromise in any way the rights of third parties, including those relating to the security of personal data.

This dissertation is presented in partial fulfillment of the requirements for the degree of Philosophiæ Diploma (PhD degree) in Pure and Applied Mathematics.

Martina Alutto, August 17, 2025

Publications from this Thesis

1. M. Alutto, L. Cianfanelli, G. Como and F. Fagnani, *On the Dynamic Behavior of the Network SIR Epidemic Model*, in IEEE Transactions on Control of Network Systems, vol. 12, no. 1, pp. 177-189, March 2025, doi: 10.1109/TCNS.2024.3448136.

2. M. Alutto, L. Cianfanelli, G. Como, F. Fagnani. *Multiple Peaks in Network SIR Models*. Proc. of the 61st IEEE Conference on Decision and Control (CDC 2022).

3. M. Alutto, G. Como, F. Fagnani. *On SIR Epidemic Models with Feedback-Controlled Interactions and Network Effects*. Proc. of the 60th IEEE Conference on Decision and Control (CDC 2021).

4. M. Alutto, L. Cianfanelli, G. Como, F. Fagnani and F. Parise, *Behavioral-Feedback SIR Epidemic Model: Analysis and Control*, Accepted to the 64th IEEE Conference on Decision and Control (CDC 2025).

5. M. Alutto, L. Cianfanelli, G. Como and F. Fagnani, *Behavioral-Feedback Network SIR Model*, Submitted.

6. M. Alutto, L. Cianfanelli, G. Como, F. Fagnani and F. Parise, *Optimal Control for Behavioral- Feedback SIR Epidemic Model*, In preparation.

Abstract

The COVID-19 pandemic has highlighted two fundamental challenges in epidemic modeling: the need to account for population heterogeneity and the crucial role of behavioral adaptations. This thesis addresses both aspects by extending the classical SIR (Susceptible-Infected-Recovered) framework to settings that incorporate network effects and endogenous behavioral feedback. The overall aim is to understand how contact patterns and behavioral responses shape epidemic dynamics, and how such understanding can inform the design of effective mitigation strategies. Adopting the classical SIR framework for its analytical tractability and generality, we first investigate a behavioral-feedback model within a homogeneous population, where the transmission rate evolves dynamically as a function of the epidemic state. In this setting, we establish a sufficient condition ensuring the unimodality of the infection curve and provide closed-form expressions for the infection peak and the final epidemic size, thus generalizing well-known results from classical SIR theory. We then extend the model to a network-based SIR framework with endogenous behavioral feedback. In this setting, the nodes of the network represent subpopulations that share similar characteristics, such as infectivity, susceptibility, activity levels and behavioral patterns. The interaction matrix, encoding the contact rates between groups, evolves dynamically in response to the epidemic state. We first analyze the asymptotic behavior of the system, deriving explicit invariants of motion for the case of constant interaction matrices, and show that when the matrix is constant and of rank-1, the limit equilibria can be characterized. We then focus on the transient dynamics, introducing a weighted aggregate infection measure and proving its unimodality under suitable conditions, thereby generalizing classical SIR properties to networked settings. We study the infection curves at the single node level and show that they can undergo at most two changes in monotonicity before eventually decreasing. We further extend some of these results to a broader class of models with state-dependent interaction matrices, emphasizing how the interplay between network structure and feedback mechanisms can give rise to complex and heterogeneous epidemic trajectories. Finally, we address an optimal control problem for behavioral-feedback SIR epidemic models, where interventions such as lockdowns are constrained by healthcare capacity. Through a geometric analysis of the system's state space, we derive optimal strategies under general monotonicity assumptions, showing that a filling-the-box policy minimizes cumulative costs. Under this optimal strategy, the infection is initially allowed to grow until the critical threshold is approached, at which point strong restrictions are applied and then gradually relaxed. We also show that, when behavioral responses violate the monotonicity assumptions, more adaptive strategies may be required. Overall, this work contributes a rigorous analytical foundation for understanding the interplay between behavior, network structure, and epidemic control, and it offers new tools for designing robust intervention strategies in the face of complex population dynamics.

Contents

List of Figures

Nomenclature

x, y, z	Fractions of susceptible, infected and recovered individuals
β	Constant infection rate
$\beta(x, y)$	State-dependent transmission rate
γ	Constant recovery rate
$b(x)$	Function describing how the transmission rate varies with the susceptible population
c	Measure of how individuals adapt their behavior based on the infected population
$R(x, y)$	Behavioral reproduction number
A	Constant interaction matrix
$A(x, y)$	State-dependent interaction matrix
a	Vector capturing susceptibility level and activity rate of subpopulations
b	Vector capturing infectivity level, activity rate and size of subpopulations
$\psi(x, y)$	Invariant of motion
$u(t)$	Exogenous control function
$u^*(t)$	Optimal control function
$\phi(t; x, y)$	Dynamical flow
Γ, Γ^-	Positive and negative semi-orbits
$J(u)$	Total cost of the control function
$V(x, y)$	Value function

1 Introduction

1.1 Motivation

Throughout history, humanity has repeatedly faced the challenges posed by epidemics. From the devastating plagues of antiquity to modern viral diseases, these crises have profoundly shaped human societies, economies and scientific paradigms. As mathematical theory developed, it became natural to apply modeling in order to describe and study the spread of infectious diseases (Kermack and McKendrick, 1927). One of the most catastrophic examples is the Black Death of the 14th century, a bubonic plague pandemic that claimed the lives of an estimated 25 million people in Europe, roughly a quarter of the population at the time (Thieme, 2003). The 20th century witnessed further devastating epidemics, including the Spanish Flu of 1918–1919, which caused an estimated 50 million deaths worldwide, surpassing even the fatalities of World War I (Taubenberger and Morens, 2006). More recently, the world has faced a series of global health emergencies, such as the SARS outbreak in 2002–2003, the H1N1 influenza pandemic in 2009 and the Ebola epidemic in West Africa between 2013 and 2016. The COVID-19 pandemic, caused by the new coronavirus SARS-CoV-2, marked a pivotal moment in the history of modern public health. First detected in December 2019 in Wuhan, China, the virus quickly spread around the world, initially affecting Asia, then Europe, North America and South America. By early 2025, more than 775 million confirmed cases and nearly 7 million deaths had been reported worldwide (World Health Organization, 2024; Our World in Data, 2024). In response to the rapid spread, governments implemented strict public health measures, including lockdowns, school closures and restrictions on mobility. These decisions were heavily influenced by the predictions of epidemiological models, which played a crucial role in guiding early intervention strategies. At the very beginning of the pandemic, when no vaccines were yet available, models highlighted the urgent need for non-pharmaceutical interventions such as social distancing, contact reduction and health system capacity planning. Later, as vaccination campaigns progressed and the situation began to improve, models continued to support decisions about easing restrictions, reopen economies and avoid resurgences. In every phase of the emergency, they helped compare different strategies and predict their potential effects, offering useful guidance for managing a rapidly evolving situation.

The COVID-19 pandemic has been a fundamental test for epidemic mathematical

models and, besides confirming their concrete utility, has also brought out a number of important limitations. In particular, two main challenges emerged: the need to better account for population heterogeneity and the necessity of modeling behavioral adaptation.

Heterogeneity played a crucial role at multiple levels during the pandemic. Different communities faced varying levels of exposure to infection, largely due to their living and working conditions. For instance, individuals living in overcrowded urban housing, frequently using public transportation, or employed in high-contact settings, such as healthcare, service industries, or other essential jobs, were more frequently exposed to situations that increased their risk of contagion. At the same time, specific demographic groups, such as the elderly or individuals with preexisting medical conditions, were far more vulnerable to severe outcomes if infected. Another important source of heterogeneity was the presence of asymptomatic individuals. Indeed, COVID-19 has ability to spread silently, especially through people who had no symptoms or had not yet developed them. This characteristic made traditional containment strategies, such as targeted isolation and contact tracing, less effective, unless combined with mass testing, which was expensive and difficult to organize. The pandemic also exposed vulnerabilities in healthcare systems worldwide: shortages of ICU beds, ventilators, personal protective equipment and testing capacity forced governments to make difficult decisions regarding resource allocation. These decisions were further complicated by the significant heterogeneity within the population, which models must accurately capture to support effective policymaking. To design effective and equitable policies, models should account for differences in activity, susceptibility, infectivity and outcomes across subpopulations. One common approach is to divide the population into distinct groups based on relevant characteristics so that policies can be tailored to the needs of each subgroup. Ignoring these differences can lead to general solutions that might not give enough protection to the people most at risk and could also waste important health and economic resources. Although models incorporating heterogeneity already existed before COVID-19, the pandemic highlighted the lack of strong theoretical results for these complex systems. Most available models could simulate epidemic evolution under heterogeneity, but they often depended heavily on numerical simulations rather than providing clear analytical insights or long-term predictions.

Another major challenge highlighted by the pandemic was the role of behavioral adaptations and individual responses. Throughout COVID-19, people's actions, whether voluntary or prompted by government measures, had a decisive impact on how the disease spread. The success of non-pharmaceutical interventions, such as social distancing, mask-wearing and later vaccination campaigns, depended heavily on public participation and on how people perceived the risk of infection. However, people's behavior was influenced by a complex mix of factors. Risk perception varied greatly between individuals and communities and was often shaped by access to information, trust in government and health authorities and the clarity and consistency of communication strategies. In many cases, misinformation and conflicting messages fueled confusion and distrust, undermining public health efforts. As the pandemic continued, additional challenges emerged: pandemic

fatigue led to a gradual decline in adherence to preventive measures, while vaccine hesitancy, driven by fear, misinformation, or distrust, complicated vaccination campaigns. These dynamics made it even harder to maintain control over the epidemic and highlighted how crucial it is to consider human behavior in epidemic modeling and in the design of effective health policies.

All of these factors highlight the critical importance of developing mathematical models that can not only predict how infections spread, but also incorporate the social and behavioral dimensions that influence epidemic outcomes. Such models are essential tools for designing more effective and realistic intervention strategies.

1.2 Related literature

1.2.1 Compartmental epidemiological models

Epidemiological models have long been essential tools for understanding how infectious diseases spread and for supporting public health decisions, such as introducing social distancing or lockdowns. The mathematical modeling of epidemics dates back to the 18th century, most notably with the study on smallpox in (Bernoulli, 1760).

In the early stages of an epidemic, when the number of infected individuals is still very small, disease transmission is better represented as a random process rather than a deterministic one. This is because, at such times, the probability of infection largely depends on the specific interactions and contact patterns between individuals, making the process inherently stochastic rather than deterministic. In these circumstances, stochastic models, which explicitly account for randomness in transmission events, offer a more realistic representation of epidemic dynamics. These models are especially useful in small populations or localized outbreaks, where the randomness of interactions plays a significant role (Daley and Gani, 2001; Britton, 2010). One of the first and most influential stochastic models is the Reed–Frost chain binomial model, introduced by W.H. Frost in 1928 and later formalized and widely applied (Abbey, 1952; Wilson and Burke, 1943). The model assumes discrete time steps, during which each susceptible individual has a certain probability of avoiding infection, depending on how many infectious individuals they come into contact with. The stochastic nature of this approach means that even with identical initial conditions, different simulation runs can lead to varying outcomes, which mirrors the unpredictable nature of real-world epidemics. Interestingly, a similar model was developed even earlier by P.D. En'ko in the late 19th century (En'ko, 1989), whose work was rediscovered and recognized decades later. Since the introduction of the Reed–Frost model, numerous extensions and refinements have been proposed. A key distinction arises when comparing the Reed–Frost model with other stochastic approaches, such as those considered in (Nowzari et al., 2016). In their study, the authors explore models where infected individuals have the opportunity to continuously infect susceptible individuals, rather than just having a single chance of transmission, as in the Reed–Frost model. This continuous risk of infection is more appropriate for diseases like the flu, where a susceptible person is always at risk when in contact with an infected individual.

In contrast, the Reed–Frost model might be better suited for modeling the spread of non-biological infections, such as an e-mail virus, where the recipient only faces a one-time decision to open the email.

While stochastic models are valuable for understanding the dynamics of small-scale outbreaks and the early stages of epidemics, they can become complex and computationally intensive. This complexity often motivates researchers to seek more tractable models that focus on the overall, average behavior of the system. This transition is formalized through mean-field limits, which rigorously show how stochastic models converge to their deterministic counterparts as the population size tends to infinity (Ethier and Kurtz, 2009; Andersson and Britton, 2012). By removing randomness and focusing on average quantities, they provide clear, predictive insights into the dynamics of large-scale outbreaks. Thanks to their analytical tractability and lower computational costs, deterministic models are widely used to design intervention strategies and guide public health policies. A major step forward in deterministic epidemic modeling came in the early 20th century, with the contributions of Kermack and McKendrick (Kermack and McKendrick, 1927; Kermack and McKendrick, 1932), who introduced the first compartmental models, establishing the foundation of modern epidemic theory (Diekmann et al., 1995). This models divide the population into distinct compartments, each representing a different stage of the disease and describe how individuals move between these compartments using differential equations. The simplest model is the SI (Susceptible–Infected) epidemic model, where individuals once infected, remain infectious forever. Although basic, this model is typically applied to diseases for which no recovery or immunity is observed, or in early outbreak stages when recovery is negligible. It has been used also in the study of computer viruses and certain sexually transmitted infections (Bailey, 1975). A more realistic variation is the SIS (Susceptible-Infected-Susceptible) epidemic model, which captures diseases that do not provide lasting immunity: individuals return to the susceptible state after recovery. This is relevant for many bacterial infections (e.g., gonorrhea), or for some strains of the common cold. On the other hand, the SIR (Susceptible-Infected-Recovered) epidemic model assumes that recovered individuals acquire permanent immunity, making it suitable for many viral infections like measles or chickenpox. Between SIS and SIR lies the SIRS (Susceptible–Infected–Recovered–Susceptible) epidemic model, which assumes that immunity lasts only for a limited time (Hethcote and Levin, 1989). After recovering, individuals eventually become susceptible again. This framework is particularly important for modeling seasonal diseases like influenza (Hethcote, 2000), where immunity fades and recurring waves of infection are common. Both SIR and SIRS models reflect different assumptions about the duration and effectiveness of immunity, which is a key factor in epidemic dynamics. In the SIR framework, immunity acts as a permanent shield that removes individuals from the transmission chain. In the SIRS setting, immunity is transient, allowing the disease to persist or re-emerge in cycles. In the SIS and SI epidemic models, immunity is either absent or irrelevant, leading to the possibility of endemic or unlimited disease spread unless other interventions are introduced.

To better reflect the complexity of real-world diseases, further model refinements

have been proposed. For instance, the SEIR (Susceptible-Exposed-Infected-Recovered) epidemic model includes a latent period between exposure and infectivity (Brauer et al., 2019). The SAIR (Susceptible-Asymptomatic-Infected-Recovered) epidemic model distinguishes between asymptomatic and symptomatic cases, which is especially important for diseases like COVID-19 (Kemper, 1978). During the last pandemic, a more detailed model called SIDHARTE was proposed (Giordano et al., 2020). This model includes compartments that reflect not only the progression of the disease but also the state in the healthcare system: Susceptible (S), Infected (I), Diagnosed (D), Hospitalized (H), in intensive care (A), Recovered (R), Threatened (T) and Extinct (E). Such detailed structures allow for more precise estimates of healthcare needs and the impact of interventions. While complex models like SIDHARTE offer greater detail, they also require a large amount of accurate data, which is not always available. Simpler models such as SIR and SIS remain widely used, especially in the early stages of an epidemic, for theoretical studies, or as building blocks for more elaborate models.

1.2.2 Network-based models

Traditional compartmental models in epidemiology often assume homogeneous mixing within a population (Anderson and May, 1991; Hethcote, 2000), meaning that every individual has an equal chance of coming into contact with any other. However, this assumption is rarely accurate in real-world scenarios. In practice, human contact patterns are uneven, influenced by factors such as social structure, geography, mobility and individual behavior. To address this limitation, network-based epidemic models have been developed. In these models, individuals or subgroups are represented as nodes in a graph and the connections between them (edges) represent potential pathways for disease transmission (Pastor-Satorras et al., 2015; Paré et al., 2020; Zino and Cao, 2021; Newman, 2002). These models introduce a contact or interaction matrix A, where each element A_{ij} quantifies the transmission rate from node j to node i. This formulation enables more realistic representations of disease transmission by incorporating heterogeneity in susceptibility, infectivity and interaction patterns (Hethcote, 1978; Nowzari et al., 2016; Fall et al., 2007; Mei et al., 2017; Ogura and Preciado, 2016). Network-based approaches provide a powerful framework to capture the structure and dynamics of real populations, making them especially relevant for studying localized outbreaks, targeted interventions and the effects of heterogeneity on disease spread.

One of the earliest network-based SIS model was proposed in (Lajmanovich and Yorke, 1976), where authors introduced a continuous-time, n-dimensional deterministic system. They identified an epidemic threshold that depends on both disease parameters and the spectral radius of the contact network. When the basic reproduction number is below this threshold, the infection dies out; when it exceeds the threshold, a unique endemic steady state arises. This idea was later expanded in (Allen, 1994), which confirmed similar threshold behavior in discrete-time models. Further studies, such as (Wang et al., 2003; Ahn and Hassibi, 2013; Ruhi and Hassibi, 2015), refined the analysis and validated the link between the threshold and the spectral radius. (Van Mieghem et al.,

2008) proposed the "intertwined" SIS model, interpreting the network SIS model as a mean-field approximation of the full Markov-chain model, a connection rigorously justified by (Sahneh et al., 2013). Subsequent developments used tools from Lyapunov theory and positive systems. (Fall et al., 2007) employed Metzler matrix theory to establish equilibrium stability conditions, while (Khanafer et al., 2016) generalized these results to weakly connected digraphs using positive system theory.

The network-based SIR epidemic model extends the scalar framework to capture diseases that confer immunity after infection. These models are more complex to analyze than their SIS counterparts due to their non-monotonic nature and higher dimensionality. However, they provide a richer and more realistic description of long-term epidemic dynamics, particularly when immunity plays a key role. One of the earliest generalizations was proposed by (Hethcote, 1978), who introduced a multi-group SIR model that incorporates births, deaths, immunization campaigns and the possible loss of immunity. In scenarios without demographic changes or loss of immunity, the model predicts convergence to the disease-free equilibrium. This line of research was extended by (Guo et al., 2008), who included vital dynamics and used Lyapunov analysis to derive sufficient conditions for the existence and global stability of endemic equilibria. In a different direction, (Youssef and Scoglio, 2011) proposed an individual-based SIR model on networks, using simulation-based methods to characterize epidemic thresholds in terms of the network's spectral radius. (Mei et al., 2017) introduced a dynamic reproduction number $R(t)$ in the network SIR context, offering a time-varying metric for assessing transmission dynamics. Several studies have also examined how network structure and population heterogeneity influence epidemic outcomes. (Ellison, 2020) showed that heterogeneous contact patterns, common in real-world networks, can lead to lower overall infection levels compared to predictions from homogeneous mixing models. Recent works have explored more detailed network topologies. For instance, (Stolerman et al., 2015) and (Das and Stolerman, 2024) modeled city-wide dynamics where neighborhoods are represented as well-mixed subpopulations and edges correspond to the movement of individuals between areas of residence and daily activity. These models allow for the analysis of equilibrium behavior and demonstrate how epidemic spread depends on mobility patterns and network topology. Given the analytical complexity of network-based SIR models, some works have focused on simplified settings involving only two interacting communities. For example, (Yang, 2024) proposed a two-population SIR network model in which two groups have distinct internal contact structures and interact differently with each other. Similarly, (Han et al., 2024) developed a two-community model where interactions occur through temporary commuters, deriving an explicit formula for the basic reproduction number and an implicit equation for the final epidemic size. Their analysis provides important insights into how inter-community connectivity affects epidemic outcomes.

1.2.3 Behavioral adaptation component

Another key limitation of the classical SIR model is the assumption of a constant transmission rate, which fails to account for behavioral adaptations. However, both historical

and contemporary evidence indicate that individuals adjust their behavior in response to perceived risk of infection, leading to changes in contact patterns that affect disease transmission. For example, during the 1918 influenza pandemic, people voluntarily avoided crowded areas (Crosby, 2003); during the SARS outbreak, a widespread use of face masks and reductions in travel were observed (Lau et al., 2005); and during the more recent COVID-19 pandemic, behavioral responses were further reinforced by government-imposed measures such as social distancing and lockdowns (Hsiang et al., 2020). While early modeling efforts mostly focused on evaluating the effects of institutional interventions like school closures (Bootsma and Ferguson, 2007), recent studies have increasingly emphasized the role of endogenous behavioral changes. These individual actions, often driven by perceived risk, can significantly influence the course of an epidemic and should be explicitly considered in disease modeling (Ferguson, 2007). To incorporate such behavioral adaptations into epidemic models, two main modeling approaches have been explored.

The first relies on *evolutionary game theory* (Sandholm, 2010), which provides a natural framework to describe how individuals make strategic decisions when facing an epidemic. In this context, people evaluate the trade-offs between adopting protective measures (e.g., vaccination, self-isolation, or social distancing) and continuing usual activities. Their choices are influenced by personal risk perception, social pressure and previous experiences. Unlike classical compartmental models where individual behavior is fixed or exogenously prescribed, game-theoretic models account for adaptive behavior, allowing individuals to switch between strategies dynamically. This approach captures more realistically the feedback loop between disease progression and behavioral response. This paradigm forms the basis of the emerging interdisciplinary field of *sociophysics* (Castellano et al., 2009), which integrates methods from statistical physics and game theory to model the co-evolution of social behavior and epidemic dynamics (Satapathi et al., 2022; Ye et al., 2021; Frieswijk et al., 2022; Paarporn and Eksin, 2023; Amaral et al., 2021; Kabir and Tanimoto, 2020; Martins et al., 2023; Certório et al., 2022). Among the most representative contributions, (Satapathi et al., 2022) and (Paarporn and Eksin, 2023) analyze SIS epidemic models in which behavioral adaptation is governed by a replicator dynamics, allowing individuals to choose between cooperating with health recommendations or defecting from them, depending on observed outcomes. In (Amaral et al., 2021), the authors propose a scalar SIR model integrated with a "quarantine game," where agents choose between continuing normal activities and voluntary self-isolation, thereby influencing the course of the epidemic. The study in (Kabir and Tanimoto, 2020) introduces a SEQIHR (Susceptible-Exposed-Quarantined-Infected-Hospitalized-Recovered) compartmental framework, where agents decide whether to comply with stay-at-home policies within a game-theoretic structure. Similarly, (Certório et al., 2022) and (Martins et al., 2023) adopt a system-theoretic perspective, demonstrating how the endemic equilibrium of a SIRS model can be controlled and stabilized through the strategic interactions of agents who modulate the transmission rate. Other works explore how social behavior spreads

via imitation and learning. For instance, (Ye et al., 2021) and (Frieswijk et al., 2022) analyze multilayer network SIS epidemic models where individuals adopt protective actions by imitating the strategies of their peers. These studies highlight how social dynamics can influence both the speed and extent of behavioral adoption. A complementary line of research emphasizes decentralized strategies, where individuals react to local infection data rather than global information. In this context, (Hota and Sundaram, 2019; Khazaei et al., 2021; Elokda et al., 2021) investigate how people adjust their contact rates or mobility in response to perceived local risk. Notably, (Elokda et al., 2021) propose a networked SAIR model, that includes an asymptomatic compartment, in which individuals continuously adapt their level of activity, number of contacts and mobility across different regions. These behavioral choices evolve over time, often on the same scale as the epidemic itself. A comprehensive overview of these behaviorally adaptive and game-theoretic epidemic models can be found in the review by (Huang and Zhu, 2022).

The second main modeling strategy incorporates behavioral changes through feedback mechanisms in the transmission dynamics. In these so-called *feedback epidemic models*, the transmission rate β is no longer assumed constant, but is instead modeled as a function of the epidemic state, typically depending on the number of infected or susceptible individuals. This approach allows the model to capture collective behavioral adaptations at the population level (Funk et al., 2010; Verelst et al., 2016). A seminal contribution in this direction is the work in (Capasso and Serio, 1978), who proposed a scalar SIR model where the transmission rate is a bounded and decreasing function of the fraction of infected y. This simple yet effective feedback captures the idea that people reduce their contacts or adopt protective measures as they become more aware of the epidemic risk. The authors showed that such a mechanism induces a unimodal infection curve, meaning the number of infected individuals rises and falls in a single wave, a pattern observed in many real-world epidemics and in the classical SIR model with constant transmission rate. This modeling framework has motivated a substantial body of research exploring how endogenous behavioral responses can mitigate epidemic severity. Several studies demonstrate that feedback-driven reductions in transmission can significantly flatten the infection curve (Baker, 2020; Franco, 2020), while preserving key stability properties of the disease-free and endemic equilibria (Korobeinikov, 2006). Recent work by (Nguyen, 2024) provides further analytical insights, establishing upper bounds on epidemic overshoot (e.g., the number of individuals infected beyond the peak) and identifying invariants of motion when the transmission rate depends only on the susceptible population. Finally, (Srivastava et al., 2024) investigates a behavioral SIRS model with ratio-dependent incidence and saturated treatment response, analyzing existence and stability of endemic equilibria under complex feedback structures. Beyond models where the transmission rate depends solely on the infected population, other works allow β to also vary with the fraction of susceptibles x. Such general formulations have been explored in (Feng and Thieme, 2000; Gao et al., 2024; Liu et al., 1987), where the rate of new infections $\beta(x, y)xy$ is modeled as an arbitrary nonlinear function of the susceptible and infected fractions. These studies establish general conditions for the existence, uniqueness and

stability of equilibria, thus extending classical compartmental models to settings with endogenous behavioral feedback. Finally, an additional line of work incorporates time-dependent transmission rates to capture delayed responses or seasonal variation. For example, (Boatto et al., 2018) study an SIR model where $\beta(t)$ varies periodically, modeling behavioral changes that follow external cycles or institutional measures.

A related but distinct modeling approach introduces behavioral adaptation as an explicit dynamic variable that responds to the observed progression of the epidemic. Instead of modifying the transmission rate directly as a function of the current state, these models incorporate a separate variable, typically representing risk perception or awareness, that evolves over time and influences individual behavior. For instance, (Zhou et al., 2020) introduces an SIS epidemic model where the transmission rate β depends on the perceived infection level, taking into account delays in perception and heterogeneity in individual risk profiles. Similarly, (Bizyaeva et al., 2024) extends this idea to a networked SIS setting with a dual-layer structure: one layer describes the physical spread of the disease through contact interactions, while the other layer models the dissemination of information. In this setting, the effective transmission rate is shaped by a dynamic risk perception variable, which evolves based on the information individuals receive through the network. While these models represent important progress, especially for SIS dynamics in both scalar and networked forms, the study of *network-based feedback SIR models* is still relatively limited. Most existing results rely on mean-field approximations and rigorous analytical insights remain scarce due to the inherent complexity introduced by network heterogeneity and individual behavioral differences. A notable exception is the recent work by (Wang et al., 2024), who analyze a networked SIR model with saturated incidence and nonlinear recovery. Their results offer valuable insights into how feedback mechanisms can shape epidemic dynamics in structured populations.

Building on these ideas, recent studies have begun to incorporate explicit models of *opinion dynamics* in multilayer network settings, where epidemic spreading co-evolves with the formation and diffusion of public attitudes and beliefs (She et al., 2022; Xu and Ishii, 2024; Xu et al., 2025). For instance, (She et al., 2022) presents an SIS epidemic model in which the infection dynamics and the prevailing opinions of the community influence each other. In contrast, (Xu and Ishii, 2024; Xu et al., 2025) develop network-based SIV (Susceptible-Infected-Vigilant) epidemic models that integrate polarizing opinion dynamics, where the transition to a vigilant state is driven by both perceived risk and social influence, ultimately altering the epidemic trajectory.

1.2.4 Optimal control of epidemic spread

The COVID-19 pandemic has brought particular attention to the use of non-pharmaceutical interventions (NPIs), such as lockdowns and mobility restrictions, especially during the initial phases of an outbreak when effective vaccines or treatments are not yet available (Flaxman et al., 2020). While highly effective in reducing transmission and preventing healthcare system collapse, these interventions also come with significant economic and

social costs. As a result, countries around the world adopted a wide range of strategies, often reflecting different priorities and trade-offs between public health goals and economic sustainability.

Broadly speaking, two classes of intervention strategies have been identified (Ferguson et al., 2020): *suppression strategies*, which aim to reduce infection numbers to very low levels and maintain them over time through strong and sustained interventions and *mitigation strategies*, which aim instead to slow down transmission without necessarily suppressing it entirely, with the goal of reducing the epidemic peak and relieving pressure on healthcare systems while limiting economic disruption. A natural framework to formalize and optimize these trade-offs is offered by optimal control theory (Zino and Cao, 2021), which allows the design of time-varying interventions that minimize a cost functional typically combining epidemic and economic objectives. Early works in this direction date back to (Morton and Wickwire, 1974), which introduces an optimal immunization strategy within the classical SIR model, laying the foundation for subsequent control-theoretic approaches to epidemic management. Later, (Behncke, 2000) extends this framework by modeling lockdown as a control input that reduces the transmission rate, while the cost function explicitly incorporates a trade-off between the severity of the epidemic and the socioeconomic impact of the intervention. Similarly, (Hansen and Day, 2011) considered both vaccination and isolation policies within an optimal control framework.

More recently, this line of research has gained renewed interest in the context of COVID-19. In (Alvarez et al., 2021; Acemoglu et al., 2021), lockdown costs are modeled as reductions in economic activity, while mortality costs take into account the risk of hospital congestion. This is achieved by introducing a lethality rate that increases with infection prevalence, resulting in a quadratic cost term. Such a formulation captures a key aspect of the recent pandemic, where overwhelmed healthcare systems led to increased mortality. In the multigroup SIR framework, (Acemoglu et al., 2021) further shows that targeted interventions, based on age or risk group, significantly outperform uniform policies, emphasizing the importance of population heterogeneity in the design of optimal strategies. Along similar lines, (Birge et al., 2020) proposes a spatial model calibrated on mobility data from New York City to evaluate geographically targeted interventions. Their results show that differentiated restrictions across neighborhoods can better contain infections while preserving more economic activity than uniform city-wide policies.

Although these studies rely heavily on numerical approaches, a few analytical results have also been derived. A notable exception is (Kruse and Strack, 2020), which addresses a finite-horizon control problem with linear epidemic cost and convex intervention cost, proving that the optimal policy is quasi-convex and of the bang-bang type, with at most two switching times. An alternative infinite-horizon formulation is considered in (Cianfanelli et al., 2021b), where a quadratic epidemic cost captures hospital congestion. The authors demonstrate that stabilizing the infection prevalence leads to better long-term outcomes than strategies focused solely on minimizing the reproduction number. (Birge et al., 2020) A different modeling approach is presented in (Miclo et al., 2022), where

a hard constraint is imposed on the maximum allowed fraction of infected individuals, representing the capacity of intensive care units (the so-called ICU constraint). This setting reflects situations where exceeding hospital capacity, as observed during COVID-19 peaks, can severely compromise patient care. Respecting this constraint guarantees access to treatment for all critical cases. The resulting optimal strategy, known as "filling the box". consists of allowing the epidemic to grow initially, then implementing a sharp lockdown to prevent crossing the threshold, followed by a gradual relaxation. A similar outcome is obtained in (Acemoglu et al., 2024), where epidemic control is coupled with optimal testing strategies. By jointly optimizing NPIs along with molecular and serological testing, the model aims to reduce both health impacts and economic costs. Feedback-based strategies under ICU constraints are also investigated in (Di Lauro et al., 2020), where simple rule-based policies adapt in real-time to the observed epidemic state, ensuring that healthcare demand remains within manageable limits. More detailed numerical studies are provided in (Djidjou-Demasse et al., 2020; Kantner and Koprucki, 2020), which explore the timing and combination of various NPIs using complex compartmental models. From a network-based perspective, (Yi et al., 2022) formulates a combinatorial optimization problem aimed at reducing infections by selectively removing edges from a contact network. This structural control approach highlights how targeted modifications to the topology of social interactions can achieve substantial epidemic mitigation with minimal disruption to mobility or economic activity.

Beyond classical optimal control on compartmental models, many recent studies have started to include behavioral feedback in epidemic models. These models aim to better capture how individuals adjust their behavior in response to perceived infection risk. For instance, (Parino et al., 2024) introduces a coupled model combining a SIS epidemic process with a population game framework where behavior and disease dynamics co-evolve over time. They define a cost function that balances health and socio-economic impacts and use the Pontryagin Maximum Principle to design optimal intervention strategies. Such formulations allows for control strategies that are not only efficient from a policy perspective, but also realistic in capturing how people actually respond to epidemics, an essential feature for the effectiveness of any public health intervention.

1.3 Main contributions

The COVID-19 pandemic highlighted two major challenges for epidemic modeling: the need to account for population heterogeneity and the critical role of behavioral adaptations. Developing models that properly address these aspects is key for improving the ability to predict and control epidemic outbreaks. This thesis directly addresses both challenges by advancing the analysis of the SIR epidemic model in settings that include behavioral feedback and network effects between different populations. We focus on understanding how contact patterns and collective behaviors affect the spread of diseases and on designing effective intervention strategies. To do this, we study both scenarios where

the population is treated as homogeneous and network-based models, where interactions happen across different subpopulations.

While more complex models (e.g., SEIR, SAIR, or SIDHARTE) offer a detailed description of specific diseases, we deliberately adopt the SIR framework. This choice is guided by its analytical tractability and by its universality: unlike more detailed models that are tailored to the peculiarities of specific pathogens, the SIR model captures the core nonlinear dynamics of contagion in a general and widely applicable way. It provides a solid foundation for studying fundamental mechanisms, such as behavioral feedback or network effects, without relying on assumptions tied to a specific epidemiological scenario. Compared to the SIS epidemic model, the higher dimensionality and lack of monotonicity in the SIR model present significant analytical challenges. These complexities motivate the development of new techniques and provide deeper insights into the long-term behavior of epidemics with feedback and interactions.

We begin in Chapter 2 with a brief recap of the classical results for the scalar SIR model and then introduce a generalized version in which the transmission rate is no longer constant, but depends dynamically on both the susceptible and infected fractions of individuals. This extension captures behavioral responses that evolve with the progression of the epidemic. Within this framework, we define a behavioral reproduction number and show that, under a broad monotonicity assumption, the infection curve is unimodal (i.e., it has at most a single peak) and the epidemic eventually fades out. This result extends the analysis of the classical SIR model and builds upon previous studies on behavioral-feedback dynamics. For a specific functional form of the state-dependent transmission rate, we further derive an invariant of motion for the behavioral-feedback SIR epidemic model, that is a quantity that remains constant along the trajectories of the system. This invariant enables a closed-form characterization of both the infection peak and the final epidemic size. These results provide useful analytical tools to better understand how behavioral feedback shapes epidemic outcomes. This work builds on and extends the results presented in (Alutto et al., 2021; Alutto et al., 2025b).

Chapter 3 builds upon the previous analysis by extending the model to a network-based SIR model with endogenous behavioral feedback. In this framework, the nodes of the network represent subpopulations that share similar characteristics, such as infectivity, susceptibility, activity level and behavioral patterns. The interaction matrix, which encodes the contact rates between subpopulations, evolves dynamically as a function of the susceptible and infected fractions across the entire network. This approach captures heterogeneous behavioral responses, including increased interactions due to low perceived risk, voluntary distancing, policy-induced restrictions, and other factors that may vary among different groups. We analyze how such adaptive interactions influence stability and long-term behavior of the epidemic. In particular, for constant interaction matrices we derive invariants of motion, and under the additional assumption of rank-1 structure, we characterize the final epidemic state directly from the initial conditions. Finally, we complement the theoretical analysis with numerical simulations, exploring how different behavioral-feedback mechanisms affect the stability region, and emphasizing the central

role of behavioral dynamics in shaping epidemic trajectories. This work is part of the results presented in (Alutto et al., 2025a; Alutto et al., 2024).

In Chapter 4, we focus on the transient behavior of the behavioral-feedback network SIR model introduced in Chapter 3. We begin by investigating a class of models where the interaction matrix is assumed to be constant over time. This setting reflects scenarios where contact patterns between subpopulations are fixed and do not adapt to the evolving epidemic state. Each entry of the interaction matrix encodes features such as inter-group contact frequency, susceptibility and infectivity. After analyzing a simplified two-subpopulation scenario, we focus on the analytically tractable class of rank-1 interaction matrices and present several novel theoretical contributions. We first introduce a weighted aggregate infection quantity and prove that it exhibits a unimodal behavior as function of time, thus generalizing classical results from the scalar SIR setting. Moreover, we investigate the transient dynamics at the node level: we show that the infection curve at each node undergoes at most two changes of monotonicity before entering a monotonic decreasing phase. Through numerical simulations, we explore scenarios in which the interaction matrix has rank higher than 1. In such cases, we observe more complex dynamics, with local infection curves potentially exhibiting multiple peaks. Finally, we extend some of the theoretical insights, obtained in the first part, to a broader class of behavioral-feedback SIR models with state-dependent interaction matrices. We analyze how different feedback structures influence the transient dynamics and identify conditions under which similar unimodality results may still hold. This chapter contributes to a deeper understanding of the interplay between network topology and epidemic dynamics and extends the analytical framework for studying networked epidemic models. This work is developed in (Alutto et al., 2024; Alutto et al., 2025a).

Finally, in Chapter 5, we address the problem of optimal epidemic control in the context of the behavioral-feedback SIR model introduced in Chapter 2. In this setting, the state-dependent transmission rate evolves with infection and susceptibility levels, capturing adaptive behavioral responses and enabling more realistic modeling of mitigation strategies. We consider an optimal control problem in which interventions, such as lockdowns, are used to limit the spread of the disease while minimizing socio-economic costs. The model includes a hard constraint on the maximum allowed fraction of infected individuals, representing, for example, the saturation threshold of healthcare facilities. The core of our analysis lies in a geometric study of the state space, where the system evolves within a simplex constrained by the infection threshold. By partitioning this simplex and analyzing the structure of the reachable sets, we are able to characterize the feasible trajectories of the system under control. Building on this geometric insight, we construct a candidate value function that represents the minimum cumulative cost required to prevent the infection from exceeding the critical threshold, starting from any given state. Under general monotonicity conditions on the transmission rate, we rigorously prove that the optimal control follows a filling-the-box strategy: the infection is initially left uncontrolled until it approaches the threshold, then a sharp intervention is applied, followed by a gradual reopening until a time after which the spread is no longer regulated. We further

demonstrate that this strategy is not universally optimal: by constructing an analytical counterexample, we show that when the monotonicity assumptions are violated, more adaptive strategies may be required. This highlights the importance of understanding how behavioral feedback mechanisms shape both epidemic dynamics and the structure of optimal interventions. The results presented here appear in (Alutto et al., 2025b; Alutto et al., 2025c).

1.4 Notation

We briefly gather here some notational conventions adopted throughout the thesis. We denote by $\mathbb{R}$,$\mathbb{R}_+$ and $\mathbb{R}_{++}$ the sets of real, nonnegative real and positive real numbers, respectively, while $\mathbb{R}_+^{n\times n}$ indicates the set of real matrices with dimension $n \times n$ and nonnegative entries. We indicate by $\mathrm{Re}(x)$ the real part of a number x. The all-1 vector and the all-0 vector are denoted by $\mathbf{1}$ and $\mathbf{0}$ respectively. The transpose of a matrix A is denoted by A^T. For x in $\mathbb{R}^n$, let $||x||_1 = \sum_i |x_i|$ and $||x||_\infty = \max_i |x_i|$ be its l_1- and l_∞- norms, while $[x]$ denotes the diagonal matrix whose diagonal coincides with x. For an irreducible matrix A in $\mathbb{R}_+^{n\times n}$, we let $\lambda_{max}(A)$ and $v_{max}(A)$ denote respectively the dominant eigenvalue of A and the corresponding left eigenvector normalized in such a way that $\mathbf{1}'v_{max}(A) = 1$, which has positive entries and is unique due to the Perron-Frobenius theorem. Inequalities between two vectors x and y in $\mathbb{R}^n$ are meant to hold true entry-wise, i.e., $x \leq y$ means that $x_i \leq y_i$ for every i, whereas $x < y$ means that $x_i < y_i$ for every i and $x \lneq y$ means that $x_i \leq y_i$ for every i and $x_j < y_j$ for some j.

We model networks as finite weighted directed graphs $\mathcal{G} = (\mathcal{V}, \mathcal{E}, A)$, where $\mathcal{V} = \{1, 2, \ldots, n\}$ is the set of nodes, $\mathcal{E} \subseteq \mathcal{V} \times \mathcal{V}$ is the set of directed links and A in $\mathbb{R}_+^{n\times n}$ is a nonnegative weight matrix, to be referred as the interaction matrix, with the property that $A_{ij} > 0$ if and only if there exists a link (i, j) in $\mathcal{E}$ directed from node i to node j. A network is connected if its interaction matrix A is irreducible.

2 Scalar SIR Epidemic Models

In this chapter, we explore dynamical models that describe the spread of infectious diseases within a homogeneously mixed population. In Section 2.1, we present the classical SIR epidemic model, first introduced and studied in (Kermack and McKendrick, 1927), and review several well-known analytical results from the literature (Brauer et al., 2019; Diekmann and Heesterbeek, 2000; Diekmann et al., 2010; Martcheva, 2015). This model captures the essential mechanisms of disease transmission and recovery, assuming constant contact and infection rates over time. In particular, we introduce a key quantity, known as the effective reproduction number $R(t)$, which describes the average number of new infections caused by an infected individual at time t. The behavior of the infection curve is closely linked to the value of $R(t)$: when $R(t) < 1$, the fraction of infected individuals decreases, while when $R(t) > 1$, it increases. Importantly, in the classical SIR model, $R(t)$ can be shown to decrease monotonically over time and to eventually fall below 1. As a consequence, the infection curve is necessarily unimodal: if $R(0) \leq 1$, the fraction of infected individuals decreases monotonically and vanishes asymptotically; if $R(0) > 1$, the infection initially grows, reaches a peak at the time $\hat{t}$ when $R(\hat{t}) = 1$, and then decreases monotonically thereafter, eventually vanishing as time becomes large. We also discuss an invariant of motion, a quantity that remains constant along system solutions, which allows for an explicit characterization of both the infection peak and the final epidemic size. While this model offers valuable insights, it does not account for the potential impact of behavioral changes in response to the evolving state of the epidemic. In real-world scenarios, individuals often adjust their behavior, such as modifying social interactions or adopting protective measures, based on the perceived risk of infection.

To address this limitation, in Section 2.2 we introduce and analyze a novel extension of the SIR model, which constitutes the main theoretical contribution of this chapter. This behavioral-feedback SIR model incorporates behavioral adaptations driven by the current infection prevalence, offering a more realistic representation of epidemic dynamics, particularly in scenarios where public awareness and behavioral responses play a significant role in influencing the disease spread. We define a behavioral reproduction number, and under a certain monotonicity assumption on the transmission rate, we show that it retains the key qualitative property of the classical SIR model: the infection curve remains unimodal, with at most a single peak. However, a notable difference is that the behavioral reproduction number is not necessarily decreasing over time. Nevertheless, once it falls below

the critical threshold of 1, it remains below 1 for all subsequent times. This property is fundamental to ensuring that, after reaching the peak, the epidemic eventually vanishes. Next, we focus on a specific functional form of the behavioral transmission rate, for which we can derive an invariant of motion. Similar to the classical case, this quantity provides a closed-form characterization of both the infection peak and the final epidemic size, extending the analytical tools of the classical model to settings that incorporate behavioral feedback.

Both models discussed in this chapter assume a homogeneous population, where all individuals are equally likely to interact with each other, without considering any subpopulation structure or network effects. For clarity, we shall refer to these models as *scalar SIR epidemic models* throughout the thesis.

2.1 Scalar SIR epidemic model

In this section, we introduce the classical SIR epidemic model, that describes the spread of a disease among a homogeneous population. This model, first proposed in (Kermack and McKendrick, 1927), serves as the foundation for much of modern epidemic theory. Here, we summarize several key analytical results that are well established in the literature. The dynamics of the model are governed by the following assumptions. The rate at which susceptible individuals become infected is proportional to the product of the fractions of susceptible and infected individuals, scaled by a constant infection rate $\beta > 0$. Infected individuals recover at a constant recovery rate $\gamma > 0$, transitioning irreversibly to the recovered compartment. Let $x(t)$, $y(t)$, and $z(t)$ denote the fractions of susceptible, infected, and recovered individuals at time $t \geq 0$, respectively.

Under these assumptions, the SIR epidemic model is described by the following system of ordinary differential equations:

$$\begin{cases} \dot{x} = -\beta xy, \\ \dot{y} = \beta xy - \gamma y, \\ \dot{z} = \gamma y. \end{cases} \tag{2.1}$$

This model offers a fundamental yet insightful framework for describing the spread of an infectious disease within a closed and homogeneously mixed population. Thanks to its simplicity and analytical tractability, the SIR epidemic model (2.1) serves as a natural starting point for the development of more advanced epidemic models, and several foundational results concerning its dynamics are well established. The following propositions are summarized from (Brauer et al., 2019).

Proposition 2.1. *Consider the SIR epidemic model (2.1), with $\beta > 0$ and $\gamma > 0$. For every initial state $(x(0), y(0), z(0))$ in*

$$\Delta = \{(x, y, z) \in \mathbb{R}^3_+ : x + y + z = 1\}, \tag{2.2}$$

it admits a unique solution $(x(t), y(t), z(t))$ *in* Δ *for* $t \geq 0$ *and*

(i) the set of equilibrium points in Δ *is*

$$\Delta^* = \{(x^*, 0, 1 - x^*) : x^* \in [0, 1]^n\} ;$$

(ii) a disease-free equilibrium $(x^*, 0, 1 - x^*)$ *in* Δ^* *is stable if* $\beta x^*/\gamma < 1$*;*

Moreover, for every initial state $(x(0), y(0), z(0))$ *in* Δ *such that* $x(0) > 0$*,* $y(0) > 0$*:*

(iii) $t \to x(t)$ *is monotonically decreasing, while* $t \to z(t)$ *is monotonically increasing;*

(iv) if $\beta x(0) \leq \gamma$*, then* $y(t)$ *is strictly decreasing for* $t \geq 0$*;*

(v) if $\beta x(0) > \gamma$*, then there exists a peak time* $\hat{t} > 0$ *such that* $y(t)$ *is strictly increasing for* t *in* $[0, \hat{t}]$ *and strictly decreasing for* t *in* $[\hat{t}, +\infty)$*.*

Proof. See (Brauer et al., 2019, Chapter 2.4). □

A key feature of the classical SIR model is the disease-free equilibrium, which corresponds to a state in which the infection is completely eradicated, i.e., $y^* = 0$. This equilibrium is stable as long as the condition $\beta x^*/\gamma < 1$ is satisfied. This condition highlights the central role of the basic reproduction number, $R_0 = \beta/\gamma$, which represents the average number of secondary infections generated by a single infectious individual in a fully susceptible population. Another important result for the SIR epidemic model is the unimodal behavior of the infection curve. The fraction of infected individuals $y(t)$ admits at most one local maximum over time. This means the epidemic follows a single wave of infections: after reaching its peak, the fraction of infected individuals monotonically decreases until the disease eventually vanishes. As the epidemic progresses, the fraction of susceptible individuals $x(t)$ decreases, which leads to a reduction in the effective reproduction number, $R(t) = \beta x(t)/\gamma$. Once $R(t)$ drops below one, the epidemic starts to decline and eventually goes to 0. This behavior is a direct consequence of the model's structure, and is illustrated in Figure 2.1.

The next result establishes an *invariant of motion* for the SIR epidemic model (2.1) in the domain Δ, that is a function $\Psi : \Delta \to \mathbb{R}$ such that $\Psi(x(t), y(t))$ remains constant along every solution of (2.1). This concept is fundamental in the study of the model (2.1), as it provides a conserved quantity that remains unchanged throughout the progression of the epidemic. In particular, the existence of such an invariant allows us to derive important characteristics of the epidemic's dynamics, including the peak of infection and the final size of the epidemic.

Proposition 2.2. *Consider the SIR epidemic model (2.1), with* $\beta > 0$*,* $\gamma > 0$*, and initial state* $(x(0), y(0), z(0))$ *in* Δ *such that* $x(0) > 0$ *and* $y(0) > 0$*. Then,*

(i) the quantity $\beta(x + y) - \gamma \log x$ *is an invariant of motion;*

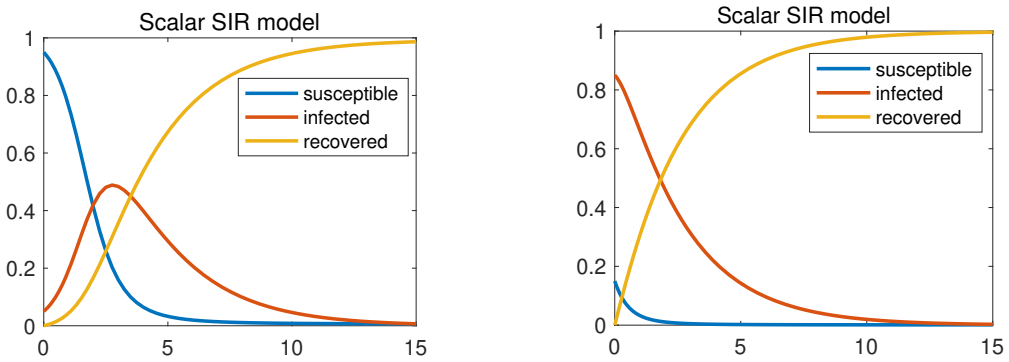

(A) (B)

FIGURE 2.1: Numerical simulation of the scalar SIR epidemic model with $\beta = 1.6$ and $\gamma = 0.4$. In plot (A), the initial condition is given by $x(0) = 0.95$ and $y(0) = 1 - x(0)$, corresponding to a scenario in which $R(0) > 1$, leading to the epidemic outbreak. In contrast, plot (B) shows a scenario with initial condition $x(0) = 0.15$ and $y(0) = 1 - x(0)$, for which $R(0) < 1$, and the infection rapidly dies out.

(ii) if $\beta x(0) > \gamma$, then the peak of infection is

$$y_{max} = -\frac{\gamma}{\beta} + \frac{\gamma}{\beta}\log\frac{\gamma}{\beta} + x(0) + y(0) - \frac{\gamma}{\beta}\log x(0); \tag{2.3}$$

(iii) there exists $x_\infty = \lim_{t\to+\infty} x(t)$ such that x_∞ is the unique solution of the equation

$$\beta x_\infty - \gamma \log x_\infty = \beta(x(0) + y(0)) - \gamma \log x(0)\,, \tag{2.4}$$

in the interval $(0, \gamma/\beta]$.

Proof. See (Brauer et al., 2019, Chapter 2.4). □

The invariant $\beta(x + y) - \gamma \log x$, as shown in Proposition 2.2(i), plays a crucial role in understanding the dynamics of the epidemic. Since it allows to derive a closed-form relationship between the fractions of susceptible and infected individuals throughout the epidemic evolution, directly linking them to the initial state, it also provides a precise estimate for the peak of the infected fraction. By setting the second equation in (2.1) equal to 0, Proposition 2.1(v) guarantees the existence of a unique instant t^* at which this condition can be met. At this particular moment, the dynamics of the epidemic reach its peak, with the susceptible fraction of the population satisfying $x(t^*) = \gamma/\beta$, while the maximum infected fraction $y(t^*) = y_{max}$ can be expressed as defined in (2.3). This result is crucial because it provides an accurate estimate of the peak infection level, which is important for designing containment policies. Furthermore, this invariant allows also for a precise characterization of the final size of the epidemic, that is determined by the value of $1 - x_\infty$, which represents the fraction of the population who has been infected over the course of the epidemic.

For this classical SIR model, invariants of motion have been used to derive exact analytical solutions (Harko et al., 2014). More broadly, this approach has been highly

effective in a variety of epidemic models, including more complex settings, where it is used to determine important quantities such as the asymptotic value of the susceptible fraction and the peak value of the infected fraction (Sontag, 2023; Feng, 2007). These quantities offer a systematic way to characterize the long-term behavior of epidemic systems, even in the presence of nonlinearities or more intricate transmission dynamics.

Despite its simplicity and theoretical significance, the classical SIR epidemic model has notable limitations that restrict its ability to accurately describe real-world epidemic dynamics. In particular, it relies on the assumption of a fully mixed population, in which each individual is equally likely to come into contact with any other, and it assumes complete homogeneity across the population in terms of susceptibility, recovery rates, and behavioral responses. The latter assumption, concerning the absence of behavioral adaptation, is especially unrealistic and will be addressed in the following section.

2.2 Behavioral-feedback scalar SIR epidemic model

To account for the influence of behavioral changes during an epidemic, we consider an extension of the classical scalar SIR model in which the infection rate is no longer constant, but instead depends on the current state of the epidemic. We introduce the following generalized SIR epidemic model, that describes the spread of a disease within a homogeneous population *with a state-dependent transmission rate*,

$$\begin{cases} \dot{x} = -\beta(x,y)xy, \\ \dot{y} = \beta(x,y)xy - \gamma y, \\ \dot{z} = \gamma y\,, \end{cases} \tag{2.5}$$

where again $x = x(t)$, $y = y(t)$ $z = z(t)$ indicate the fractions of susceptible, infected and recovered individuals in the population, respectively. The transmission rate is now a function $\beta : [0,1]^2 \to (0,+\infty)$, that captures an endogenous behavioral reaction to the epidemics through a modification of the interaction level, that is assumed to be a $\mathcal{C}^1$ function of $(x(t), y(t))$, while $\gamma > 0$ represents the constant recovery rate, as in (2.1). We shall refer to (2.5) as the behavioral-feedback SIR (BF-SIR) epidemic model.

This section presents original results on the qualitative and quantitative behavior of the BF-SIR epidemic model (2.5). Despite the added complexity introduced by the feedback mechanism, we show that several key properties of the classical model, such as the unimodality of the infection curve and the existence of an invariant of motion, can be preserved under certain assumptions. This allows for a tractable yet more realistic representation of epidemic dynamics in contexts where individual behavior is reactive to the epidemic evolution.

Example 2.1. *Let*

$$\beta(x,y) = \frac{b(x)}{1+cy}\,, \tag{2.6}$$

where the function $b : [0,1] \to (0,+\infty)$ is non-decreasing, differentiable and captures how the transmission rate varies with the number of susceptibles: a higher fraction of susceptibles may lead to a lower perceived risk, encouraging social interactions and riskier behaviors that facilitate contagion. The constant $c \geq 0$ measures how susceptibles adapt their behavior based on the presence of infected individuals. Observe that this class of models includes as a special case the classical SIR epidemic model (2.1), where $c = 0$ and b is a positive constant. This model generalizes (Franco, 2020; Baker, 2020), by adding a dependence on x.

The next result establishes the well-posedness of the model by showing that the set Δ, defined by (2.2), is positively invariant also for the BF-SIR epidemic model (2.5), and provides some preliminary results on the dynamics.

Proposition 2.3. *For every initial state $(x(0), y(0), z(0))$ in Δ, the BF-SIR epidemic model (2.5) admits a unique solution $(x(t), y(t), z(t))$ in Δ for $t \geq 0$. Moreover,*

(i) $t \to x(t)$ is monotonically non-increasing for all $t \geq 0$;

(ii) $y(t) > 0$ for all $t \geq 0$ if and only if $y(0) > 0$;

(iii) there exists $x_\infty \in \mathbb{R}$ such that

$$\lim_{t \to +\infty} (x(t), y(t), z(t)) = (x_\infty, 0, 1 - x_\infty)\,.$$

Proof. Since the vector field of (2.5) is Lipschitz with respect to (x, y, z), local existence and uniqueness for the Cauchy problem related to the ODE (2.5) is a standard result (Hale, 2009, p. I.3). By integrating the equations in (2.5), assuming initial condition $(x(0), y(0), z(0))$ in Δ, we get

$$x(t) = x(0) \exp\left(\int_0^t (-\beta(x(\tau), y(\tau)) y(\tau))\, d\tau \right), \tag{2.7}$$

$$y(t) = y(0) \exp\left(\int_0^t (\beta(x(\tau), y(\tau)) x(\tau) - \gamma)\, d\tau \right), \tag{2.8}$$

$$z(t) = z(0) + \gamma \int_0^t y(\tau)\, d\tau\,. \tag{2.9}$$

Moreover, the sum of equations in (2.5) gives

$$\dot{x}(t) + \dot{y}(t) + \dot{z}(t) = 0\,, \tag{2.10}$$

All this implies that, as long as the solution $(x(t), y(t), z(t))$ exists, we must have that

$$x(t) \geq 0,\ y(t) \geq 0,\ z(t) \geq 0, \qquad x(t) + y(t) + z(t) = 1\,. \tag{2.11}$$

In other terms, as long as the solution exists, it lives in Δ. In particular, this implies that the solution is globally defined, (Knauf, 2018, Section 3.3).

The proof of the remaining statements is as follows.

(i) It follows from (2.11) and the first equation in (2.5).

(ii) It follows directly from (2.8), since the exponential cannot be 0.

(iii) Since $x(t)$ and $x(t)+y(t)=1-z(t)$ are monotonic functions, they both admit a limit:

$$x_\infty := \lim_{t\to+\infty} x(t), \;\; \xi_\infty := \lim_{t\to+\infty} [x(t)+y(t)]\,.$$

As a consequence, the following limit

$$y_\infty = \lim_{t\to+\infty} y(t) = \xi_\infty - x_\infty \geq 0\,, \tag{2.12}$$

exists. Suppose now by contradiction that $y_\infty > 0$. This means that there exist $T, \varepsilon > 0$ such that $y(t) > \varepsilon$, for all $t \geq T$. Then, we get

$$\begin{aligned}
\lim_{t\to+\infty}[x(t)+y(t)] &= x(0)+y(0)-\gamma\int_0^\infty y(\tau)d\tau \\
&= x(0)+y(0)-\gamma\lim_{t\to+\infty}\int_0^t y(\tau)d\tau \\
&\leq x(0)+y(0)-\gamma\lim_{t\to+\infty}\int_T^t y(\tau)d\tau \\
&< x(0)+y(0)-\gamma\varepsilon\lim_{t\to+\infty}(t-T) \\
&= -\infty\,.
\end{aligned}$$

As this is an absurd, it must be $y_\infty = 0$. Then, the result follows from (2.11). □

To facilitate our analysis, we define the following sets

$$\mathcal{S} = \left\{(x,y)\in\mathbb{R}^2_+ : x+y\leq 1\right\},$$

$$\mathcal{S}_+ = \left\{(x,y)\in\mathbb{R}^2_{++} : x+y\leq 1\right\},$$

and observe that there exists an invertible map $s:\mathcal{S}\to\Delta$ such that $s(x,y)=(x,y,1-x-y)$. For this reason, from now on, we shall omit the variable z when denoting the state.

2.2.1 Reproduction number

In this subsection, we analyze the transient behavior of the infection dynamics, showing that, under a monotonicity condition, the infection curve exhibits a unimodal behavior, i.e. it has at most one peak. We define a *behavioral reproduction number* as

$$R(x,y) = \frac{1}{\gamma}\beta(x,y)x\,. \tag{2.13}$$

Note that the BF-SIR epidemic model (2.5) can be rewritten in $\mathcal{S}$ in terms of the reproduction number (2.13) as

$$\begin{cases} \dot{x} = -R(x,y)\gamma y, \\ \dot{y} = (R(x,y)-1)\,\gamma y, \end{cases} \tag{2.14}$$

We will establish the next result under the assumption that β is of class $\mathcal{C}^1$ satisfying the condition

$$x\frac{\partial \beta}{\partial x}(x,y) + \beta(x,y) > 0\,, \qquad \forall (x,y) \in \mathcal{S}\,, \tag{2.15}$$

Note that (2.15) implies that the reproduction number is increasing with respect to the fraction of susceptible individuals, i.e.,

$$\frac{\partial R}{\partial x}(x,y) > 0\,, \qquad \forall (x,y) \in \mathcal{S}\,. \tag{2.16}$$

The following result shows that $R(x,y)$ plays the same exact role than the reproduction number for the classical SIR model.

Proposition 2.4. *Let $R(x,y)$ satisfy condition (2.16). Consider the BF-SIR epidemic model (2.14) with initial state (x_0,y_0) in $\mathcal{S}$ such that $y_0 > 0$. Then, for every solution $(x(t),y(t)) \in \mathcal{S}$ the following facts hold:*

(i) if $R(x_0,y_0) \leq 1$, $t \mapsto y(t)$ strictly decreases for $t \geq 0$;

(ii) if $R(x_0,y_0) > 1$, there exists a peak time $\hat{t} > 0$ such that $t \mapsto y(t)$ strictly increases for t in $[0,\hat{t}]$ and strictly decreases for $t \geq \hat{t}$.

Proof. (i) We first notice that if $x_0 = 0$, then $x(t) = 0$ at all time and consequently $R(x(t),y(t)) = 0$ at all time. We now consider the case when $x_0 > 0$ that yields (by uniqueness of the solution) $x(t) > 0$ at all time, while $y(t) > 0$ at all time follows from Proposition 2.3(ii). In this case, we can now compute the time derivative of $R(t)$:

$$\gamma \dot{R} = \dot{x}\left[\beta + x\frac{\partial \beta}{\partial x}\right] + x\frac{\partial \beta}{\partial y}\dot{y}\,. \tag{2.17}$$

Notice that if for some $t^* \geq 0$ it happens that $R(x(t^*),y(t^*)) = 1$, then from the sign of $\dot{x}$, the standing fact that $x > 0$ at all time and (2.15), we have that the first term in the right-hand side of (2.17) is always negative. Finally, the third term is 0 at t^* since $\dot{y}(t^*) = 0$. We conclude that $\dot{R}(x(t^*),y(t^*)) < 0$, then $R(t)$ is strictly decreasing. As $R(x_0,y_0) \leq 1$, this implies that for sure there exists $\varepsilon > 0$ such that $R(x(t),y(t)) < 1$ for every $t \in (0,\varepsilon]$. We claim that $R(x(t),y(t)) < 1$ for every $t > 0$. If not, by contradiction, there exists $t^* > 0$ such that $R(x(t^*),y(t^*)) = 1$ and $R(x(t),y(t)) < 1$ for every $t \in (0,t^*)$. This contradicts the fact that $R(x(t),y(t))$ is strictly decreasing at t^*. The condition $R(x(t),y(t)) < 1$ for every $t > 0$ implies that $\dot{y}(t) < 0$ for every $t > 0$ and yields the thesis.

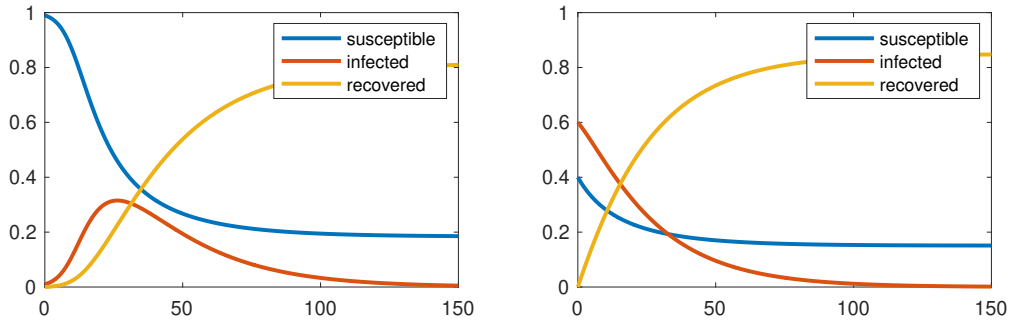

(A) (B)

FIGURE 2.2: Numerical simulation of the behavioral feedback SIR model with a transmission rate of the form defined in Example (2.1), with $b(x) = 0.35x$ and $c = 1.5$. In plot (A), the initial condition is given by $x_0 = 0.99$ and $y_0 = 1 - x_0$, corresponding to a scenario in which $R(x_0, y_0) > 1$, leading to the epidemic outbreak. In contrast, plot (B) shows a scenario with initial condition $x_0 = 0.4$ and $y_0 = 1 - x_0$, for which $R(x_0, y_0) < 1$, and the infection rapidly dies out.

(ii) If $R(x(t), y(t)) > 1$ for every t, then $y(t)$ would be strictly increasing at all times and could not converge to 0, violating Proposition 2.3(iii). Therefore, $\hat{t} = \min\{t \geq 0 \,|\, R(x(t), y(t)) = 1\}$ must exist finite. Then $y(t)$ is increasing up to $\hat{t}$. For $t > \hat{t}$, previous point (i) implies that $y(t)$ is strictly decreasing. □

Remark 2.1. *Note that Proposition 2.4 mirrors Proposition 2.1(iv)-(v), by establishing the unimodality of the infection curve under the assumption that the reproduction number increases with respect to the fraction of susceptible individuals, as stated in* (2.16).

A numerical simulation of the BF-SIR epidemic model is presented in Figure 2.2. The state-dependent transmission rate considered is $\frac{0.35x}{1+1.5y}$, that satisfies condition (2.15), while the recovery rate is $\gamma = 0.05$. The plot in Figure 2.2(A) depicts the solution corresponding to the initial condition $x_0 = 0.99$ and $y_0 = 1 - x_0$, for which $R(x_0, y_0) > 1$. Under this scenario, the fraction of infected individuals has a unimodal behavior, attaining a single peak before decreasing monotonically. In contrast, the plot in Figure 2.2(B) show the solution with initial condition $x_0 = 0.4$ and $y_0 = 1 - x_0$, satisfying $R(x_0, y_0) < 1$. As showed in Proposition 2.4(i), in this case the fraction of infected individuals decreases monotonically to zero.

While, Figure 2.3 shows a numerical simulation of the BF-SIR epidemic model (2.5) where condition (2.15) is not satisfied. Indeed, the transmission rate is given by $\beta(x, y) = x^2 - x + \frac{0.2}{3y+0.1}$, leading to a non-monotone dependence of $R(x, y)$ on the fraction of susceptibles, while the recovery rate is set to $\gamma = 0.025$. The simulation starts from the initial condition $x_0 = 0.95$, $y_0 = 1 - x_0$. As illustrated in the plot, the infection curve displays a multimodal behavior, characterized by the presence of two peaks. This example serves as a counterexample to the general unimodality result previously established under the monotonicity condition (2.15). In the absence of such monotonicity, the infection curve can lose its classical unimodal structure, leading to more complex epidemic dynamics with

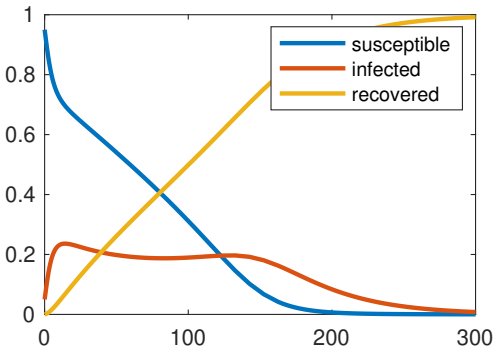

FIGURE 2.3: Numerical simulation of the behavioral-feedback SIR model with a transmission rate that does not satisfy condition (2.15). The initial state is $x_0 = 0.95$ and $y_0 = 1 - x_0$. The fraction of infected individuals exhibits a multimodal behavior with multiple peaks.

multiple waves and peaks of infection. This highlights the critical role of the behavioral feedback structure in shaping the qualitative properties of epidemic trajectories. Even when the monotonicity condition does not hold, it is often still possible to identify a time $\hat{t}$ after which the infection curve becomes monotonically decreasing toward zero. This marks the point where the fraction of susceptibles falls below the so-called *herd immunity level*, a threshold of critical importance for the design of effective control strategies.

2.3 A special case of non-constant behavioral feedback transmission rate

In this section, we refine our analysis by considering a special case of the non-constant behavioral feedback transmission rate $\beta(x, y)$, introduced in Example 2.1. Compared to the general behavioral feedback transmission rate case, this special setting is more analytically tractable, as it admits an invariant of motion and exploit it to characterize the orbits of the BF-SIR epidemic model (2.5), estimating infection peak and the final epidemic size. Such information is crucial for informing the design of containment strategies aimed at reducing the burden of an epidemic on public health systems.

Therefore, we now consider the dynamics corresponding to the setting of Example 2.1, that is

$$\begin{cases} \dot{x} = -\dfrac{b(x)}{1+cy} xy, \\ \dot{y} = \dfrac{b(x)}{1+cy} xy - \gamma y. \end{cases} \tag{2.18}$$

Within this framework, the effective reproduction number can be expressed as:

$$R(x, y) = \frac{xb(x)}{\gamma(1+cy)}\,. \tag{2.19}$$

The assumptions that $c \geq 0$ and that $b(x) > 0$ is differentiable and non-decreasing imply that

$$R_x(x,y) = \frac{b(x) + xb'(x)}{\gamma(1+cy)} > 0\,, \tag{2.20}$$

$$R_y(x,y) = \frac{-cxb(x)}{\gamma(1+cy)^2} \leq 0\,, \tag{2.21}$$

for every state (x,y) in $\mathcal{S}$, namely, the reproduction number is increasing with respect to the fraction of susceptible individuals x and non-increasing with respect to the fraction of infected individuals y.

For our analysis, it will prove convenient to also define

$$\rho(x,y) = 1 - \frac{1}{R(x,y)} = 1 - \frac{\gamma(1+cy)}{xb(x)}\,, \tag{2.22}$$

for all (x,y) in $\mathcal{S}_+$ and observe that $\rho(x,y) \geq 0$ if and only if $R(x,y) \geq 1$.

2.3.1 Invariant of motion

As done in Section 2.1 for the classical SIR model, we can derive an invariant of motion for the BF-SIR epidemic model (2.18) in the domain $\mathcal{S}_+$. Recall that an invariant of motion is a function $\Psi : \mathcal{S}_+ \to \mathbb{R}$ such that $\Psi(x(t), y(t))$ remains constant along every solution of (2.18). Assuming that $\Psi(x,y)$ is differentiable on $\mathcal{S}_+$, the chain rule, together with system (2.14), implies that Ψ is an invariant of motion if and only if, for every $(x,y) \in \mathcal{S}_+$,

$$\begin{aligned} 0 &= \dot{\Psi} \\ &= \Psi_x \dot{x} + \Psi_y \dot{y} \\ &= \gamma y \left((R(x,y) - 1)\Psi_y - R(x,y)\Psi_x \right)\,. \end{aligned}$$

or, equivalently, if and only if

$$\Psi_x(x,y) = \rho(x,y)\Psi_y(x,y)\,, \tag{2.23}$$

for every (x,y) in $\mathcal{S}_+$, where $\rho(x,y)$ is given by (2.22).

Proposition 2.5. *For every $x_0 > 0$, a constant $c \geq 0$ and a differentiable non-decreasing function $b : [0,1] \to (0,+\infty)$, let*

$$g(x) = \int_{x_0}^{x} \frac{\gamma c}{sb(s)} \mathrm{d}s \leq 0\,, \tag{2.24}$$

and

$$\psi(x,y) = ye^{-g(x)} - \int_{x_0}^{x} e^{-g(s)} \left(-1 + \frac{\gamma}{sb(s)} \right) \mathrm{d}s\,. \tag{2.25}$$

Then, $\psi(x,y)$ is differentiable in $\mathcal{S}_+$ with

$$\psi_y(x,y) = e^{-g(x)}\,, \qquad \psi_x(x,y) = e^{-g(x)}\rho(x,y)\,. \tag{2.26}$$

Moreover, $\psi(x,y)$ is an invariant of motion for the BF-SIR epidemic model (2.18) in $\mathcal{S}_+$.

Proof. The first equation in (2.26) can be obtained by direct computation. To prove the second one, note that

$$\begin{aligned}
\psi_x(x,y) &= -ye^{-g(x)}g'(x) + e^{-g(x)}\left(1 - \frac{\gamma}{xb(x)}\right) \\
&= -ye^{-g(x)}\frac{\gamma c}{xb(x)} + e^{-g(x)}\left(1 - \frac{\gamma}{xb(x)}\right) \\
&= e^{-g(x)}\left(1 - \frac{\gamma(1+cy)}{xb(x)}\right) \\
&= e^{-g(x)}\rho(x,y) \\
&= \psi_y(x,y)\rho(x,y)\,.
\end{aligned}$$

Since (2.23) is satisfied, $\psi(x,y)$ is an invariant of motion. □

Remark 2.2. *Note that Proposition 2.5 establishes a result analogous to that in Proposition 2.2(i) for the classical SIR epidemic model, under the assumption of a specific state-dependent transmission rate, as illustrated in Example 2.1.*

2.3.2 Peak of infection

Leveraging the derivation of the invariant of motion, we will characterize the maximum infection peak of the BF-SIR epidemic model. To establish the result, observe that, since $b(x)$ is positive, differentiable and non-decreasing, the function $f(x) := xb(x)$ is differentiable and strictly increasing in $[0,1]$, and thus invertible. Let us start with a technical lemma.

Lemma 2.1. *Suppose that there exists an initial condition (x_0,y_0) in $\mathcal{S}_+$ such that $R(x_0,y_0) > 1$. Define the value $\tilde{x}_\gamma = f^{-1}(\gamma)$ and the function $\tilde{x}$ as*

$$\tilde{x}(y) := f^{-1}(\gamma(1+cy)), \quad c > 0\,, \tag{2.27}$$

then $\tilde{x}_\gamma \in (0,1)$ and $\tilde{x}(y) \in (0,1]$ for all $y \in \left(0, \min\{1, \frac{f(1)-\gamma}{c\gamma}\}\right]$.

Proof. First observe that since there exists an initial condition $(x_0,y_0) \in \mathcal{S}_+$ such that $R(x_0,y_0) > 1$, from (2.20) and (2.21), we obtain $R(1,0) > 1$ which means $f(1) > \gamma$. Hence, $\tilde{x}_\gamma$ is well defined. From $f(\tilde{x}_\gamma) = \gamma$, the fact that $\gamma \in (0, f(1))$ and monotonicity of $f(x)$, it follows that $\tilde{x}_\gamma \in (0,1)$.

Next, note that since

$$c > 0, \qquad \frac{f(1)-\gamma}{c\gamma} > 0, \qquad y \le \frac{f(1)-\gamma}{c\gamma}\,,$$

it follows that $\gamma(1+cy) \leq f(1)$. Hence, $\tilde{x}(y)$ is well defined. From $f(\tilde{x}(y)) = \gamma(1+cy) \in (0, f(1)]$ and monotonicity of f, we obtain $\tilde{x}(y) \in (0, 1]$. □

Define now the value y_c as

$$y_c = \begin{cases} 1 & \text{if } c = 0, \\ \min\left\{1, \frac{f(1)-\gamma}{c\gamma}\right\} & \text{if } c > 0. \end{cases} \tag{2.28}$$

Building on the previous lemma, we can now proceed to characterize the peak infection level in the BF-SIR epidemic model.

Proposition 2.6. *Consider the BF-SIR epidemic model (2.18). Let (x_0, y_0) be the initial state in $\mathcal{S}$ with $y_0 > 0$. Then,*

(i) if $R(x_0, y_0) \leq 1$, then $y(t) \leq y_0$ for all $t \geq 0$;

(ii) if $R(x_0, y_0) > 1$, define

$$\phi(y) := \psi\left(f^{-1}(\gamma(1+cy)), y\right), \tag{2.29}$$

for all $y \in (0, y_c]$, then ϕ is invertible and $y(t) \leq \phi^{-1}(\psi(x_0, y_0))$ for all $t \geq 0$.

Proof. (i) Let $(x(t), y(t))$ be the solution of the BF-SIR epidemic model (2.18), with initial state (x_0, y_0) in $\mathcal{S}$. If $R(x_0, y_0) \leq 1$, from Proposition 2.4(i), the fraction of infected $y(t)$ attains its maximum value at its initial state y_0.

(ii) Assume now that $R(x_0, y_0) > 1$. From Proposition 2.4(ii), there exists a peak time $\hat{t} > 0$ such that $\dot{y}(\hat{t}) = 0$. Since $y_0 > 0$ implies $y(t) > 0$ for all $t \geq 0$, from (2.14), it follows that, $R(x(\hat{t}), y(\hat{t})) = 1$, that is

$$x(\hat{t})\, b(x(\hat{t})) = \gamma(1 + cy(\hat{t}))\,, \tag{2.30}$$

where $y(\hat{t}) > y_0$. It follows from (2.30) that $y(\hat{t}) \in (0, y_c]$. Hence, by Lemma 2.1, the fraction of susceptibles at the peak time $\hat{t}$ is

$$x(\hat{t}) = f^{-1}\left(\gamma(1 + cy(\hat{t}))\right) = \tilde{x}(y(\hat{t}))\,. \tag{2.31}$$

Moreover, note that $R(\tilde{x}(y), y) = 1$ for $y \in (0, y_c]$, which in turn is equivalent to

$$\rho(\tilde{x}(y), y) = 0, \quad \forall y \in (0, y_c]\,, \tag{2.32}$$

by definition of ρ. From Proposition 2.5, it follows that $\psi(x(\hat{t}), y(\hat{t})) = \psi(x_0, y_0)$. Moreover, (2.29) and (2.30) imply

$$\phi(y(\hat{t})) = \psi(\tilde{x}(y(\hat{t})), y(\hat{t})) = \psi(x(\hat{t}), y(\hat{t})) = \psi(x_0, y_0)\,. \tag{2.33}$$

From (2.26) and (2.32), $\phi(y)$ is differentiable with derivative

$$\begin{aligned}\phi'(y) &= \psi_x(\tilde{x}(y), y)\frac{c\gamma}{f'(\tilde{x}(y))} + \psi_y(\tilde{x}(y), y) \\ &= e^{-g(\tilde{x}(y))}\rho\left(\tilde{x}(y), y\right)\frac{c\gamma}{f'(\tilde{x}(y))} + e^{-g(\tilde{x}(y))} \\ &= e^{-g(\tilde{x}(y))} \\ &> 0\,.\end{aligned}$$

This means that ϕ is invertible and from (2.33) we get

$$y(\hat{t}) = \phi^{-1}(\psi(x_0, y_0))\,.$$

Proposition 2.4(ii) implies that $y(t) \leq y(\hat{t}) = \phi^{-1}(\psi(x_0, y_0))$ for all $t \geq 0$. □

Remark 2.3. *Note that from Proposition 2.3(ii), if $y_0 = 0$ then the fraction of infected $y(t)$ will remain 0 for all $t \geq 0$. Then, for all (x_0, y_0) in $\mathcal{S}$ we can define the peak of infection as*

$$\max_{t\geq 0} y(t) = \begin{cases} y_0 & \text{if } R(x_0, y_0) \leq 1 \text{ or } y_0 = 0 \\ \phi^{-1}(\psi(x_0, y_0)) & \text{if } R(x_0, y_0) > 1,\ y_0 > 0. \end{cases} \tag{2.34}$$

Remark 2.4. *Proposition 2.6(ii) and Proposition 2.2(ii) characterize the infection peak for the BF-SIR and classical SIR models, respectively, both relying on the invariant of motion, the former in the case of a state-dependent transmission rate as in the functional form of Example 2.1.*

Understanding the maximum value of $y(t)$ is crucial, as social planners typically aim to keep the proportion of infected individuals below a predetermined threshold, while simultaneously minimizing the economic and social costs associated with limiting economic activity and social interactions. This threshold often reflects the healthcare system's capacity to provide adequate care to infected patients. Ensuring that the infection level remains below this critical value is essential to guarantee that all patients receive the necessary medical attention and to prevent the healthcare system from becoming overwhelmed.

In Chapter 5 of this thesis, we will formulate and analyze an optimal control problem that incorporates this type of constraint, balancing public health considerations with the need to mitigate the economic cost.

2.3.3 Size of epidemic

Having derived the invariant of motion for the BF-SIR epidemic model (2.18), we can now also define the size of epidemic, similar to the analysis done for the classical case in Proposition 2.2(iii).

Let us first define, for all (x_0, y_0) in $\mathcal{S}$ such that $y_0 > 0$,

$$x_c = \begin{cases} x_0 & \text{if } R(x_0, y_0) \leq 1\,, \\ x(\hat{t}) & \text{if } R(x_0, y_0) > 1\,. \end{cases} \tag{2.35}$$

where $x(\hat{t})$ is the fraction of susceptibles at the peak time $\hat{t}$, defined in (2.31).

Proposition 2.7. *Consider the BF-SIR epidemic model (2.18). Let (x_0, y_0) be the initial state in $\mathcal{S}$ with $y_0 > 0$. Given the g function defined in (2.24), then $x_\infty = \lim_{t\to+\infty} x(t)$ is the unique solution of the equation*

$$\int_{x_\infty}^{x_0} e^{-g(s)} \left(-1 + \frac{\gamma}{sb(s)}\right) \mathrm{d}s = y_0\,, \tag{2.36}$$

in the interval $(0, x_c]$.

Proof. From the invariant of motion (2.25) and the characterization of the asymptotic state of the model in Proposition 2.3(iii) where $y_\infty = 0$, it follows that $\psi(x_0, y_0) = \psi(x_\infty, 0)$, that is

$$\begin{aligned} \psi(x_0, y_0) = y_0 e^{-g(x_0)} &= y_0 \\ &= y_\infty e^{-g(x_\infty)} - \int_{x_0}^{x_\infty} e^{-g(s)} \left(-1 + \frac{\gamma}{sb(s)}\right) \mathrm{d}s \\ &= -\int_{x_0}^{x_\infty} e^{-g(s)} \left(-1 + \frac{\gamma}{sb(s)}\right) \mathrm{d}s\,. \end{aligned}$$

By rearranging the equations, we obtain

$$\int_{x_\infty}^{x_0} e^{-g(s)} \left(-1 + \frac{\gamma}{sb(s)}\right) \mathrm{d}s = y_0\,.$$

We can define the function

$$h(x) := \int_{x}^{x_0} e^{-g(s)} \left(-1 + \frac{\gamma}{sb(s)}\right) \mathrm{d}s\,,$$

that is differentiable with first derivative as follows

$$h'(x) = -e^{-g(x)} \left(-1 + \frac{\gamma}{xb(x)}\right)\,,$$

for all x in $(0, x_c]$. Note that if $R(x_0, y_0) \leq 1$, then from (2.20), (2.21) it follows that $R(x, 0) = xb(x)/\gamma \leq 1$ for all x in $(0, x_c]$. While, if $R(x_0, y_0) > 1$, from Proposition

(2.4)(ii) we get that there exists a time instant $\hat{t}$ such that $R(x(\hat{t}), y(\hat{t})) = 1$ and again from (2.20), (2.21) it follows that $R(x, 0) = xb(x)/\gamma \leq 1$ for all x in $(0, x_c]$. Therefore, $h'(x) \leq 0$ for all x_∞ in $(0, x_c]$ and thus it is invertible, then there exists $x_\infty = h^{-1}(y_0)$. □

Remark 2.5. *As for the classical SIR epidemic model (2.1), the final size of the epidemic can be precisely characterized by the value $1 - x_\infty$, which represents the total fraction of the population that has been infected over the course of the epidemic. Note also that the result in 2.7 mirrors that of Proposition 2.2(iii) for the classical case.*

2.3.4 Some final remarks

After revisiting the scalar SIR model in Section 2.1, we introduced in Section 2.2 the behavioral-feedback SIR epidemic model, showing that the unimodality of the infection curve is preserved whenever the behavioral reproduction number increases with respect to the fraction of susceptible individuals. Building on this, in Section 2.3, we analyzed a special functional form for a non-constant transmission rate and we derived an invariant of motion for the behavioral-feedback SIR epidemic model in Subsection 2.3.1. This result enabled a closed-form characterization of both the infection peak (Subsection 2.3.2) and the final epidemic size (Subsection 2.3.3). It is worth noting that alternative functional forms for the transmission rate could also be considered, provided they satisfy the same analytical conditions. For example, one could use

$$\beta(x, y) = b(x)(1 - cy) \qquad c \in [0, 1)\,,$$

and

$$\beta(x, y) = b(x)e^{-ky} \qquad k \geq 0\,,$$

where the function $b : [0, 1] \to (0, +\infty)$ is again a non-decreasing and differentiable function of the fraction of susceptibles. However, the form presented in Example 2.1 was chosen primarily for analytical convenience. In particular, this rational expression enabled the derivation of an invariant of motion. While alternative decreasing functions of the infected fraction, such as the ones presented above, are also viable and potentially more realistic in some contexts, they lead to more complex dynamics and may not yield closed-form expressions for those quantities. Therefore, the selected form serves as a tractable yet representative example to illustrate the theoretical framework.

3 Asymptotic Behavior and Stability of Network Behavioral-Feedback SIR Epidemic Model

The classical SIR epidemic model, discussed in Chapter 2, relies on several strong homogeneity assumptions. It assumes a fully mixed population in which all individuals are equally likely to interact, share the same susceptibility and infectivity, and recover at the same rate. These assumptions, while simplifying the analysis, rarely hold in real-world scenarios, where contact patterns, susceptibility, and recovery behaviors often exhibit significant heterogeneity. To better capture these complexities, network-based epidemic models have been developed (Pastor-Satorras et al., 2015; Paré et al., 2020; Zino and Cao, 2021). In these models, nodes represent subpopulations that share similar characteristics, such as infectivity, susceptibility, and interaction rates. This allows for a natural aggregation of individuals, enabling a more structured yet tractable description of epidemic dynamics. For instance, nodes can correspond to age groups, geographic regions, or communities with distinct patterns of susceptibility, infectivity, and social activity levels. Another key limitation of the classical SIR model is the assumption of a constant transmission rate, which fails to account for behavioral adaptations in response to epidemic severity. Historical and contemporary evidence suggests that individuals often modify their behavior, such as reducing social contacts or adopting preventive measures, in reaction to perceived risk. This limitation was partially addressed in Chapter 2 by introducing a scalar SIR model with behavioral feedback, where the transmission rate depends on the current epidemic state.

In this chapter, we extend the analysis to a network-based SIR model with behavioral feedback. Unlike standard network models with fixed contact structures, we consider an adaptive interaction matrix A whose entries evolve dynamically based on the current epidemic state. Specifically, each element A_{ij} is modeled as a function of the susceptible x and infected y fractions of individuals, thereby capturing heterogeneous behavioral responses such as voluntary distancing, behavioral fatigue, or policy-induced restrictions across different subpopulations. Our main objective in this chapter is to investigate how this feedback and the network mechanism affects the stability properties of the epidemic dynamics. Section 3.2 is devoted to this analysis, where we characterize the stability

region of the disease-free equilibrium and, in the case of constant interaction matrices, derive explicit invariants of motion. In Section 3.4, we build on these invariants and show that, under the additional assumption of a rank-1 interaction matrix, they can be exploited to describe the long-term dynamics of the system and to determine the final epidemic state directly from the initial conditions. Finally, in Section 3.5, we complement the theoretical analysis with numerical simulations, which reveal how different functional forms of the behavioral-feedback interaction matrix influence the size and geometry of the stability region. These results underline the importance of accounting for adaptive behavior in network epidemic models and provide valuable insights for the design of effective and targeted intervention strategies.

3.1 Model definition

We consider a system of n interacting subpopulations, each composed of indistinguishable individuals. A subpopulation is represented by a node of a state-dependent network $\mathcal{G} = (\mathcal{V}, \mathcal{E}, A(x, y))$, where (i, j) belongs to $\mathcal{E}$ if and only if $A_{ij}(x, y) > 0$ for some state (x, y) in $[0, 1]^{2n}$. For each subpopulation $i \in \{1, \dots, n\}$, the variables $x_i(t)$, $y_i(t)$, and $z_i(t)$ denote the fractions of susceptible, infected, and recovered individuals, respectively. The entries $A_{ij}(x, y)$ represent the infection rate from subpopulation j to subpopulation i, and are dynamically modulated by the current epidemic state. Their dependence on the fraction of susceptible x and infected y individuals across the network, allows the model to capture behavioral adaptations; for instance, a reduction in contact with highly infected groups or an increase in activity among low-risk ones, thereby embedding a feedback mechanism between epidemic prevalence and social interaction patterns. Finally, a positive parameter γ models the recovery rate, which is assumed to be homogeneous across the network.

The network behavioral-feedback SIR (BF-SIR) epidemic model with irreducible interaction matrix $A : [0, 1]^{2n} \to \mathbb{R}_+^{n \times n}$ of class $\mathcal{C}^1$ and recovery rate $\gamma > 0$, is then the autonomous system of ordinary differential equations

$$\begin{cases} \dot{x}_i = -x_i \displaystyle\sum_{j=1}^{n} A_{ij}(x, y) y_j \\ \dot{y}_i = x_i \displaystyle\sum_{j=1}^{n} A_{ij}(x, y) y_j - \gamma y_i \\ \dot{z}_i = \gamma y_i \end{cases} \qquad \forall i = 1, \dots, n\,. \tag{3.1}$$

In this section, we first prove a well-posedness result for the system, showing that solutions exist and are unique. We then characterize the space in which the trajectories evolve and describe the set of equilibrium points.

Example 3.1. *Consider a class of models with interaction matrix*

$$A_{ij}(x, y) = g_i(x_i) f_j(y_j)$$

for all $i, j = 1, \dots, n$, *where* $g_i : [0,1] \to [0,\infty)$ *is a non-decreasing function of* x_i *and* $f_j : [0,1] \to [0,\infty)$ *is non-increasing in* y_j. *Here,* $g_i(x_i)$ *reflects the susceptibility and social activity rate of subpopulation* i, *depending on the local fraction of susceptibles* x_i. *A higher fraction of susceptibles may lead to a lower perceived risk, which encourages riskier social interactions and behaviors that increase both susceptibility and contagion. On the other hand,* $f_j(y_j)$ *captures how a higher fraction of infected individuals in subpopulation* j *leads to a reduction in outgoing interactions, as others respond by limiting contact to reduce their risk of infection. This factorized structure of the interaction matrix models the impact of adaptive behavior on epidemic dynamics through varying interaction rates between subpopulations.*

The following result gathers some properties of the network BF-SIR epidemic model, with a generalization of (Mei et al., 2017, Theorem 7).

Proposition 3.1. *Consider the network BF-SIR epidemic model* (3.1) *with an irreducible interaction matrix* $A : [0,1]^{2n} \to \mathbb{R}_+^{n \times n}$ *and recovery rate* $\gamma > 0$. *Then, for every initial condition* $(x(0), y(0), z(0))$ *in*

$$\Delta = \left\{(x, y, z) \in [0,1]^{3n} : x + y + z = \mathbf{1}\right\},$$

it admits a unique $\mathcal{C}^1$ *solution on* $\mathbb{R}_+^n$, *denoted by* $(x(t), y(t), z(t))$ *in* Δ. *Moreover,*

(i) for every $i = 1, \dots, n$, $x_i(t)$ *is non-increasing for* $t \geq 0$, *and* $x_i(0) > 0$ *if and only if* $x_i(t) > 0$ *for every* $t \geq 0$;

(ii) if $y(0) \gneq \mathbf{0}$, *then* $y(t) > \mathbf{0}$ *for every* $t > 0$;

(iii) there exists x^* *in* $\mathbb{R}_+^n$ *such that* $\mathbf{0} \leq x^* \leq x(0)$ *and*

$$\lim_{t \to +\infty} x(t) = x^*, \qquad \lim_{t \to +\infty} y(t) = \mathbf{0}; \tag{3.2}$$

(iv) the set of equilibrium points in Δ *is*

$$\Delta^* = \{(x^*, \mathbf{0}, \mathbf{1} - x^*) : x^* \in [0,1]^n\}.$$

Proof. Note that the vector field of (3.1) is $\mathcal{C}^1$ with respect to (x, y, z), then existence and uniqueness for the Cauchy problem related to the ODE (3.1) is a standard result (Hale, 2009, Chapter I.3), (Knauf, 2018, Chapter 3.2). We now apply Nagumo's theorem (Blanchini and Miani, 2007), since for every point belonging to the boundary of Δ, the vector field of the dynamics is either tangent, or points inside the set Δ. Therefore for $(x(0), y(0), z(0))$ in Δ, it follows that $(x(t), y(t), z(t))$ belong to Δ for all $t > 0$, which means that Δ is a positively invariant set for the system (3.1). In particular, this implies that the solution is globally defined (Knauf, 2018, Section 3.3).

(i) The invariance of Δ implies that $x(t)$, $y(t)$ and $A(x(t), y(t))$ have non-negative entries for every time t. Therefore,

$$\dot{x}_i(t) = -x_i(t) \sum_{j=1}^{n} A_{ij}(x, y) y_j(t) \leq 0$$

for all $i = 1, \ldots, n$ and $t \geq 0$. By integrating the first equation of (3.1), for each node i we get

$$x_i(t) = x_i(0) \exp\left(- \int_0^t \sum_{j=1}^{n} A_{ij}(x(\tau), y(\tau)) y_j(\tau) \mathrm{d}\tau \right),$$

hence $x_i(t) > 0$ for every $t \geq 0$ if and only if $x_i(0) > 0$.

(ii) Assume by contradiction the existence of $i \in \{1, \ldots, n\}$ and $T > 0$ such that $y_i(T) = 0$. Then, (3.1) implies that $\dot{y}_i(T) \geq 0$, which yields $\dot{y}_i(t) = 0$ for all $t \in [0, T]$ otherwise $y_i(t)$ would be negative for some $t < T$. By (3.1), this would imply that $y_j(t) = 0$ for all $t \in [0, T]$ for all j such that $A_{ij}(x, y) > 0$. We could iterate this argument and, using the irreducibility of $A(x, y)$, we would reach the contradiction that $y(t) = \mathbf{0}$ for all $t \in [0, T]$.

(iii) Observe that the sum of the first two equations of (3.1) is

$$\dot{x}_i(t) + \dot{y}_i(t) = -\gamma y_i(t) \leq 0, \tag{3.3}$$

for all i. Since $x_i(t)$ and $x_i(t) + y_i(t)$ are monotonic functions, they both admit a limit:

$$x_i^* := \lim_{t \to +\infty} x_i(t), \qquad \xi_i^* := \lim_{t \to +\infty} [x_i(t) + y_i(t)] .$$

As a consequence, the following limit

$$y_i^* = \lim_{t \to +\infty} y_i(t) = \xi_i^* - x_i^* \geq 0$$

exists. Suppose now by contradiction that $y_i^* > 0$. This means that there exist $T, \varepsilon > 0$ such that $y_i(t) > \varepsilon$, for all $t \geq T$. Then, we get

$$\begin{aligned}
\xi_i^* = \lim_{t \to +\infty} [x_i(t) + y_i(t)] &= x(0) + y(0) - \gamma \int_0^{\infty} y_i(\tau) d\tau \\
&= x_i(0) + y_i(0) - \gamma \lim_{t \to +\infty} \int_0^t y_i(\tau) d\tau \\
&< x_i(0) + y_i(0) - \gamma \lim_{t \to +\infty} \int_T^t y_i(\tau) d\tau \\
&< x_i(0) + y_i(0) - \gamma\varepsilon \lim_{t \to +\infty} (t - T) = -\infty
\end{aligned}$$

As this is a contradiction, it must be $y_i^* = 0$ and this is valid for all $i \in \{1, \ldots, n\}$. From the invariance of Δ, for every $(x(0), y(0), z(0))$ in Δ, the trajectory $(x(t), y(t), z(t))$

converges to some equilibrium of the form $(x^*, \mathbf{0}, \mathbf{1}-x^*)$ and from point (i), $x(0) \geq x^* \geq \mathbf{0}$.

(iv) Note that a point $(x^*, y^*, z^*) \in \Delta$ is an equilibrium if and only if

$$\mathbf{0} = -[x^*]A(x^*, y^*)y^*\,, \qquad \mathbf{0} = [x^*]A(x^*, y^*)y^* - \gamma y^*\,, \qquad \mathbf{0} = \gamma y^*\,.$$

This implies that any point of the form $(x^*, \mathbf{0}, \mathbf{1} - x^*)$ is an equilibrium, referred to as a *disease-free equilibrium*. Moreover, these are the only equilibrium points, since any point with $y^* \neq \mathbf{0}$ would not satisfy the equilibrium conditions given above. □

Notice that, from Proposition 3.1, the third equation of (3.1) can be omitted since the dynamics of the recovered fraction of individuals $z_i = 1-x_i-y_i$ can be deduced from that of the fractions of susceptible individuals x_i and of infected individuals y_i, respectively, for every subpopulation i in $\mathcal{V}$. The model (3.1) can then be more compactly rewritten in the following vectorial form

$$\begin{cases} \dot{x} = -[x]A(x, y)y\,, \\ \dot{y} = [x]A(x, y)y - \gamma y\,, \end{cases} \tag{3.4}$$

for all x and y belonging to the positively invariant set

$$\mathcal{S} = \left\{(x, y) \in [0, 1]^{2n} : x + y \leq \mathbf{1}\right\}\,.$$

We refer to the set of equilibrium points within $\mathcal{S}$ as

$$\mathcal{S}^* = \{(x^*, \mathbf{0}) : x^* \in [0, 1]^n\}\,.$$

3.2 Stability results

In this section, we analyze the stability properties of the network BF-SIR epidemic model. We first investigate general conditions under which the disease-free equilibrium is stable, focusing on the influence of the feedback structure encoded in the interaction matrix. We also provide an example that allows for a more detailed characterization of the stability condition.

We begin by establishing a general stability result.

Theorem 3.1. *Consider the network BF-SIR epidemic model (3.4) with irreducible interaction matrix $A : [0, 1]^{2n} \to \mathbb{R}_+^{n\times n}$ and recovery rate $\gamma > 0$. Then, for every initial state $(x(0), y(0))$ in $\mathcal{S}$:*

(i) if

$$\lambda_{\max}([x^*]A(x^*, \mathbf{0})) > \gamma\,, \tag{3.5}$$

then $(x^*, \mathbf{0}) \in \mathcal{S}^*$ is unstable,

(ii) if

$$\lambda_{\max}([x^*]A(x^*,\mathbf{0})) < \gamma\,, \tag{3.6}$$

then $(x^*,\mathbf{0}) \in \mathcal{S}^*$ *is stable.*

Proof. First observe that the Jacobian matrix of (3.4) evaluated in a disease-free equilibrium $(x^*,\mathbf{0})$ is

$$J(x^*,\mathbf{0}) = \begin{bmatrix} 0 & -[x^*]A(x^*,\mathbf{0}) \\ 0 & [x^*]A(x^*,\mathbf{0}) - \gamma I \end{bmatrix}. \tag{3.7}$$

It then follows that half of the eigenvalues are equal to 0, while the remaining ones correspond to the eigenvalues of the $n \times n$ dimension matrix $[x^*]A(x^*,\mathbf{0}) - \gamma I$. According to the linearization theorem, the stability analysis depends on the sign of the real part of the eigenvalues of the Jacobian matrix (3.7), which is determined by

$$\max\{\mathrm{Re}(\lambda) :\ \lambda \in \sigma(J(x^*,\mathbf{0}))\} = \max\{0, \lambda_{\max}([x^*]A(x^*,\mathbf{0})) - \gamma\}\,.$$

(i) It is immediate that if $\lambda_{\max}([x^*]A(x^*,\mathbf{0})) > \gamma$ then $\max\{\mathrm{Re}(\lambda) :\ \lambda \in \sigma(J(x^*,\mathbf{0}))\} > 0$, so that $(x^*,\mathbf{0})$ is linearly unstable.

(ii) Instead, if $\lambda_{\max}([x^*]A(x^*,\mathbf{0})) < \gamma$, then we shall use the center manifold theory (Bacciotti, 2006; Guckenheimer and Holmes, 1983), by analyzing the stable and center spaces. In this case, the stable subspace is given by

$$\mathcal{V}_S = \{(\mathbf{0}, y) :\ y \in [0,1]^n\}\,,$$

while the center subspace is

$$\mathcal{V}_C = \{(x, \mathbf{0}) :\ x \in [0,1]^n\}\,.$$

Since $\mathcal{V}_C$ coincides with the set of equilibrium points, as stated in Proposition 3.1(iv), we can exploit center manifold theory to analyze the stability of the disease-free equilibrium by studying the dynamics restricted to the manifold $\mathcal{V}_C$. The reduced equation on this manifold is given by $\dot{x} = 0$, which implies that the equilibrium $(x^*,\mathbf{0})$ is stable for the reduced system. Consequently, stability holds also for the system (3.4). □

The next result provides sufficient conditions for the monotonicity of stability condition (3.6).

Proposition 3.2. *Consider the network BF-SIR epidemic model* (3.4) *with* $\mathcal{C}^1$ *irreducible interaction matrix* $A : [0,1]^{2n} \to \mathbb{R}_+^{n\times n}$ *and recovery rate* $\gamma > 0$. *If the following conditions*

hold:

$$A_{ij} + x_i \frac{\partial A_{ij}}{\partial x_i} \geq 0\,, \tag{3.8}$$

$$\frac{\partial A_{ij}}{\partial x_k} \geq 0 \tag{3.9}$$

for every i, j and k such that $k \neq i$, then the stability condition of the equilibrium $(x^*, \mathbf{0})$ given by (3.6) is monotone.

Proof. From conditions (3.8)-(3.9), it follows that

$$\frac{\partial}{\partial x}[x]A(x, \mathbf{0}) \geq 0\,. \tag{3.10}$$

Therefore, for any x, z in $[0, 1]^n$ such that $x \leq z$, we get

$$[x]A(x, \mathbf{0}) \leq [z]A(z, \mathbf{0}). \tag{3.11}$$

Recalling a standard property of nonnegative square matrices, such that if $B \leq C$ entry-wise, then $\lambda_{\max}(B) \leq \lambda_{\max}(C)$ (Meyer, 2000), we obtain that

$$\lambda_{\max}([x]A(x, \mathbf{0})) \leq \lambda_{\max}([z]A(z, \mathbf{0}))\,. \tag{3.12}$$

This implies that if the equilibrium $(z, \mathbf{0})$ is stable, then every equilibrium of the form $(x, \mathbf{0})$ with $x \leq z$ is also stable. □

Theorem 3.1 provides a stability condition for the disease-free equilibrium points of the network BF-SIR model, based on the dominant eigenvalue $\lambda_{\max}([x^*]A(x^*, \mathbf{0}))$. This quantity plays a crucial role in determining whether a given equilibrium is stable. In Chapter 4, we will further explore how this eigenvalue governs the evolution of a weighted aggregate of the infected fractions, under specific conditions.

Remark 3.1. *For the class of behavioral-feedback network SIR models introduced in Example 3.1, the interaction matrix takes the form $A(x, y) = g(x)f(y)^T$, where $g, f : [0, 1]^n \to \mathbb{R}^n$ are vector-fields. This formulation highlights that $A(x, y)$ has a rank-1 structure, that varies over time. As a consequence, the dominant eigenvalue of $A(x, y)$ is given by $f(y)^T g(x)$, corresponding to the trace of $A(x, y)$. While, the associated dominant left-eigenvector of $A(x, y)$ is $f(y(t))$ for all $t \geq 0$.*

3.3 Invariants of motion for constant interaction matrices

We now consider a simplified version of the model in which the interaction matrix A is constant, i.e., it does not depend on the current fractions of susceptible and infected individuals. This assumption corresponds to a scenario where contact rates between

subpopulations remain fixed over time and are not influenced by the evolution of the epidemic. Although simplified, this setting allows for a more tractable analysis and serves as a useful reference for interpreting the behavior of more complex models with adaptive or state-dependent interactions. In this framework, we show that, for the network SIR model (3.1) with constant interaction matrix, it is possible to identify a set of invariants of motion. These quantities play a key role in understanding the long-term behavior of the system and, as shown in Chapter 2 for scalar SIR epidemic models, they can be used to relate the final state to the initial state.

Proposition 3.3. *Consider the connected network SIR epidemic model (3.1) with constant interaction matrix $A \in \mathbb{R}^{n\times n}$. Then, for every $i = 1, \dots, n$, the quantity*

$$h_i = x_i \exp\left(-\frac{1}{\gamma}\sum_j A_{ij}(x_j + y_j)\right) \tag{3.13}$$

is an invariant of motion.

Proof. Equations (3.1) and (3.3) imply that

$$\begin{aligned}
\dot{h}_i &= \left(\dot{x}_i - x_i\frac{1}{\gamma}\sum_j A_{ij}(\dot{x}_j + \dot{y}_j)\right)\exp\left(-\frac{1}{\gamma}\sum_j A_{ij}(x_j + y_j)\right)\\
&= \left(-x_i\sum_j A_{ij}y_j - x_i\frac{1}{\gamma}\sum_j A_{ij}(-\gamma y_j)\right)\exp\left(-\frac{1}{\gamma}\sum_j A_{ij}(x_j + y_j)\right)\\
&= 0\,,
\end{aligned}$$

thus proving the result. □

From Proposition 3.1 and Proposition 3.3, the invariants of motion (3.13) at equilibrium satisfy

$$x_i^* \exp\left(-\frac{1}{\gamma}\sum_{j=1}^{n} A_{ij}\, x_j^*\right) = h_i(0), \quad i = 1, \dots, n,$$

where x_i^* denotes the limit fraction of susceptibles for subpopulation i, and $h_i(0)$ depends only on the initial state. Solving this system would, in principle, yield the limit equilibrium points of the model. However, in the general case this is a coupled set of n nonlinear equations in n unknowns, for which existence and uniqueness of a meaningful solution are not guaranteed. To gain a clearer understanding of the system's dynamics and to analytically characterize the limit equilibrium point as a function of the initial state, in the next section we consider a special case where the interaction matrix $A \in \mathbb{R}^{n\times n}$ is constant and has rank-1. This structure effectively allows for an explicit characterization of the final epidemic size as a function of the initial conditions.

3.4 Constant rank-1 interaction matrices

To further simplify the analysis and derive analytical insights into the long-term behavior of the epidemic, we now consider a special case where the interaction matrix $A \in \mathbb{R}^{n\times n}$ is constant and has rank-1. Specifically, we assume that

$$A = ab^T, \tag{3.14}$$

where $a = [a_1, \dots, a_n]^T$ and $b = [b_1, \dots, b_n]^T$ are two vectors with strictly positive entries. This formulation corresponds to replacing the functions $g_i(x_i)$ and $f_j(y_j)$ in the behavioral-feedback model introduced in Example 2.1 with positive constants a_i and b_j, respectively. As a result, the entries of A no longer vary over time or with the state of the epidemic. From an epidemiological perspective, the vector a captures both the *susceptibility* and the *activity level* of individuals in each subpopulation. In particular, a_i reflects how likely individuals in group i are to become infected and how frequently they interact. Conversely, the vector b represents the *infectivity*, *activity*, and *relative size* of each subpopulation: the entry b_j measures how infectious and socially active individuals in group j are, as well as how numerous they are within the overall population.

Under this assumption, the network BF-SIR epidemic model (3.1) simplifies to the following system of equations:

$$\begin{cases} \dot{x}_i = -a_i x_i \bar{y}, \\ \dot{y}_i = a_i x_i \bar{y} - \gamma y_i, \qquad \forall i = 1, \dots, n, \\ \dot{z}_i = \gamma y_i, \end{cases} \tag{3.15}$$

where

$$\bar{y} = \sum_{j=1}^{n} b_j y_j \tag{3.16}$$

is a weighted aggregate of infected individuals that drives the infection rate in all subpopulations. This quantity combines the prevalence of infection in each group with their corresponding size, infectivity and activity levels, and serves as a global measure of infectious pressure within the system.

This rank-1 formulation includes the class of models studied in (Ellison, 2020), where the matrix A is also assumed to be symmetric. More broadly, such structures have been used to design optimal epidemic control policies in heterogeneous populations, as discussed in (Acemoglu et al., 2021). The assumption of a rank-1 constant interaction matrix allows for significant analytical tractability and captures key heterogeneities across groups, even if it does not capture *homophily*, that is, the tendency of individuals to preferentially interact within their own group or with similar individuals. This limitation may reduce the realism of the model in certain contexts, such as age-structured or spatially localized populations, where within-group interactions are typically more frequent.

3.4.1 Limit equilibrium points

In this subsection, we leverage the invariants of motion associated with the rank-1 network SIR model (3.15) to derive the final epidemic size as a function of the initial state. To carry out our analysis, it is useful to define two different types of weighted aggregates of the susceptible individuals in the population. These are given by:

$$\bar{x} = \sum_{j=1}^{n} b_j x_j \,, \tag{3.17}$$

$$\tilde{x} = \sum_{j=1}^{n} a_j b_j x_j \,. \tag{3.18}$$

The first quantity, $\bar{x}$, represents a weighted average of the susceptible individuals, where the weights account for each subpopulation's size, activity and infectivity levels. The second quantity, $\tilde{x}$, adds a further weighting by the susceptibility. We begin by introducing a technical result that will serve as the foundation for deriving these invariants.

Lemma 3.1. *Fix two vectors $a > \mathbf{0}$ and $b > \mathbf{0}$ in $\mathbb{R}^n$. Then, for every (x, y) in $\mathcal{S}\setminus\{(x,\mathbf{0}) : \tilde{x} \geq \gamma\}$, the following hold:*

(i) the equation

$$\xi = \sum_{i=1}^{n} b_i x_i \exp(a_i(\xi - \overline{x} - \overline{y})/\gamma) \,, \tag{3.19}$$

admits exactly one solution in the interval $[0, \overline{x}]$ that is denoted by $\xi = \varphi(x, y)$;

(ii) $\varphi(x, y) = \overline{x}$ if and only if $y = \mathbf{0}$ or $x = \mathbf{0}$;

(iii) $\varphi(x, y) = 0$ if and only if $x = \mathbf{0}$;

(iv) $\varphi(x, y)$ is continuous on $\mathcal{S} \setminus \{(x,\mathbf{0}) : \tilde{x} \geq \gamma\}$.

Proof. For $x = \mathbf{0}$, equation (3.19) reduces to $\xi = 0$, which has a unique solution $\varphi(\mathbf{0}, y) = 0 = \overline{x}$. This proves claims (i)–(ii) in the special case $x = \mathbf{0}$ and the "if" part of claim (iii). For $x \gneq \mathbf{0}$, consider the function $g : \mathbb{R}_+ \to \mathbb{R}$ defined by

$$g(\xi) = \sum_{j=1}^{n} b_j c_j \exp(a_j \xi/\gamma) - \xi \,,$$

where $c_j = x_j \exp(-a_j(\overline{x}+\overline{y})/\gamma)$, for $1 \leq j \leq n$. Observe that equation (3.19) is equivalent to $g(\xi) = 0$. We have that:

(a) $g(\xi)$ is differentiable and strictly convex in $\xi \geq 0$;

(b) $g(0) = \sum_j b_j c_j > 0$ and $g(\xi) \overset{\xi\to+\infty}{\longrightarrow} +\infty$;

(c) $g(\overline{x}) = \sum_j b_j x_j \exp(-a_j \overline{y}/\gamma) - \overline{x} \leq \sum_j b_j x_j - \overline{x} = 0$, with equality if and only if $y = \mathbf{0}$;

(d) if $y = \mathbf{0}$ then $g'(\overline{x}) = \sum_j a_j b_j x_j/\gamma - 1 = \tilde{x}/\gamma - 1 < 0$.

Points (a)–(c) imply that $g(\xi)$ has at least one and at most two zeros. By (b), $\varphi(x, y) > 0$ for $x \gneq \mathbf{0}$, proving the "only if" part of (iii). For $y \gneq \mathbf{0}$, by points (b)–(c), $g(\xi)$ has one zero in $(0, \overline{x})$ and another one in $(\overline{x}, +\infty)$, proving claim (i) and the "only if" part of claim (ii). For $y = \mathbf{0}$, (b)–(d) imply that $g(\xi)$ has no zeros in $[0, \overline{x})$ and $g(\overline{x}) = 0$, proving claims (i) and the "if" part of claim (ii). Finally, since $g'(\varphi(x, y)) < 0$ for $y \gneq 0$, the Implicit Function Theorem implies that $\varphi(x, y)$ is differentiable for (x, y) in $\mathcal{S}$ such that $x \gneq \mathbf{0}$. Continuity of $\varphi(x, y)$ on the whole space $\mathcal{S} \setminus \{(x, \mathbf{0}) : \tilde{x} \geq \gamma\}$ then follows upon noting that $0 \leq \varphi(x, y) \leq \overline{x} \overset{x \to \mathbf{0}}{\longrightarrow} 0$, so that

$$\lim_{x \to 0} \varphi(x, y) = 0 = \varphi(\mathbf{0}, y)\,.$$

□

Our next result generalizes in a network setting Proposition 2.2(i)-(iii), as it characterizes the dependence of the limit equilibrium point on the initial state for the network SIR epidemic model with irreducible rank-1 interaction matrix. First, note that from Proposition 3.3, for every $i = 1, \ldots, n$, the quantity

$$h_i = x_i \exp(-a_i(\overline{x} + \overline{y})/\gamma) \tag{3.20}$$

is an invariant of motion for the rank-1 connected network SIR epidemic model (3.15).

Proposition 3.4. *Consider the rank-1 connected network SIR epidemic model (3.15). Then, for every initial state $(x(0), y(0))$ in $\mathcal{S}$,*

$$\lim_{t \to +\infty} x(t) = \Phi(x(0), y(0))\,, \tag{3.21}$$

where, for every (x, y) in $\mathcal{S}$ and $1 \leq i \leq n$,

$$\Phi_i(x, y) = x_i \exp\left(a_i\big(\varphi(x, y) - \overline{x} - \overline{y}\big)/\gamma\right)\,,$$

where $\varphi(x, y)$ is defined as in Lemma 3.1(i).

Proof. It follows from Proposition 3.1(iv) that (3.2) holds true for some $\mathbf{0} \leq x^* \leq x(0)$, so that point Proposition 3.3 and (3.20) imply that

$$h_i(x(0), y(0)) = h_i(x(t), y(t)) \overset{t \to +\infty}{\longrightarrow} h_i(x^*, 0)\,. \tag{3.22}$$

Let $\overline{x}^* = \sum_i b_i x_i^*$. It then follows from (3.20) and (3.22) that

$$\begin{aligned} x_i^* \exp(-a_i \overline{x}^*/\gamma) &= h_i(x^*, 0) \\ &= h_i(x(0), y(0)) \\ &= x_i(0) \exp(-a_i(\overline{x}(0) + \overline{y}(0))/\gamma)\,, \end{aligned}$$

so that

$$\lim_{t\to+\infty} x_i(t) = x_i^* = x_i(0)\exp(a_i(\bar{x}^* - \overline{x}(0) - \overline{y}(0))/\gamma)\,.$$

Multiplying both sides of the above by b_i and summing up over $i = 1,\dots,n$ shows that $\overline{x}^*$ is indeed a solution of (3.19). Now, observe that Proposition 3.1(i) ensures that $\bar{x}(t)$ is non-increasing in t, so that necessarily $\overline{x}^*$ belongs to the interval $[0,\overline{x}(0)]$. By Lemma 3.1(i), $\varphi(x(0),y(0))$ is the unique solution of (3.19) in $[0,\overline{x}(0)]$, so that necessarily $\overline{x}^* = \varphi(x(0),y(0))$, thus completing the proof. □

Remark 3.2. *In the absence of behavioral feedback, the stability of the disease-free equilibrium $(x^*,\mathbf{0})$ can also be established through the use of the invariants of motion h_i defined in (3.20), offering an alternative to the approach used in Theorem 3.1. Note that in this case the dominant eigenvalue, that determines the stability of disease-free equilibrium, becomes*

$$\lambda_{\max}([x^*]A) = \sum_{j=1}^{n} a_j b_j x_j^*\,,$$

and a proof of stability of the equilibrium point $(x^*,\mathbf{0})$ can be derived in term of the invariant of motion h_i and the quantity $\Phi(x,y)$.

Remark 3.3. *In Chapter 2, invariants of motion were introduced for scalar epidemic models to determine the limiting value of the fraction of susceptible individuals and the peak value of the fraction of infected individuals. This approach has also been applied to other compartmental models (Feng, 2007), and to models with time-varying transmission rates (Sontag, 2023). For the classical scalar SIR model and its variant with equal death and birth rates, this method has even led to exact analytical solutions (Harko et al., 2014). The novelty of Proposition 2.5 lies in its application to a network SIR epidemic model with n subpopulations, forming a $2n$-dimensional system, and in determining n invariants of motion for this system. Proposition 3.4 then utilizes the form of these invariants to characterize the functional dependence of the limiting equilibrium point on the initial state.*

3.5 Region of stability

Understanding the stability properties of an epidemic model is a key step toward designing effective and targeted control strategies. In particular, identifying the set of initial conditions and system parameters that lead to a stable disease-free state is crucial to guide interventions that can prevent the uncontrolled spread of the infection. From a public health perspective, an ideal outcome corresponds to reaching an equilibrium in which the largest possible fraction of the population remains uninfected. Control policies should therefore aim to steer the system toward such favorable configurations, minimizing the total number of infections while ensuring that the disease does not re-emerge in the long term.

We define the *stability region* of network BF-SIR epidemic model (3.1) as:

$$\mathcal{S}^{**} = \{(x, \mathbf{0}) \in \mathcal{S}^* : (3.6)\} \ .$$

This set identifies the stable equilibrium points, as per Theorem 3.1. In this region of the state space, the infection naturally dies out over time, even in the absence of additional interventions. Assuming that the subpopulations have equal size (the definition can be adapted if the subpopulations have different size), we define

$$\mathcal{X} = \underset{\substack{x\in[0,1]^n:\\ (x,y)\in\overline{S}^{**}}}{\operatorname{argmax}} \frac{1}{n}\sum_{j=1}^{n} x_j$$

as the set of points inside the closure of the stability region that maximize the fraction of susceptible agents. By construction, $\mathcal{X}$ belongs to the boundary of $\mathcal{S}^{**}$. Identifying both the stability region and the set $\mathcal{X}$ is crucial to design effective control strategies. Indeed, in optimal control problems with infinite time horizons, the cost of control policies that do not steer the system towards stable equilibrium points diverges in time (Cianfanelli et al., 2021a). Hence, a sustainable control policy should drive the system toward a stable equilibrium with as large as possible fraction of susceptible agents, that is, in the stability region and as close as possible $\mathcal{X}$, to minimize the overall spread of the infection while ensuring long-term stability. The set $\mathcal{X}$ was first informally introduced in (Ellison, 2020) to discuss the effects of heterogeneity when a planner aims to design a control that drives the system toward stable equilibrium points that maximize the fraction of susceptible agents in the network SIR model with no feedback and with rank-1 symmetric interaction matrices. In what follows, we investigate how the shape and size of this stability region change depending on the network structure and the behavioral feedback mechanisms encoded in the interaction matrix $A(x, y)$. To build intuition, we consider a simplified scenario with only two subpopulations and visualize the stability region in the (x_1, x_2) plane.

Models comparison

To explore the role of different behavioral assumptions and network configurations, we compare a selection of models, each characterized by a specific form of the interaction matrix $A(x, y)$. In all cases, we fix the recovery rate to $\gamma = 1$ and analyze how the structure of A affects the shape of the stability region. Figure 3.1 shows the resulting regions (in green) for various models, plotted in the (x_1, x_2) plane. Since the stability condition in Theorem 3.1 only depends on the susceptible fractions, the comparison focuses on how different functional dependencies of A on x affect stability.

(A) *Homogeneous:* $A = 1.5\mathbf{1}\mathbf{1}^T$. This simple case corresponds to an arbitrary partitioning of a fully homogeneous population into two subgroups, allowing separate analysis of epidemic dynamics under different initial conditions. This approach has been used to assess targeted lockdown strategies, especially when individuals are

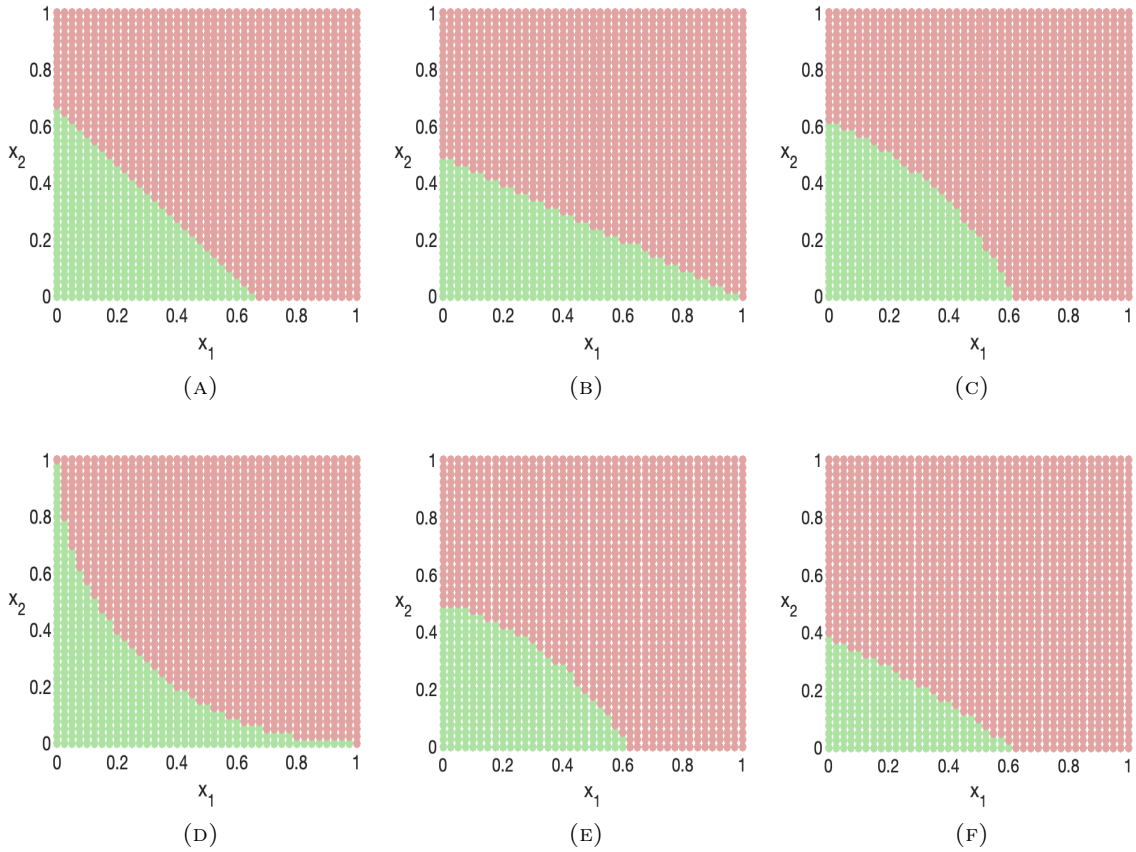

FIGURE 3.1: Stability region of two nodes network SIR epidemic models with different interaction matrices.

grouped by age with uniform intra- and inter-group contact rates (Acemoglu et al., 2021).

(B) *Constant Rank-1:*

$$A = \begin{bmatrix} 1 & 2 \\ 1 & 2 \end{bmatrix},$$

where we model an higher infectivity rate for the subpopulation 2. This class of models has been analyzed in Section 3.4.

(C) *Local positive feedback:* $A_{ij}(x, y) = 1 + x_i$ for $j = 1, 2$. In this scenario individuals increase their interaction levels in response to a higher fraction of susceptibles in their subpopulation. Since $x_i = 1 - y_i - z_i$, this type of interaction is inversely related to the fraction of individuals who have been or are currently infected. This mechanism reflects a behavioral tendency where lower perceived infection risk leads to increased social interactions.

(D) *Local negative feedback:* $A_{ij}(x, y) = 2 - x_i$ for $i, j = 1, 2$. In this case, the interaction rate decreases as the fraction of susceptibles increases, aligning with the progression

of the infected population. This behavior may represent the effect of increasing *pandemic fatigue*, where individuals progressively reduce their adherence to restrictive measures as the epidemic evolves.

(E) *Local mixed feedback:*

$$A = \begin{bmatrix} 1 + x_1 & 1 + x_1 \\ 2 - x_2 & 2 - x_2 \end{bmatrix}.$$

In this setting, the first subpopulation exhibits a positive feedback response to its own fraction of susceptibles, while the second subpopulation follows a negative feedback response. This hybrid model captures the coexistence of different behavioral patterns within a population, reflecting a diverse range of individual reactions to epidemic evolution.

(F) *Global mixed feedback:*

$$A = \begin{bmatrix} 1 + (x_1 + x_2) & 1 + (x_1 + x_2) \\ 3 - (x_1 + x_2) & 3 - (x_1 + x_2) \end{bmatrix}.$$

In this model, the first subpopulation exhibits a positive feedback mechanism relative to the total fraction of susceptibles. These are individuals who reduce their interactions as the infection spreads, similar to those who adhered to strict social distancing measures during the COVID-19 pandemic. In contrast, the second subpopulation shows negative feedback relative to the total fraction of susceptibles. This behavior patterns individuals who had to maintain high levels of interaction, such as health-care workers, delivery personnel, and other essential workers. This distinction in behavioral responses is a more general scenario, similar to the categorization of individuals into *risk-averters* and *risk-tolerators*, analyzed in works such as (Bizyaeva et al., 2024) and (Zhou et al., 2020).

Implications for control

As emphasized by (Ellison, 2020) and further explored in (Cianfanelli et al., 2021b) when dealing with optimal control problems over an infinite time horizon, it is crucial for the system to converge to a stable long-run state. If the epidemic dynamics do not stabilize, but instead continue to oscillate or persist indefinitely, the associated social or economic costs would accumulate without bound. In such cases, the overall outcome becomes suboptimal or even infeasible from a policy standpoint. In the context of epidemic control, this means that an effective strategy should drive the system toward a stable equilibrium where the disease eventually dies out. Ideally, this target state should also minimize the total number of infections over time, i.e., it should preserve as large a fraction of the susceptible population as possible.

Depending on the specific structure of the interaction matrix, the optimal target state can vary significantly. Below, we summarize the implications for each of the models presented above:

- In the homogeneous case (A), where both subpopulations behave identically, the boundary of the stability region $\mathcal{S}^{**}$ is symmetric. In this case, every point on the boundary of $\mathcal{S}^{**}$ belongs to $\mathcal{X}$, implying that the planner should steer the system as close as possible to this boundary. All such boundary points are equivalent in terms of their effect on the system's long-term behavior, which is not surprising, since the model is effectively equivalent to a scalar SIR model with no structural heterogeneity in the interaction patterns.

- In the rank-1 case (B), it may be preferable to target a state where the fraction of susceptibles is higher in node 1 than in the more infectious subpopulation (node 2), since it has a stronger influence on disease spread. Due to this heterogeneity, $\mathcal{X}$ is indeed the singleton that contains the maximally asymmetric equilibrium on the boundary of $\mathcal{S}^{**}$ where all agents that have been infected and are now recovered belong to the most infective subpopulation.

- For local positive feedback (C), a balanced distribution of susceptibles is favorable due to the convex shape of the stability region $\mathcal{S}^{**}$. This is because increasing the susceptible fraction in one subpopulation enhances contact rates, making imbalanced states less favorable from a stability perspective. The convexity of the stability region and the structure of A imply that $\mathcal{X}$ is the singleton that contains the maximally symmetric equilibrium on the boundary of the stability region, therefore the planner should drive the system in the stability region and as close as possible to such equilibrium.

- In the local negative feedback case (D), an uneven distribution of susceptibles can be advantageous. Specifically, allowing one subpopulation to absorb the majority of the infections can help maintain a higher susceptible fraction in the other group, effectively preserving part of the population through a form of natural segmentation. In this case, the convexity of $[0,1]^2 \backslash \mathcal{S}^{**}$ and the structure of A imply that $\mathcal{X}$ contains the two maximally asymmetric equilibrium points on the boundary of the stability region. Hence, the planner should promote lockdown in a single population to drive the system as close as possible to these asymmetric equilibrium points where all agents that have been infected belong to the same population.

- In mixed-feedback scenarios (E-F), local dependence indicates that a balanced distribution of susceptibles is still a viable strategy, while with global dependence it may be preferable to allow higher infection levels in the second subpopulation, which is less responsive or more exposed (e.g., essential workers).

Behavioral Feedback Enhances Stability

We now explore how behavioral feedback mechanisms can positively influence the stability and overall trajectory of epidemic dynamics. In particular, we compare the behavior

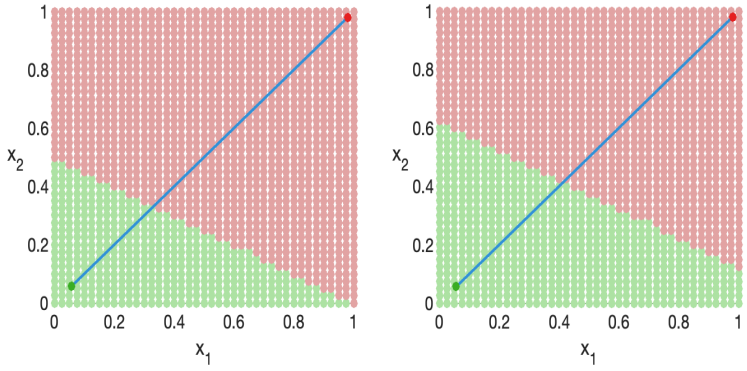

FIGURE 3.2: Stability region and trajectory of two nodes network SIR epidemic models with different interaction matrices.

of two network epidemic models: one with static interactions and one with feedback-modulated interactions.

In Figure 3.2, we compare the trajectories of the two models to highlight the effects of behavioral feedback on epidemic dynamics. Plot (A) shows the homogeneous scenario, where the interaction matrix is given by $A = 1.5I$, along with the system trajectory starting from the initial conditions $x_1(0) = x_2(0) = 0.98$ and $y_1(0) = y_2(0) = 0.02$. Conversely, plot (B) illustrates the system dynamics under the feedback interaction matrix with entries:

$$\tilde{A}_{ij} = \delta A_{ij}(1 + 1.3\, y_i)\,, \quad \forall i, j = 1, \ldots, n,$$

where δ is a scaling parameter and A is the same base matrix used in the homogeneous case. The initial conditions remain the same as in plot (A), allowing for a direct comparison between the two settings. Since both models share the same dependence on the fraction of susceptibles, they exhibit qualitatively similar stability regions. Moreover, when $\delta = 1$, the stability region would have exactly the same size as in the homogeneous case. In plot (B), the simulation is performed with $\delta = 0.8$, and we observe that this modification leads to an expected expansion of the stability region.

The main insight from this comparison is that incorporating behavioral feedback, where contact patterns adapt to the epidemic state, can significantly improve the stability properties of the system without altering the long-term fraction of susceptible individuals. In particular, the network BF-SIR epidemic model reaches the same equilibrium as the homogeneous model but with a smoother trajectory and fewer infections along the way. This helps to mitigate epidemic overshooting, a phenomenon in which the number of infections temporarily exceeds what is necessary to achieve herd immunity, causing excessive suppression of the susceptible population. Avoiding overshooting is crucial not only to reduce the burden on healthcare systems and the economic cost of infections but also to limit long-term disruptions in population behavior and immunity. Therefore, models that incorporate endogenous behavioral responses provide valuable tools for designing more effective and sustainable epidemic control strategies.

In this chapter, we developed a network-based SIR model with behavioral-feedback mechanisms, in which the interaction matrix evolves in response to the epidemic state. This framework captures essential features such as heterogeneous risk perception and adaptive contact reduction across subpopulations. In Section 3.2, we characterized the stability region of the disease-free equilibrium. In Section 3.3, for the case of constant interaction matrices, we derived invariants of motion that provide structural insights into the dynamics and in the special rank-1 setting (Section 3.4), these invariants enabled a characterization of the long-term behavior and of the equilibrium points. In Section 3.5, we presented numerical simulations that illustrate the impact of different feedback mechanisms on epidemic outcomes. Overall, these results highlight the importance of accounting for both network structure and behavioral adaptation when designing effective intervention strategies.

4 Dynamics of Behavioral-Feedback Network SIR Epidemic Model

In this chapter, we focus on the transient dynamics of the behavioral-feedback network SIR (BF-SIR) epidemic model introduced in Chapter 3. Our goal is to investigate how the epidemic evolves over time across a network of interacting subpopulations, paying particular attention to the shape and complexity of infection trajectories before reaching equilibrium.

To make the analysis more tractable, we begin by studying a simplified version of the model in which the entries of the interaction matrix $A = (A_{ij})$ are assumed to be constant. This means that the contact patterns between individuals from different subpopulations do not change over time and are not influenced by the current state of the epidemic. Although this is a simplifying assumption, it reflects scenarios where interaction rates are driven by characteristics, such as susceptibility, infectivity and activity, that remains fixed during the epidemic. Within this framework, we introduce new theoretical results that deepen the understanding of the dynamic behavior of the network SIR epidemic model with n nodes in Section 4.1. We first highlight a particularly interesting case: a two-node network SIR model where the infection curve in one of the nodes exhibits bimodal behavior, with two distinct infection peaks. This phenomenon illustrates how even simple network structures can generate rich transient dynamics. Motivated by this example, we then focus on a particularly important and analytically convenient case: the rank-1 network SIR model, already introduced in Section 3.4. In this context, we make two main contributions. First, we introduce a time-varying, weighted aggregate index of infected individuals that we prove to be unimodal throughout the evolution of the epidemic. This quantity generalizes the behavior observed in scalar SIR models. Second, we investigate the transient dynamics at the level of individual nodes. Specifically, we provide a detailed classification of the infection curves for each subpopulation and prove that the infection level at each node can exhibit at most two changes in monotonicity. This result sets a general bound on the complexity of local epidemic trajectories. We then present numerical simulations that explore what happens when the interaction matrix has higher rank. In these more complex cases, the transient infection curves at individual nodes may exhibit multiple peaks, indicating more intricate and less predictable dynamics. In Section 4.2, we take a step further by generalizing some of these results to a broader class of network

BF-SIR epidemic models. In particular, we examine how the structure of the feedback mechanism affects the transient behavior and explore whether similar properties hold when the interaction matrix depends dynamically on the state of the epidemic.

4.1 Network SIR epidemic model

We adopt the same modeling framework introduced in the previous chapter, where a population is divided into n interacting subpopulations, each associated with a node of a network and composed of indistinguishable individuals. Here, we focus on the case where the interaction matrix $A \in \mathbb{R}_+^{n\times n}$ is constant, i.e., it does not vary over time nor depend on the state variables. As before, each subpopulation $i \in 1, \dots, n$ is described by the state variables $x_i(t)$, $y_i(t)$, and $z_i(t)$, representing the fractions of susceptible, infected, and recovered individuals, respectively, with the constraint $x_i(t) + y_i(t) + z_i(t) = 1$ for all times. The network SIR epidemic model with interaction matrix A in $\mathbb{R}_+^{n\times n}$ and recovery rate $\gamma > 0$ is then the autonomous system of ordinary differential equations:

$$\begin{cases} \dot{x}_i = -x_i \sum_j A_{ij} y_j \\ \dot{y}_i = x_i \sum_j A_{ij} y_j - \gamma y_i \\ \dot{z}_i = \gamma y_i \end{cases} \qquad \forall i = 1, \dots, n\,. \tag{4.1}$$

This model has been previously studied in (Mei et al., 2017) and (Nowzari et al., 2016). In these works, it has been proven that all solutions converge to an equilibrium point of the form $(x^*, \mathbf{0}, \mathbf{1} - x^*) \in \mathbb{R}_+^{3n}$ and that the unstable equilibrium points are those such that

$$\lambda_{\max}(\operatorname{diag}(x^*)A) > \gamma$$

where $\lambda_{\max}$ is the dominant eigenvalue of the nonnegative matrix $\operatorname{diag}(x^*)A$. We have extended these results in Theorem 3.1 to the more general case in which the interaction matrix A depends dynamically on the state variables. In particular, we have provided conditions that guarantee not only the convergence to an equilibrium but also the stability properties of the equilibrium points in the presence of state-dependent interactions.

Moreover, under the assumption of strong connectivity of the graph $\mathcal{G}$, (Mei et al., 2017, Theorem 7) shows that the quantity

$$R(t) = \lambda_{\max}(\operatorname{diag}(x(t))A)/\gamma$$

is decreasing along solutions of (4.1) and it serves a role similar to the one played by the reproduction number in the scalar SIR model. According to their result and indicating by $v_{\max}(t)$ the left eigenvector corresponding to the dominant eigenvalue at time t, if $R(0) \leq 1$, then the weighted average of the infected individuals, $v_{\max}(0)^T y(t)$, decays monotonically to zero. On the other hand, if $R(0) > 1$, then the weighted average $v_{max}(0)^T y(t)$ will initially increase, indicating an epidemic outbreak. There exists a time

instant $\tau > 0$ such that $R(\tau) \leq 1$,after which the weighted average $v_{max}(\tau)^T y(t)$ will be monotonically decreasing to 0 for t in $[\tau, +\infty)$.

This result creates a parallelism with classical SIR theory (see Proposition 2.1(iv)-(v)), identifying an aggregate quantity of infected individuals that exhibits a unimodal behavior. However, since the quantity $v_{max}(\tau)^T y(t)$ explicitly depends on the fraction of susceptibles $x(\tau)$, the quantity $v_{max}(0)^T y(t)$ may not be unimodal in general. Moreover, several simulations highlight how the infection dynamics at individual nodes can display complex patterns, including multimodal behaviors with multiple peaks. In the following, we will investigate these phenomena in detail, aiming to identify sufficient conditions under which such behaviors can emerge.

Homogeneous two-nodes network

We begin our analysis of the network SIR model by considering a minimal setting with two interacting subpopulations. This simplified scenario provides a useful starting point to investigate how the epidemic dynamics at the level of individual nodes can differ from the behavior observed in the scalar SIR model. As shown in Proposition 2.1(iv)-(v), the scalar SIR model typically exhibits a unimodal infection curve. However, in the two-node network case, we demonstrate that this property may no longer hold: under certain conditions, the infection curve of one subpopulation can display multiple peaks, revealing a richer and more complex dynamic.

To explore this phenomenon, we study the network SIR model (4.1) with $n = 2$ subpopulations, assuming a fully connected interaction structure given by the matrix $A = \mathbf{1}\mathbf{1}^T$ and a unit recovery rate $\gamma = 1$. This framework represents a completely homogeneous population, where all individuals have equal chances of interacting with one another, irrespective of their subpopulation. It was also used in the stability comparison analysis in Section 3.5 of the previous chapter. The two-node setup can thus be interpreted as a simple partitioning of an otherwise well-mixed population, allowing us to isolate and examine the effects of asymmetric initial conditions on the epidemic evolution in each subpopulation. Indeed, let us consider an initial state as

$$y_1(0) = 1 - x_1(0) = \varepsilon\,, \quad y_2(0) = 1 - x_2(0) = 0\,, \tag{4.2}$$

for some $\varepsilon > 0$ such that

$$\frac{1-\varepsilon}{2-\varepsilon}(1 - \log(2-\varepsilon)) > \varepsilon\,. \tag{4.3}$$

Note that the range of such values of ε is nonempty since the function

$$g(\varepsilon) = \frac{1-\varepsilon}{2-\varepsilon}(1 - \log(2-\varepsilon)) - \varepsilon$$

is continuous in the interval $[0, 1]$ and $g(0) = \frac{1}{2}(1 - \log 2) > 0$. Observe that, with these initial states, from (4.1) we have

$$\dot{y}_1(0) = x_1(0)(y_1(0) + y_2(0)) - y_1(0) = -\varepsilon^2 < 0\,, \tag{4.4}$$

which implies that $y_1(t)$ is strictly decreasing for sufficiently small $t > 0$. We now show that $y_1(t)$ cannot remain decreasing for all values of $t \geq 0$, but will necessarily become strictly increasing in a certain time range, before eventually starting to decrease again and vanish as t grows large.

Towards this goal, first observe that the aggregate variables

$$\overline{x} = x_1 + x_2\,, \qquad \overline{y} = y_1 + y_2\,,$$

satisfy an autonomous scalar SIR epidemic model

$$\dot{\overline{x}} = -\overline{x}\,\overline{y}\,, \qquad \dot{\overline{y}} = (\overline{x} - 1)\overline{y}\,. \tag{4.5}$$

Then, since $\dot{\overline{y}}(0) = (\overline{x}(0) - 1)\overline{y}(0) > 0$, Proposition 2.1(v) implies that there exists a peak time $\hat{t} > 0$ at which $\dot{\overline{y}}(\hat{t}\,) = 0$, i.e., $\overline{x}(\hat{t}\,) = 1$. This fact, Proposition 2.2(ii) and (4.2) imply that

$$\overline{y}(\hat{t}\,) = \overline{x}(0) + \overline{y}(0) - \overline{x}(\hat{t}\,) + \log \frac{\overline{x}(\hat{t}\,)}{\overline{x}(0)} = 1 - \log(2 - \varepsilon)\,. \tag{4.6}$$

Since $\dot{x}_2 = -x_2\overline{y}$ and $x_2(0) = 1$, we have that

$$x_2(\hat{t}\,) = \exp\left(- \int_0^{\hat{t}} \overline{y}(t)\mathrm{d}t \right) = \frac{\overline{x}(\hat{t}\,)}{\overline{x}(0)} = \frac{1}{2 - \varepsilon}\,, \tag{4.7}$$

where the second equality follows from integrating the first equation in (4.5) and the last one follows from (4.2). It then follows from (4.6) and (4.7) that

$$\dot{y}_2(\hat{t}\,) = x_2(\hat{t}\,)\overline{y}(\hat{t}\,) - y_2(\hat{t}\,) = \frac{1 - \log(2 - \varepsilon)}{2 - \varepsilon} - y_2(\hat{t}\,)\,. \tag{4.8}$$

Now, assume by contradiction that $\dot{y}_1(t) \leq 0$ for all $t \geq 0$. In particular, this would imply that $y_1(\hat{t}\,) \leq y_1(0) = \varepsilon$, so that

$$y_2(\hat{t}\,) = \overline{y}(\hat{t}\,) - y_1(\hat{t}\,) \geq 1 - \log(2 - \varepsilon) - \varepsilon\,,$$

follows by (4.6). Recalling that $\dot{\overline{y}}(\hat{t}\,) = 0$, substituting the above in the right-hand side of (4.8), and using (4.3), we would then get

$$\begin{aligned} \dot{y}_1(\hat{t}\,) &= \dot{\overline{y}}(\hat{t}\,) - \dot{y}_2(\hat{t}\,) \\ &\geq \frac{1 - \varepsilon}{2 - \varepsilon}\,(1 - \log(2 - \varepsilon)) - \varepsilon > 0\,, \end{aligned}$$

thus contradicting the assumption that $\dot{y}_1(t) \leq 0$ for $t \geq 0$. It then follows that there must exist some values of time $t \geq 0$ such that $\dot{y}_1(t) > 0$. Combining with (4.4) and the fact $\lim_{t \to +\infty} y_1(t) = 0$, as established in Proposition 3.1(iii), this implies that the infection curve $t \mapsto y_1(t)$ is multimodal. That is, it does not simply rise and fall once, as in the standard scalar SIR model, but instead exhibits multiple phases of increase and decrease. More specifically, the analysis presented later in Section 4.1.1 shows that this

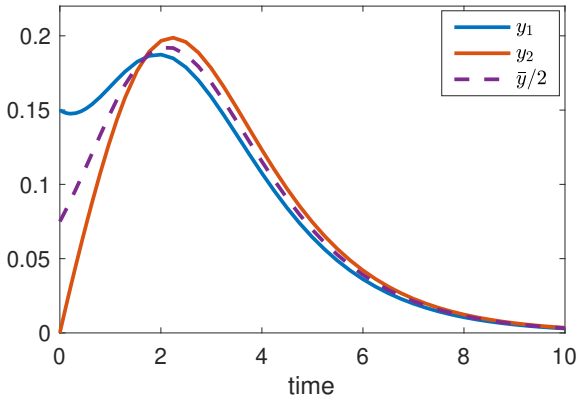

FIGURE 4.1: Numerical simulation of the network SIR epidemic model with $n = 2$ nodes with interaction matrix $A = \mathbf{1}\mathbf{1}^T$, recovery rate $\gamma = 1$, and initial state $y_1(0) = 1 - x_1(0) = 0.15$ and $y_2(0) = 1 - x_2(0) = 0$ satisfying (4.2)-(4.3).

behavior follows a particular structure, illustrated in Figure 4.1. Initially, $y_1(t)$ decreases over an interval $[0, \check{t}_1]$, reaching a local minimum at some time $\check{t}_1 > 0$. It then increases again until reaching a second peak at a later time $\hat{t}_1 > \check{t}_1$, after which it finally decreases for all $t \geq \hat{t}_1$. This pattern reveals how even in a simple two-node setting, the epidemic dynamics can exhibit unexpectedly rich and nontrivial behavior.

As previously noted, the network SIR epidemic model analyzed in this part can be seen as an extension of the classical scalar SIR model, where the population is split into two equally sized subpopulations that differ only in their initial conditions. In particular, we assume that all initially infected individuals are concentrated in the first subpopulation, while the second subpopulation starts entirely susceptible. The model parameters are selected in such a way that, if the two subpopulations were isolated, the first would display a typical decline in infections over time, eventually reaching a disease-free state through exponential decay. However, because the two subpopulations interact, the presence of the susceptible individuals in the second subpopulation allows the infection to spread further. Eventually, the infection may return to the first subpopulation, triggering a second wave of infection. This results in a non-monotonic infection curve for the first subpopulation, where the initial peak occurs at time 0, followed by a decrease and then a resurgence leading to a second, delayed peak. This phenomenon highlights how inter-subpopulation interactions can significantly influence the local epidemic trajectories, even after an apparent decline.

4.1.1 Rank-1 network SIR epidemic model

We now focus on the special case introduced in Section 3.4 of the previous chapter, where the interaction matrix A is irreducible and has rank-1, as defined in equation (3.14). This structure simplifies the analysis while still capturing key heterogeneities across subpopulations. In particular, it allows us to derive explicit analytical results that provide deeper insight into the system's dynamics (3.15) and its transient behavior.

Unimodality of the weighted aggregate infection curve

In this part, we analyze the evolution of the weighted aggregate of infected individuals, denoted by $\bar{y}$ and defined in (3.16). We will show that this aggregate quantity always exhibits a unimodal behavior over time. In other words, even though infection levels at the individual node level may display complex or multimodal behaviors, the aggregate weighted infection curve has a single peak.

The following result describes the dynamics of the weighted aggregates $\bar{x}$, defined in (3.17), and $\bar{y}$ of susceptible and, respectively, infected individuals. In particular, it shows that the logarithmic time derivative of $\bar{y}$ equals the difference between the weighted aggregate of susceptible individuals $\tilde{x}$, defined in (3.18), and the recovery rate γ. This relationship provides a key insight into the monotonicity properties of $\bar{y}$ and lays the foundation for proving its unimodality.

Lemma 4.1. *Consider the rank-1 connected network SIR epidemic model (3.15). Then,*

$$\begin{cases} \dot{\bar{x}} = -\bar{y}\tilde{x}\,, \\ \dot{\bar{y}} = \bar{y}\,(\tilde{x} - \gamma)\ . \end{cases} \tag{4.9}$$

Proof. By taking the time derivative of both sides of (3.17) and substituting it in (3.15), we get

$$\dot{\bar{x}} = \sum_{j=1}^{n} b_j \dot{x}_j = -\bar{y} \sum_{j=1}^{n} b_j a_j x_j = -\bar{y}\tilde{x}\,,$$

thus proving the first equation in (4.9). Analogously, by taking the time derivative of both sides of (3.16) and substituting the second equation in (3.15), we get

$$\dot{\bar{y}} = \sum_{j=1}^{n} b_j \dot{y}_j = \bar{y} \sum_{j=1}^{n} b_j a_j x_j - \gamma\bar{y} = \bar{y}\,(\tilde{x} - \gamma)\ ,$$

thus proving the second equation in (4.9). □

The following is the main result of this part. It shows that the weighted aggregate infection curve $t \mapsto \bar{y}(t)$ is always unimodal. Moreover, it reveals a dichotomy in the shape of this curve that depends on the initial value of the weighted aggregate of infected individuals $\tilde{x}(0)$.

Theorem 4.1. *Consider the rank-1 connected network SIR epidemic model (3.15). Let the initial state $(x(0), y(0))$ in $\mathcal{S}$ be such that*

$$\mathbf{0} \lneq x(0) \leq \mathbf{1} - y(0) \lneq \mathbf{1}\,. \tag{4.10}$$

Then, $\tilde{x}(t)$ is strictly decreasing for $t \geq 0$ and

$$\lim_{t \to +\infty} \tilde{x}(t) < \gamma\,. \tag{4.11}$$

Moreover:

(i) if

$$\tilde{x}(0) \leq \gamma\,, \tag{4.12}$$

then $\overline{y}(t)$ is strictly decreasing for $t \geq 0$;

(ii) if

$$\tilde{x}(0) > \gamma\,, \tag{4.13}$$

then there exists $\hat{t} > 0$ such that $\overline{y}(t)$ is strictly increasing on $[0, \hat{t}]$ and strictly decreasing on $[\hat{t}, +\infty)$.

Proof. By the way $\tilde{x}$ is defined in (3.18) and using the equations in (3.15), we can express its time derivative as

$$\dot{\tilde{x}} = \sum_{j=1}^{n} a_j b_j \dot{x}_j = -\overline{y} \sum_{j=1}^{n} a_j^2 b_j x_j\,. \tag{4.14}$$

Now, the rightmost inequality in (4.10) and Proposition 3.1(ii) imply that $y(t) > \mathbf{0}$ for every $t > 0$, whereas the leftmost inequality in (4.10) and Proposition 3.1(i) imply that there exists some i in $\{1, \dots, n\}$ such that $x_i(t) > 0$ for every $t \geq 0$. From (4.14), and since $a > \mathbf{0}$ and $b > \mathbf{0}$, we get that

$$\begin{aligned} \dot{\tilde{x}}(t) &= -\overline{y}(t) \sum_{j=1}^{n} a_j^2 b_j x_j(t) \\ &\leq -a_i^2 b_i x_i(t) \overline{y}(t) \\ &< 0\,, \end{aligned} \tag{4.15}$$

for every $t > 0$. Inequality (4.15) implies that $t \mapsto \tilde{x}(t)$ is strictly decreasing for $t \geq 0$. Now, let

$$\tilde{x}(\infty) = \lim_{t \to +\infty} \tilde{x}(t)\,.$$

If $\tilde{x}(0) \leq \gamma$, then $\tilde{x}(\infty) < \tilde{x}(0) \leq \gamma$, so that (4.11) is satisfied. On the other hand, if $\tilde{x}(0) > \gamma$, assume by contradiction that $\tilde{x}(\infty) \geq \gamma$. Then $\tilde{x}(t) > \gamma$ for every $t \geq 0$, so that, by (4.9),

$$\dot{\overline{y}}(t) = \overline{y}(t)\,(\tilde{x}(t) - \gamma) \geq 0\,, \qquad \forall t \geq 0\,.$$

The above would imply that $\overline{y}(t)$ is nondecreasing, so that

$$\lim_{t \to +\infty} \overline{y}(t) \geq \overline{y}(0) > 0\,,$$

thus contradicting Proposition 3.1(iii). Hence, we have $\tilde{x}(\infty) < \gamma$ also when $\tilde{x}(0) > \gamma$, thus completing the proof of the first part of the statement.

(i) If $\tilde{x}(0) \leq \gamma$, by point (i) we have that $\tilde{x}(t) < \gamma$ for $t > 0$. Hence, (4.9) implies that

$$\dot{\overline{y}}(t) = \overline{y}(t)\,(\tilde{x}(t) - \gamma) < 0 \qquad \forall t > 0\,,$$

thus showing that $\overline{y}(t)$ is strictly decreasing for $t \geq 0$.

(ii) If $\tilde{x}(0) > \gamma$, by point (i), $\tilde{x}(t)$ is strictly decreasing and

$$\lim_{t \to +\infty} \tilde{x}(t) < \gamma\,.$$

Then, there necessarily exits a time $\hat{t} > 0$ such that $\tilde{x}(t) > \gamma$ for $0 \leq t < \hat{t}$, $\tilde{x}(\hat{t}) = \gamma$, and $\tilde{x}(t) < \gamma$ for $t > \hat{t}$. It then follows from (4.9) that $\overline{y}(t)$ is strictly increasing for t in $[0, \hat{t}]$ and strictly decreasing for t in $[\hat{t}, +\infty)$, thus proving (ii). □

Remark 4.1. *The quantity $\tilde{x}(t)$ acts as a time-varying analogue of the reproduction number for the aggregate infection dynamics. In particular, the threshold condition $\tilde{x}(0) = \gamma$ separates two qualitatively different behaviors of the curve $t \mapsto \bar{y}(t)$. When $\tilde{x}(0) > \gamma$, the infection initially grows and reaches a single peak before declining. Conversely, when $\tilde{x}(0) \leq \gamma$, the infection starts decreasing immediately. This highlights the central role of $\tilde{x}(t)$ in governing the transient evolution of the epidemic at the population level.*

Remark 4.2. *As mentioned earlier, (Mei et al., 2017) shows that for irreducible interaction matrices, if $\lambda_{\max}([x(\tau)]A) < \gamma$ for some $\tau \geq 0$, the weighted aggregate $v_{\max}(\tau)^T y(t)$ decreases monotonically to 0. Conversely, if $\lambda_{\max}([x(0)]A) > \gamma$, then $v_{\max}(0)^T y(t)$ initially grows exponentially. This result has been generalized in Theorem 3.1. For rank-1 interaction matrices of the form $A = ab^T$, the vector $v_{\max}(t)$ simplifies to b for all $t \geq 0$. This allows us to conclude that the weighted aggregate $v_{\max}(t)^T y(t)$, which we denote as $\overline{y}(t)$, is unimodal. We will try to generalize this result for a broader class of behavioral-feedback interaction matrices.*

Dynamic behavior of the infection in the single subpopulations

Inspired by the analysis on the homogeneous two-node network at the beginning of this section, this part focuses on the analysis of infection curves for each individual subpopulation within the context of the rank-1 connected network SIR epidemic model.

We first define the quantities

$$w_i = \tilde{x} - \gamma - a_i \overline{y}\,, \qquad i = 1, \ldots, n\,, \tag{4.16}$$

which represent how the rate of new infections in each subpopulation evolves over time. These quantities provide a measure of the relative change in the infection rate, accounting for both the dynamics of the epidemic and the parameters that influence the spread. Indeed, from the second equation in (3.15) observe that the rate of new infections in node

i is described by the quantity $f_i = a_i x_i \bar{y}$. Moreover, considering the time derivative of f_i, we have

$$\frac{\dot{f}_i}{f_i} = \frac{\dot{\bar{y}}}{\bar{y}} + \frac{\dot{x}_i}{x_i} = \tilde{x} - \gamma - a_i \bar{y} = w_i.$$

Hence, w_i is the logarithmic derivative of the rate of new infections in node i. Let also

$$\hat{t} = \inf\{t \geq 0 : \tilde{x}(t) \leq \gamma\} \tag{4.17}$$

denote the peak time of the weighted aggregate of infected individuals $\bar{y}$, and observe that Theorem 4.1 implies that $\hat{t} < +\infty$. Also, for every $i = 1, \dots, n$, let

$$\bar{t}_i = \inf\{t \geq 0 : w_i(t) \leq 0\} = \inf\{t \geq 0 : \tilde{x}(t) \leq \gamma + a_i \bar{y}(t)\}$$

be the first time instant at which the rate of new infections in node i starts decreasing, and notice that

$$\bar{t}_i \leq \hat{t}\,, \tag{4.18}$$

and $\bar{t}_i \leq \bar{t}_j$ if and only if $a_j \leq a_i$. Hence, it is possible to order these time instants from the entries of vector a.

The following are two useful technical results.

Lemma 4.2. *Consider the rank-1 network SIR epidemic model (3.15) and every initial state $(x(0), y(0))$ in $\mathcal{S}$ such that $y(0) \gneq \mathbf{0}$. Then, for every $i = 1, \dots, n$,*

(i) $\dot{w}_i(t) < -a_i \bar{y} w_i(t)$ *for every* $t \geq 0$*;*

(ii) $w_i(t)$ *is strictly decreasing for* $0 \leq t \leq \bar{t}_i$*;*

(iii) $w_i(t) < 0$ *for every* $t > \bar{t}_i$*;*

(iv) for every $t \geq 0$*,*

$$\ddot{y}_i(t) = a_i x_i(t) \bar{y}(t) w_i(t) - \gamma \dot{y}_i(t)\,; \tag{4.19}$$

(v) if $\dot{y}_i(t) = 0$ *for some* $t \geq \bar{t}_i$*, then* t *cannot be a local minimum point of* $y_i(t)$*.*

Proof. (i) From the first equation (3.15), we have that

$$\dot{\tilde{x}} = \sum_i a_i b_i \dot{x}_i = -\bar{y} \sum_i a_i^2 b_i x_i \leq 0\,. \tag{4.20}$$

By Proposition 3.1(ii), the assumption $y(0) \gneq \mathbf{0}$ implies that

$$y(t) > 0\,, \qquad \forall t > 0\,, \tag{4.21}$$

so that in particular

$$\bar{y}(t) = \sum_j b_j y_j(t) > 0\,, \qquad \forall t \geq 0\,. \tag{4.22}$$

It then follows from (4.16),(4.9), (4.20), and (4.22) that

$$\begin{aligned}\dot{w}_i &= \dot{\tilde{x}} - a_i \dot{\overline{y}} \\ &= \dot{\tilde{x}} - a_i \overline{y}(\tilde{x} - \gamma) \\ &= \dot{\tilde{x}} - a_i \overline{y} w_i - a_i^2 \overline{y}^2 \\ &< -a_i \overline{y} w_i \,,\end{aligned}$$

thus proving the claim.

(ii) For $0 \le t \le \bar{t}_i$, we have $w_i(t) \ge 0$ so that, by point (i) and (4.22), we have that $\dot{w}_i(t) < -a_i \overline{y}(t) w_i(t) \le 0$. This implies that $w_i(t)$ is strictly decreasing for $0 \le t \le \bar{t}_i$.

(iii) It follows from (i) that, for every $t_i^* \ge 0$ such that $w_i(t_i^*) = 0$, we have

$$\dot{w}_i(t_i^*) < -a_i \overline{y}(t_i^*) w_i(t_i^*) = 0 \,,$$

so that $w_i(t) < 0$ for $t > t_i^*$. If $w_i(0) \le 0$ so that $\bar{t}_i = 0$, this implies that $w_i(t) < 0$ for all $t > 0 = \bar{t}_i$. On the other hand, $w_i(0) > 0$ so that $\bar{t}_i > 0$, it follows that $w_i(t) < 0$ for all $t > \bar{t}_i$.

(iv) Taking the derivative of both sides of the second line in (3.15) and substituting the first line of (3.15) and (4.9) yield

$$\begin{aligned}\ddot{y}_i &= a_i \left(\dot{x}_i \, \overline{y} + x_i \, \dot{\overline{y}}\right) - \gamma \dot{y}_i \\ &= a_i \, x_i \, \overline{y} \, (\tilde{x} - \gamma - a_i \overline{y}) - \gamma \dot{y}_i \\ &= a_i \, x_i \, \overline{y} \, w_i - \gamma \dot{y}_i \,,\end{aligned}$$

thus proving (4.19).

(v) Assume by contradiction that $t \ge \bar{t}_i$ is a local minimum point of $y_i(t)$ with $\dot{y}_i(t) = 0$. By (4.19), we then have

$$\ddot{y}_i(t) = a_i x_i(t) \overline{y}(t) w_i(t) - \gamma \dot{y}_i(t) = \gamma y_i(t) w_i(t) \,, \tag{4.23}$$

where the last identity holds true since, by the second equation in (3.15), $\dot{y}_i(t) = 0$ is equivalent to

$$a_i x_i(t) \overline{y}(t) = \gamma y_i(t) \,. \tag{4.24}$$

Equations (4.23) and (4.21) imply that

$$\operatorname{sgn}(\ddot{y}_i(t)) = \operatorname{sgn}(w_i(t)) \,. \tag{4.25}$$

Now, recall that by point (iii) we have $w_i(t) \le 0$ for every $t \ge \bar{t}_i$. If $w_i(t) < 0$, then

equation (4.25) implies that $\ddot{y}_i(t) < 0$, so that t cannot be a local minimum point for $y_i(t)$. On the other hand, if $w_i(t) = 0$, by point (i) and (4.22) we get that

$$\dot{w}_i(t) < -a_i \overline{y}(t) w_i(t) = 0\,, \tag{4.26}$$

while (4.25) implies that $\ddot{y}_i(t) = 0$. Hence, taking the derivative of both sides of (4.19), by (4.24) and $w_i(t) = 0$, we get

$$\begin{aligned} \dddot{y}_i(t) &= a_i x_i(t) \overline{y}(t) \dot{w}_i(t) + a_i (\dot{(x_i(t)} \overline{y}(t))) w_i(t) - \gamma \ddot{y}_i(t) \\ &= \gamma y_i(t) \dot{w}_i(t) \\ &< 0\,, \end{aligned}$$

where the last inequality follows from (4.21) and (4.26). Together with $\dot{y}_i(t) = \ddot{y}_i(t) = 0$, the above implies that t is an inflection point for $y_i(t)$, hence it particular it is not a local minimum point. We have thus proven that $y_i(t)$ cannot have any stationary minimum points in the interval $[\bar{t}_i, +\infty)$. □

Proposition 4.1. *Consider the connected rank-1 network SIR epidemic model (3.15) with initial state $(x(0), y(0))$ in $\mathcal{S}$ such that $y(0) \gneq \mathbf{0}$. Then, for every $i = 1, \dots, n$,*

(i) $y_i(t)$ admits at most one local minimum time $\check{t}_i \geq 0$.

Moreover, if such local minimum time $\check{t}_i$ exists,

(ii) it satisfies

$$0 \leq \check{t}_i \leq \bar{t}_i\,, \tag{4.27}$$

with $\check{t}_i = \bar{t}_i = 0$ if and only if $w_i(0) \leq 0$ and $\dot{y}_i(0) > 0$;

(iii) it cannot occur after any stationary local maximum point of $y_i(t)$.

Proof. If $w_i(0) \leq 0$, then $\bar{t}_i = 0$ and Lemma 4.2(v) implies that no stationary point $t \geq 0$ of $y_i(t)$ can be a local minimum point. It follows that the only local minimum point of $y_i(t)$ can possibly be $\check{t}_i = 0$, which is the case if and only if $\dot{y}_i(0) > 0$. Hence the claims are proved in the special case $w_i(0) \leq 0$.

On the other hand, if $w_i(0) > 0$, then $\bar{t}_i > 0$ and the interior extremum theorem and Lemma 4.2(v) imply that there cannot be any minimum points of $y_i(t)$ in the interval $[\bar{t}_i, +\infty)$. This proves point (ii). We are then left with studying local minimum points of $y_i(t)$ in the interval $[0, \bar{t}_i)$. Let $s \geq 0$ be a stationary local maximum point of $y_i(t)$, and let u in $(s, \bar{t}_i)$ be a (necessarily stationary) local minimum point of $y_i(t)$. Then,

$$\dot{y}_i(s) = \dot{y}_i(u) = 0\,, \tag{4.28}$$

and

$$\ddot{y}_i(s) \leq 0\,, \qquad \ddot{y}_i(u) \geq 0\,. \tag{4.29}$$

Notice that we cannot have $y_i(s) = 0$ or otherwise $y_i(t) = 0$ in a neighborhood of s (as s is a local maximum point for $y_i(t)$) thus contradicting Proposition 3.1(ii). Hence, we get

$$\begin{aligned} 0 \geq \ddot{y}_i(s)/y_i(s) &= a_i x_i(s)\overline{y}(s)w_i(s)/y_i(s) - \gamma\dot{y}_i(s)/y_i(s) \\ &= \gamma w_i(s) \\ &> \gamma w_i(u) \\ &= a_i x_i(u)\overline{y}(u)w_i(u)/y_i(u) - \gamma\dot{y}_i(u)/y_i(u) \\ &= \ddot{y}_i(u)/y_i(u) \\ &\geq 0\,, \end{aligned} \tag{4.30}$$

where the first and the last inequalities above follow from (4.29), the first and the last identities follow from (4.19), the other two identities from (4.28) and the fact that, by the second equation in (3.15), $a_i x_i(t)\bar{y}(t) = \gamma y_i(t)$ when $\dot{y}_i(t) = 0$, and the strict inequality in the middle holds true because of Lemma 4.2(ii). As (4.30) is a contradiction, this shows that a local minimum point $u < \bar{t}_i$ of $y_i(t)$ cannot follow any stationary local maximum point $s \geq 0$ of $y_i(t)$, thus proving point (iii).

Finally, to prove point (i), assume by contradiction that there exist two distinct local minimum points $r < u$ of $y_i(t)$ in the interval $[0, \bar{t}_i)$. Then, there would necessarily exist a local maximum point of $y_i(t)$ in the interval (r, u). But, since $s > r \geq 0$, such local maximum point would also be stationary, thus violating point (iii). Therefore, there cannot exist two distinct local minimum points $r < u$ of $y_i(t)$ in the interval $[0, \bar{t}_i)$, thus completing the proof of point (i). □

Remark 4.3. *Equations (4.27) and (4.18) imply that the local minimum point of y_i can never occur after the peak of the weighted aggregate of infected individuals $\bar{y}$. Hence, if at some time $\tau \geq 0$ both $\dot{\bar{y}}(\tau) \leq 0$ (so that $\bar{y}$ has peaked at some time $\hat{t} \leq \tau$) and $\dot{y}_i(\tau) < 0$ (so that the epidemic in i is currently regressing), then $y_i(t)$ will remain decreasing for all $t \geq \tau$.*

As a consequence of Proposition 4.1, we get the following result classifying the possible dynamic behaviors of the fraction of infected individuals in the single subpopulations of the network SIR epidemic model with rank-1 interaction matrix. This classification is based on the study of the sign of two quantities:

$$\dot{y}_i(0) = a_i x_i(0)\overline{y}(0) - \gamma y_i(0),$$

$$w_i(0) = \tilde{x}(0) - \gamma - a_i\overline{y}(0).$$

Theorem 4.2. *Consider the connected rank-1 network SIR epidemic model (3.15) with initial state $(x(0), y(0))$ in $\mathcal{S}$ such that $y(0) \gneq \mathbf{0}$. Then, for every $i = 1, \ldots, n$,*

(i) if

$$\dot{y}_i(0) \leq 0\,, \tag{4.31}$$

and

$$w_i(0) \leq 0\,, \tag{4.32}$$

then $y_i(t)$ is strictly decreasing for $t \geq 0$;

(ii) if

$$\dot{y}_i(0) > 0\,, \tag{4.33}$$

or if

$$\dot{y}_i(0) = 0\,, \tag{4.34}$$

and

$$w_i(0) > 0\,, \tag{4.35}$$

then there exists a peak time $\hat{t}_i > 0$ such that $y_i(t)$ is strictly increasing on $[0, \hat{t}_i]$ and strictly decreasing on $[\hat{t}_i, +\infty)$;

(iii) if

$$\dot{y}_i(0) < 0\,, \tag{4.36}$$

and

$$w_i(0) > 0\,, \tag{4.37}$$

then either $y_i(t)$ is strictly decreasing for $t \geq 0$ or there exist a local minimum time $\check{t}_i$ and a peak time $\hat{t}_i$ such that $0 < \check{t}_i < \hat{t}_i$ and $y_i(t)$ is strictly decreasing on $[0, \check{t}_i]$, strictly increasing on $[\check{t}_i, \hat{t}_i]$, and strictly decreasing on $[\hat{t}_i, +\infty)$;

Proof. (i) If (4.32) holds true, then $\bar{t}_i = 0$. On the other hand, (4.31) and Proposition 4.1(ii) rule out the possibility that there exists any minimum point for $y_i(t)$. Therefore, $y_i(t)$ is strictly decreasing for $t \geq 0$.

(ii) If (4.33) holds true, then Proposition 4.1(i) implies that $\check{t}_i = 0$ is the only minimum point of $y_i(t)$. On the other hand, if (4.34) and (4.35) both hold true, then it follows from (4.19) that

$$\begin{aligned} \ddot{y}_i(0) &= a_i x_i(0) \overline{y}(0) w_i(0) - \gamma \dot{y}_i(0) \\ &= \gamma \overline{y}^2(0) w_i(0) \\ &> 0\,, \end{aligned}$$

(where the second identity follows from the fact that, by the second equation in (3.15), $a_i x_i(t) \bar{y}(t) = \gamma y_i(t)$ when $\dot{y}_i(t) = 0$) thus implying that also in this case $\check{t}_i = 0$ is a local minimum point for $y_i(t)$.

Since $y(0) \gneq \mathbf{0}$ and, by Proposition 4.1(i), $y_i(t)$ cannot have another local minimum points besides $\check{t}_i = 0$, it follows that exists a peak time $\hat{t}_i > 0$ such that $y_i(t)$ is strictly increasing for t in $[0, \hat{t}_i]$ and strictly decreasing for t in $[\hat{t}_i, +\infty)$.

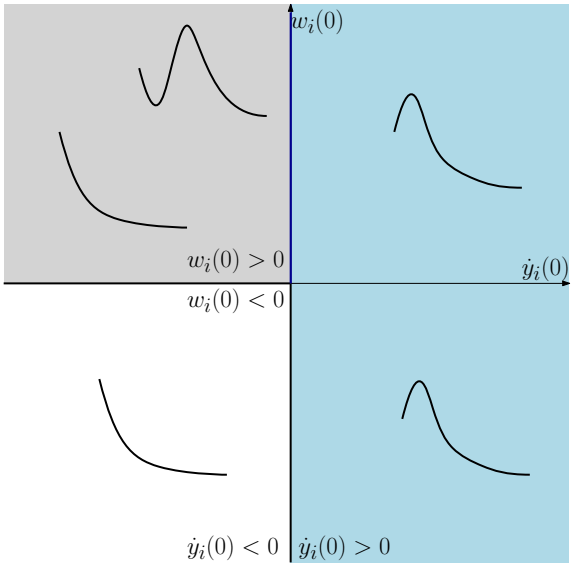

FIGURE 4.2: Conceptual illustration of Theorem 4.2.

(iii) From (4.36), 0 is a non-stationary local maximum point of $y_i(t)$. Since, by Proposition 4.1(i), $y_i(t)$ can have at most one local minimum point, and by Proposition 3.1(v),

$$\lim_{t\to+\infty} y_i(t) = 0 < y_i(0)\,, \tag{4.38}$$

it follows that either $y_i(t)$ is strictly decreasing for $t \geq 0$ (in case there is no local minimum point) or, if a local minimum point $\check{t}_i > 0$ exists, then there exists also a peak time $\hat{t}_i > \check{t}_i$ so that $y_i(t)$ is strictly increasing on $[0, \hat{t}_i]$ and strictly decreasing on $[\hat{t}_i, +\infty)$. □

The previous result provides a classification of the behavior of infection curves of the single subpopulations and Figure 4.2 offers a conceptual illustration of this classification. In particular, observe that if $\dot{y}_i(0) = 0$, then the behavior of the single infection curves depends only on the sign of $w_i(0)$: in this case, Theorem 4.2 provides a tight condition.

In Theorem 4.2, each condition is considered from the perspective of the single subpopulation i. However, note that if (4.31) is true for all $i = 1, \ldots, n$, meaning that the infection curves are initially decreasing, then they will decrease forever. To see this, one can multiply both sides of (4.31) by b_i and sum over i. This gives $\tilde{x}(0) < \gamma$, which implies that $w_i(0) < 0$ for all i.

Sufficient conditions for multimodal infection curves

We now consider a particular class of rank-1 interaction matrices in the form

$$A = \beta \mathbf{1} b^T\,, \tag{4.39}$$

with $\beta > 0$ and $\mathbf{1}^T b = 1$. This is a special case of the one studied in the previous part, where the vector a has all equal entries and the components of b sum up to 1.

This model represents a scenario in which all individuals have the same susceptibility to the disease but exhibit different levels of infectivity. A practical example could be individuals wearing medical masks, who might become infected with the same probability as others but transmit the disease at different rates depending on their level of protection. A simple special case of this class of matrices is $A = \mathbf{1}\mathbf{1}^T$, which was explored in Subsection 4.1. The network SIR epidemic model with this interaction matrix is particularly relevant for control applications, as demonstrated in (Acemoglu et al., 2021). Even if the dynamics at the individual nodes are homogeneous, meaning the infection spreads at the same rate across all individuals, it can still be valuable to classify individuals into multiple groups. This classification can be crucial when considering the effects of differentiated control policies. For example, control measures may be adjusted based on factors such as age, since the costs of implementing these measures and the epidemic costs (in terms of disease spread) may vary significantly across different age groups or other demographic factors.

We observe that, for rank-1 interaction matrices in the form (4.39), the dynamics become

$$\begin{cases} \dot{x}_i = -\beta x_i \bar{y}, \\ \dot{y}_i = \beta x_i \bar{y} - \gamma y_i \,, \end{cases} \tag{4.40}$$

for every $i = 1, \dots, n$, and

$$\begin{cases} \dot{\overline{x}} = -\beta \overline{x}\, \overline{y}, \\ \dot{\overline{y}} = \overline{y}\,(\beta \overline{x} - \gamma) \,, \end{cases} \tag{4.41}$$

since $\overline{x}$ and $\tilde{x}$ differ in a constant term only. The next result provides sufficient conditions for multimodality of the infection curve at the single node level and encompasses the analysis at the beginning of this section. We first need to define auxiliary functions

$$g_i(\varepsilon) = \frac{1-\varepsilon}{1-b_i\varepsilon}\left(1 - \frac{\gamma}{\beta} + \frac{\gamma}{\beta}\log\frac{\gamma}{\beta(1-b_i\varepsilon)}\right) - \varepsilon \,. \tag{4.42}$$

Notice that

$$g_i(0) = 1 - \frac{\gamma}{\beta} + \frac{\gamma}{\beta}\log\frac{\gamma}{\beta}, \qquad g_i(1) = -1 \,.$$

As a consequence, when $\gamma/\beta < 1$, g_i admits zeros in $[0,1]$ and we put

$$\overline{\varepsilon}_i = \min\left\{\varepsilon \in [0,1] : \, g_i(\varepsilon) = 0\right\}. \tag{4.43}$$

Proposition 4.2. *Consider the rank-1 network SIR epidemic model (3.15) with $a = \beta\mathbf{1}$ and $\mathbf{1}^T b = 1$. Consider a subpopulation i in $\{1, \dots, n\}$ and an initial state $(x(0), y(0))$ in $\mathcal{S}$ that satisfy the following conditions:*

$$x(0) + y(0) = \mathbf{1} \,, \tag{4.44}$$

$$\beta x_i(0)\bar{y}(0) - \gamma y_i(0) < 0 \,, \tag{4.45}$$

$$\beta \overline{x}(0) > \gamma \,, \tag{4.46}$$

$$0 < y_i(0) < \overline{\varepsilon}_i \,. \tag{4.47}$$

Then, there exist a local minimum time $\check{t}_i$ and a peak time $\hat{t}_i$ such that $0 < \check{t}_i < \hat{t}_i$ and $y_i(t)$ is strictly decreasing on $[0, \check{t}_i]$, strictly increasing on $[\check{t}_i, \hat{t}_i]$, and strictly decreasing on $[\hat{t}_i, +\infty)$.

Proof. From (4.45) and (4.40) it follows that $\dot{y}_i(0) < 0$, which implies that $y_i(t)$ is strictly decreasing for sufficiently small $t > 0$. On the other hand, (4.41) and (4.46) imply that $\bar{y}(t)$ is strictly increasing for sufficiently small $t > 0$. Since $\overline{x}$ and $\overline{y}$ satisfy the scalar autonomous SIR epidemic model (4.41), this implies that $\overline{y}(t)$ has a peak at some time $\hat{t} > 0$ and

$$\overline{x}(\hat{t}) = \frac{\gamma}{\beta}\,. \tag{4.48}$$

From Proposition 2.2(ii) we obtain that the peak value of the weighted aggregate of infected individuals is

$$\begin{aligned} \overline{y}(\hat{t}\,) &= \overline{x}(0) + \overline{y}(0) - \overline{x}(\hat{t}) + \frac{\gamma}{\beta}\log\frac{\overline{x}(\hat{t})}{\overline{x}(0)} \\ &= 1 - \frac{\gamma}{\beta} + \frac{\gamma}{\beta}\log\frac{\gamma}{\beta\overline{x}(0)}\,, \end{aligned} \tag{4.49}$$

where the second equality follows from (4.44) and (4.48). Moreover, (4.40) and (4.41) imply that $x_i(t)/x_i(0) = \overline{x}(t)/\overline{x}(0)$, for $i = 1, \ldots, n$, and $t \geq 0$. Therefore, using (4.48) we obtain

$$x_i(\hat{t}) = \frac{\gamma}{\beta}\frac{x_i(0)}{\overline{x}(0)}\,, \tag{4.50}$$

We now prove that $y_i(t)$ cannot remain decreasing for all $t > 0$. Assume by contradiction that $\dot{y}_i(t) \leq 0$ for all t in $[0, \hat{t}]$. In particular, this implies that $y_i(\hat{t}) \leq y_i(0)$. This together with (4.50) and (4.49) imply that

$$\begin{aligned} 0 &\geq \dot{y}_i(\hat{t}\,) \\ &= \beta x_i(\hat{t}\,)\bar{y}(\hat{t}\,) - \gamma y_i(\hat{t}\,) \\ &= \gamma\frac{x_i(0)}{\overline{x}(0)}\left(1 - \frac{\gamma}{\beta} + \frac{\gamma}{\beta}\log\frac{\gamma}{\beta\overline{x}(0)}\right) - \gamma y_i(\hat{t}\,) \\ &\geq \gamma\left[\frac{x_i(0)}{\overline{x}(0)}\left(1 - \frac{\gamma}{\beta} + \frac{\gamma}{\beta}\log\frac{\gamma}{\beta\overline{x}(0)}\right) - y_i(0)\right]\,. \end{aligned} \tag{4.51}$$

Notice that, because of the assumptions on b, we have that $\overline{x}(0) = 1 - \overline{y}(0) \leq 1 - b_i y_i(0)$. Since the last expression in (4.51) is decreasing in $\overline{x}(0)$ and $x_i(0) = 1 - y_i(0)$, we get that

$$\gamma g_i(y_i(0)) \leq 0\,. \tag{4.52}$$

By (4.46), we necessarily have that $\gamma/\beta < 1$. This implies that $g_i(0) > 0$ and, with (4.52), that $y_i(0) \geq \bar{\varepsilon}_i$, thus violating (4.43). This contradiction implies that $y_i(t)$ cannot remain decreasing for all $t > 0$. The claim then follows from Theorem 4.2. □

Remark 4.4. *Observe that the set of model parameters and initial states that satisfy the assumptions of Proposition 4.2 is nonempty. To prove this, consider a network with n nodes, where the interaction matrix is given by (4.39) with parameters $\beta > \gamma$ and*

$$b_1 < \min\left\{\frac{\gamma}{\beta}, 1 - \frac{\gamma}{\beta}\right\}. \tag{4.53}$$

Next, fix an initial state $(x(0), y(0))$ in the set $\mathcal{S}$ such that $0 < y_1(0) < \bar{\varepsilon}_1$ and $y_j(0) = 0$ for $2 \leq j \leq n$. Notice that $\overline{y}(0) = b_1 y_1(0)$. A straightforward check confirms that both (4.45) and (4.46) are automatically satisfied, imposing no additional restrictions on $y_1(0)$. Thus, all the assumptions of Proposition 4.2 hold.

Observe that, under the assumptions of Proposition 4.2, we can derive an upper bound for the stationary infection peaks that can occur in a node i. Let $\hat{t}_i$ be the peak time for node i, such that $\dot{y}_i(\hat{t}_i) = 0$. From (4.40), this implies that

$$y_i(\hat{t}_i) = \frac{\beta}{\gamma} x_i(\hat{t}_i)\overline{y}(\hat{t}_i)\,. \tag{4.54}$$

Since the weighted aggregate of infected individuals is bounded above by its peak infection value, i.e. $\overline{y}(t) \leq \overline{y}(\hat{t}\,)$ for $t \geq 0$, and the fraction of susceptible individuals is monotonically decreasing over time, we can derive the following upper bound for $y_i(\hat{t}_i)$:

$$\begin{aligned} y_i(\hat{t}_i) &\leq \frac{\beta x_i(0)}{\gamma}\overline{y}(\hat{t}) \\ &= \frac{\beta x_i(0)}{\gamma}\left(\overline{x}(0) + \overline{y}(0) - \overline{x}(\hat{t}) + \frac{\gamma}{\beta}\log\frac{\overline{x}(\hat{t}\,)}{\overline{x}(0)}\right) \\ &= x_i(0)\left(\frac{\beta}{\gamma} - 1 + \log\frac{\gamma}{\beta\overline{x}(0)}\right), \end{aligned}$$

where the first equivalence follows from (4.49), and the final equality comes from (4.48) and (4.44).

As discussed in Chapter 2, accurately estimating the peak level of infections is crucial for designing effective containment policies. Knowing in advance how high the infection curve may rise allows policymakers to assess whether healthcare capacities, such as hospital beds or ICU units, will be sufficient, and to plan timely interventions to mitigate the epidemic's impact.

4.1.2 Numerical Simulations

In this subsection, we present the results of several numerical simulations of the network SIR epidemic model. These simulations aim to illustrate the dynamics of disease spread across different types of networks with varying interaction matrices and initial conditions.

We start by reporting the infections curves of a network SIR epidemic model (4.1) with $n = 5$ nodes and rank-1 interaction matrix. In Figure 4.3, the interaction matrix is

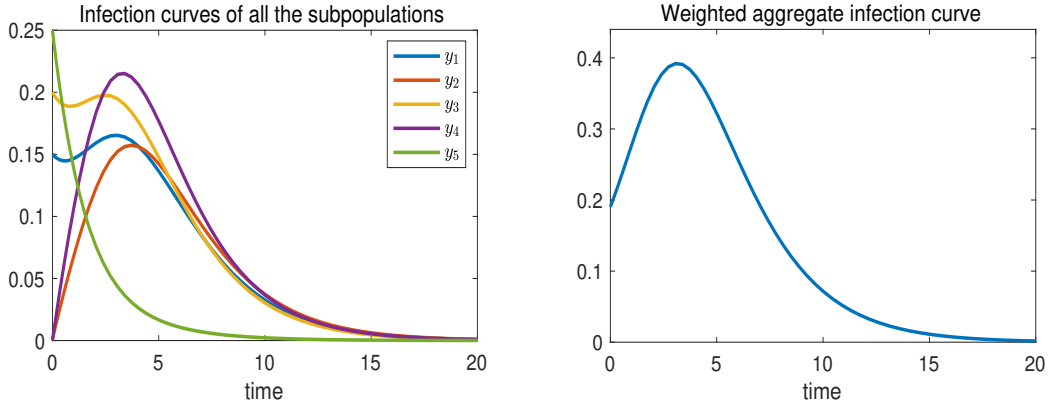

FIGURE 4.3: Numerical simulations of the network SIR epidemic model with $n = 5$ nodes and rank-1 interaction matrix.

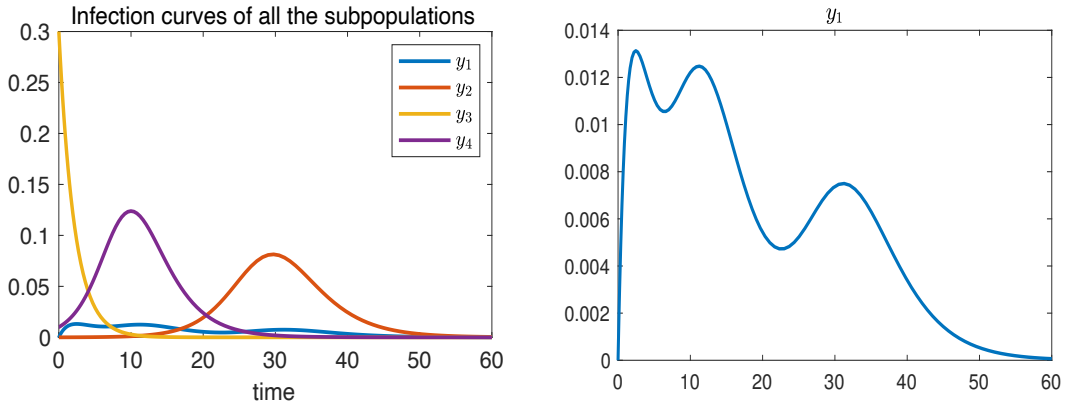

FIGURE 4.4: Simulations of the network SIR model in a non-homogeneous network with 4 nodes and full-rank interaction matrix.

$A = ab^T$ with $a = (0.1, 0.25, 0.6, 1, 0.2)$ and $b = (0.45, 0.4, 0.6, 0.65, 0.01)$, and the recovery rate is $\gamma = 0.6$. The initial state has entries $x_1(0) = 0.85$, $x_2(0) = 0.999$, $x_3(0) = 0.8$, $x_4(0) = 1$, $x_5(0) = 0.75$, and $y(0) = \mathbf{1} - x(0)$. The left-hand side plot in Figure 4.3 shows that the infection curves of nodes 1 and 3 are both multimodal with two changes of monotonicity: for both $i = 1$ and $i = 3$, the fraction of infected individuals $y_i(t)$ is strictly decreasing for times t in $[0, \check{t}_i]$, it is strictly increasing in $[\check{t}_i, \hat{t}_i]$, and it is strictly decreasing for t in $[\hat{t}_i, +\infty)$. The bottom plot displays the weighted aggregate infection curve $t \mapsto \overline{y}(t)$, which is unimodal with a peak in $\hat{t}$. This behavior aligns with the result proven in Theorem 4.1. Furthermore, as a consequence of Proposition 4.1(ii) (see also Remark 4.3), we observe that $\check{t}_i \leq \hat{t}$ for $i = 1, 3$. This implies that the local minimum in the infection curve for each of these nodes occurs before or at the peak time of the weighted aggregate infection.

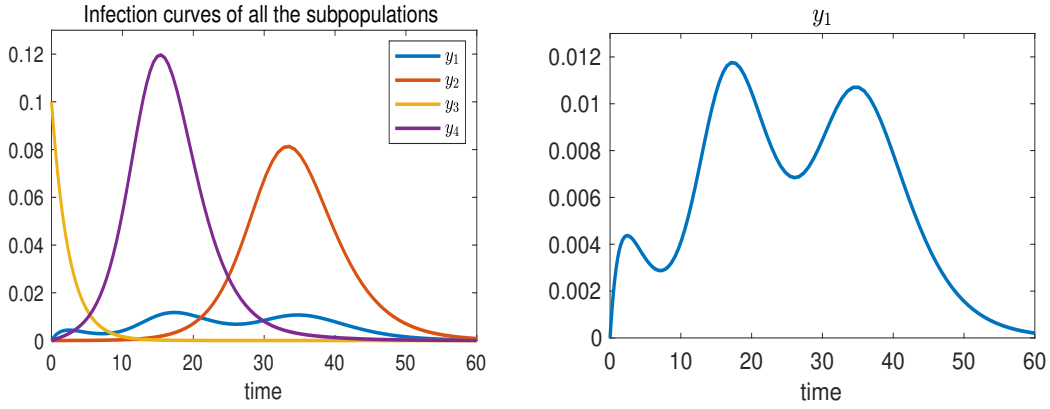

FIGURE 4.5: Numerical simulation of the network SIR epidemic model with $n = 4$ nodes and full-rank interaction matrix.

Next, in Figure 4.4, we report numerical simulations of a network SIR epidemic model with $n = 4$ nodes, recovery rate $\gamma = 0.5$, and interaction matrix

$$A = \begin{pmatrix} 0.05 & 0.05 & 0.05 & 0.05 \\ 0.0001 & 0.8 & 0.0001 & 0.0001 \\ 0.0001 & 0.0001 & 0.05 & 0.0001 \\ 0.0009 & 0.0009 & 0.0009 & 0.0009 \end{pmatrix}.$$

Initial conditions are $x_1(0) = x_2(0) = 1$, $y_1(0) = y_2(0) = 0$, $x_3(0) = 0.3 = 1 - y_3(0)$, $x_4(0) = 0.99 = 1 - y_4(0)$, i.e. subpopulation 3 has 30% of infected individuals while subpopulation 4 has 1% of infected individuals at time $t = 0$. In this simulation, the infection curve for node 1 exhibits three peaks, which is characteristic of non-rank-1 interaction matrices. We also observe significant delays between the peaks of infection in different nodes. This behavior highlights that, while rank-1 interaction matrices typically restrict infection curves to two peaks, more complex, full-rank matrices can give rise to multiple peaks, even in small networks. This distinction is crucial when modeling epidemic dynamics in networks with more intricate interaction structures.

Finally, Figure 4.5 presents another simulation for a network SIR epidemic model with $n = 4$ nodes, recovery rate $\gamma = 0.5$, and the interaction matrix

$$A = \begin{pmatrix} 0.05 & 0.07 & 0.05 & 0.05 \\ 0.0001 & 0.8 & 0.0001 & 0.0001 \\ 0.0001 & 0.0001 & 0.1 & 0.0001 \\ 0.01 & 0.01 & 0.01 & 0.9 \end{pmatrix}.$$

The initial state has entries $x_1(0) = x_2(0) = x_4(0) = 1$, $y_1(0) = y_2(0) = y_4(0) = 0$, and $x_3(0) = 0.9 = 1 - y_3(0)$, i.e., all subpopulations are initially completely susceptible except for subpopulation 3 that has 10% of infected individuals at time $t = 0$. In this scenario, the infection curve for node 1 again displays three peaks. Notably, the second and third peaks are higher than the first one, suggesting that multiple peaks in the infection curves could result from varying network dynamics, potentially due to the interaction matrix's

structure. These additional peaks warrant further investigation, especially when designing targeted interventions or control strategies. This further confirms that the limitation of infection curves to two peaks is a specific feature of rank-1 interaction matrices. This is an interesting feature of the network SIR epidemic model especially since actual epidemic data often displays multimodal infection curves with multiple peaks occurring at different times in different subpopulations. (See, e.g., (Our World in Data, 2024) for COVID-19 infection curves in the different countries.)

4.2 Unimodality in the network BF-SIR model

After analyzing the case of constant rank-1 interaction matrices, we now move to a more general and realistic setting. In this extended model, the interaction matrix still has rank-1, but its entries evolve as functions of the epidemic state. This extension captures the adaptive nature of contact patterns in response to changing levels of infection. We focus on the class of models introduced in Example 3.1 and we derive conditions under which an aggregate weighted fraction of infected individuals exhibits global unimodality. Specifically, under the assumptions of Example 3.1, the equations of the behavioral network SIR epidemic model (3.1) can be rewritten as follows:

$$\begin{cases} \dot{x}_i = -x_i g_i(x_i) \displaystyle\sum_{j=1}^{n} f_j(y_j) y_j \\ \dot{y}_i = x_i g_i(x_i) \displaystyle\sum_{j=1}^{n} f_j(y_j) y_j - \gamma y_i \end{cases} \qquad \forall i = 1, \dots, n. \tag{4.55}$$

Observe that the rate of new infections in node i due to the infected individuals in subpopulation j is described by the function

$$w_{ij}(x_i, y_j) = x_i g_i(x_i) f_j(y_j) y_j,$$

which represents the force of infection from node j to node i and incorporates both susceptibility and infectivity modulated by behavioral responses.

To analyze the overall evolution of the epidemic across the network, we now introduce the following weighted aggregate of infected individuals,

$$\bar{y}(t) = \sum_{j=1}^{n} f_j(y_j(t)) y_j(t)\,. \tag{4.56}$$

This quantity generalizes the aggregate infection variable (3.16) by incorporating behavioral responses via the weighting functions $f_j(y_j)$. It provides a global measure of the infection level across the network, where each subpopulation's contribution is modulated to reflect heterogeneities in behavioral responses or infectivity. The following result shows that the weighted aggregate infection curve $t \mapsto \bar{y}(t)$ is unimodal, under some assumptions

on the rate of new infections $w_{ij}(x_i, y_j)$ defined above. This can be seen as a generalization of Theorem 4.1 to this broader class of rank-1 network BF-SIR epidemic models.

To analyze its behavior, consider the time derivative of $\bar{y}$:

$$\dot{\bar{y}} = \sum_{j=1}^{n} \dot{y}_j \Big[f_j'(y_j) y_j + f_j(y_j) \Big]. \tag{4.57}$$

Theorem 4.3. *Consider the rank-1 network BF-SIR epidemic model (4.55). Let the initial state $(x(0), y(0))$ in $\mathcal{S}$ be such that $x(0) \gneq \mathbf{0}$, $y(0) \gneq \mathbf{0}$. If the following hold:*

$$\frac{\partial^2 w_{ij}}{\partial y_j^2}(x_i, y_j) \leq 0 \tag{4.58}$$

$$\frac{\partial w_{ij}}{\partial y_j}(x_i, y_j) > 0 \tag{4.59}$$

$$\frac{\partial w_{ij}}{\partial x_i}(x_i, y_j) > 0 \tag{4.60}$$

for all $i, j = 1, \ldots, n$. Then, $\overline{y}(t)$ has at most one peak, i.e.

(i) if $\dot{\bar{y}}(0) < 0$, then $\overline{y}(t)$ is strictly decreasing for $t \geq 0$;

(ii) if $\dot{\bar{y}}(0) > 0$, then there exists $\hat{t} > 0$ such that $\overline{y}(t)$ is strictly increasing on $[0, \hat{t}]$ and strictly decreasing on $[\hat{t}, +\infty)$.

Proof. (i) We prove the result by contradiction. If not, by continuity, there exists $\tau > 0$ such that $\dot{\bar{y}}(\tau) = 0$ and $\dot{\bar{y}}(\tau) < 0$ for all $t < \tau$. We compute the second time derivative of $\bar{y}$,

$$\ddot{\bar{y}} = \sum_{j=1}^{n} \Big[f_j''(y_j) y_j + 2 f_j'(y_j) \Big] \dot{y}_j^2 + \sum_{j=1}^{n} \Big[f_j'(y_j) y_j + f_j(y_j) \Big] \ddot{y}_j \tag{4.61}$$

where, from (4.55),

$$\ddot{y}_j = \dot{x}_j g_j(x_j) \bar{y} + x_j g_j'(x_j) \dot{x}_j \bar{y} + x_j g_j(x_j) \dot{\bar{y}} - \gamma \dot{y}_j \tag{4.62}$$

for all $j = 1, \ldots, n$. We study the sign of $\ddot{\bar{y}}(\tau)$ and from (4.58) the first sum in (4.61) is always non-positive, then we get

$$\ddot{\bar{y}}(\tau) \leq \sum_{j=1}^{n} [f_j'(y_j) y_j + f_j(y_j)] \ddot{y}_j \tag{4.63}$$

Substituting (4.62) in (4.63), from (4.55) and $\dot{\bar{y}}(\tau) = 0$ we get

$$\ddot{\bar{y}}(\tau) \leq \bar{y} \sum_{j=1}^{n} \Big[f_j'(y_j) y_j + f_j(y_j) \Big] \Big[g_j(x_j) + x_j g_j'(x_j) \Big] \dot{x}_j < 0$$

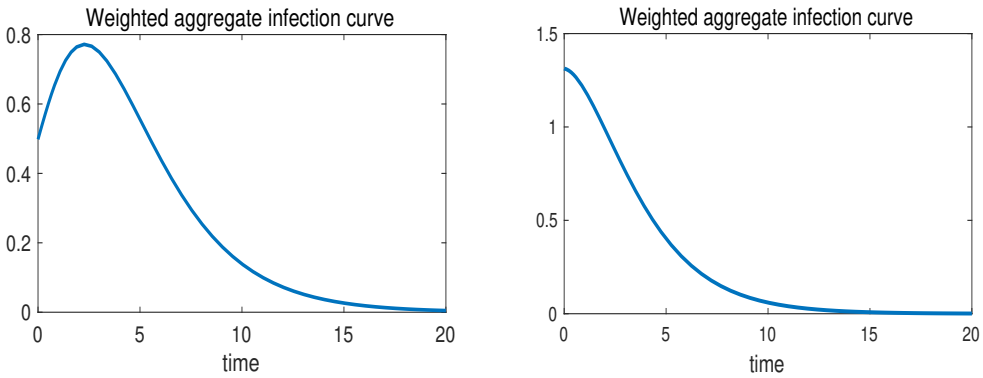

(A) (B)

FIGURE 4.6: Numerical simulations of the aggregate infection curve of the network BF-SIR epidemic model (4.1), simulated under different initial conditions, with $n = 5$ nodes and a rank-1 feedback interaction matrix of the form defined in (4.64), where $g_i(x_i) = 0.15(1 + x_i)$.

where the last inequality follows from assumptions (4.59), (4.60) and Proposition 3.1(i). By continuity, we can state that $\ddot{\bar{y}}(t) < 0$ in an interval $[\tau - \varepsilon, \tau]$ for some $\varepsilon > 0$. Since $\dot{\bar{y}}(t)$ is decreasing in $[\tau - \varepsilon, \tau]$ and stays strictly below 0 for all $t < \tau$ for the assumption made, it follows that also $\dot{\bar{y}}(\tau) < 0$ contrarily to what we had assumed. This yields the result.

(ii) Notice that there must exist $t > 0$ such that $\dot{\bar{y}}(t) < 0$. Indeed, if not, there exist some j for which $\dot{y}_j(t) > 0$ for all t and y_j could not converge to 0. Therefore, $\hat{t} = \min\{t \geq 0 : \dot{\bar{y}}(t) = 0\}$ must exist finite. Then $\bar{y}(t)$ is increasing up to $\hat{t}$. For $t > \hat{t}$, previous point (i) implies that $\bar{y}$ is strictly decreasing. □

Remark 4.5. *The assumptions (4.58) and (4.59) require that the rate of new infections w_{ij} is increasing and concave with respect to y_j, while condition (4.60) ensures that is increasing with respect to x_i. These assumptions have a clear epidemiological motivation: the increase of w_{ij} with respect to y_j reflects the idea that more infected individuals lead to a higher transmission risk. The concavity captures saturation effects: when many individuals are already infected, the impact of an additional one tends to diminish, for example due to limited contact opportunities. Similarly, the monotonicity with respect to x_i simply reflects that a larger susceptible population increases the potential for new infections.*

Remark 4.6. *An example of the interaction matrix between subpopulations that satisfy (4.58), (4.59), (4.60) is the following, that has rank-1 and its entries are:*

$$A_{ij} = \frac{g_i(x_i)}{1 + y_j} \quad \forall i, j = 1, \ldots, n, \tag{4.64}$$

where $g_i : [0, 1] \to [0, \infty)$ is an arbitrary non-decreasing function of x_i.

Figure 4.3 displays the aggregate infection curves $t \mapsto \overline{y}(t)$ for the network BF-SIR epidemic model (4.1), simulated under different initial conditions, with $n = 5$ nodes and a rank-1 feedback interaction matrix of the form defined in (4.64), where $g_i(x_i) = 0.15(1 + x_i)$. The recovery rate is set to $\gamma = 0.6$. In particular, Figure 4.3(A) shows a simulation where the initial condition is given by $x(0) = [0.85,\ 0.999,\ 0.8,\ 1,\ 0.75]$, and $y(0) = \mathbf{1} - x(0)$, for which $\dot{\overline{y}}(0) > 0$. In this case, the weighted aggregate infection curve $\overline{y}(t)$ is unimodal, reaching its peak at time $\hat{t}$, as established in Theorem 4.3(ii). In contrast, Figure 4.3(B) illustrates a simulation with a different initial condition: $x(0) = [0.55,\ 0.7,\ 0.6,\ 0.6,\ 0.75]$, and again $y(0) = \mathbf{1} - x(0)$, for which $\dot{\overline{y}}(0) < 0$. Here, the aggregate infection curve is monotonically decreasing over time, which is also consistent with the result stated in Theorem 4.3(i).

Having analyzed the case of rank-1 behavioral interaction matrices, we now move toward a general class of network BF-SIR epidemic models, still described by system (3.1), with the aim of characterizing their transient behavior.

Inspired by the approach in Mei et al., 2017, we explore the role of the dominant eigenvalue of the matrix $[x(t)]A(x(t), y(t))$ in governing the transient dynamics. This matrix captures the interaction between susceptible and infected individuals across the network, modulated by behavioral responses. The next result focuses on a class of models where the dominant eigenvalue of $[x(t)]A(x(t), y(t))$ can be interpreted as a time-varying effective reproduction number that drives the epidemic's evolution. Drawing an analogy with the classical scalar SIR model, we introduce the following time-dependent feedback reproduction number:

$$R(t) = \frac{\lambda_{\max}([x(t)]A(x(t), y(t)))}{\gamma}. \tag{4.65}$$

This reproduction number provides valuable insight into the behavior of an aggregate infection index over time, under certain assumptions. Before presenting the formal result, we define $v_{\max}(t)$ as the left eigenvector associated with the dominant eigenvalue of the matrix $[x(t)]A(x(t), y(t))$.

Proposition 4.3. *Consider the network BF-SIR epidemic model (3.4) with irreducible interaction matrix $A : [0, 1]^{2n} \to \mathbb{R}_+^{n\times n}$ and recovery rate $\gamma > 0$. Assume that*

$$[A(x, y)y]A(x, y) + \frac{\partial A(x, y)}{\partial x}[x][A(x, y)y] > 0\,, \tag{4.66}$$

$$\frac{\partial A(x, y)}{\partial y}[x][A(x, y)y] + A(x, y)[x]A(x, y) \leq 0\,, \tag{4.67}$$

$$A(x, y) + \frac{\partial A(x, y)}{\partial y}[y] \geq 0\,. \tag{4.68}$$

If $R(0) > 1$ and $y(0) > \mathbf{0}$, then for small time, the weighted average $t \mapsto v_{\max}(0)^T y(t)$ grows exponentially fast and then there exists $\tau > 0$ such that $R(\tau) \leq 1$. Then, for every $t \geq \tau$, the weighted infection curve $t \mapsto v_{\max}(\tau)^T y(t)$ is monotonically decreasing to zero.

Proof. By left multiplying $\dot{y}(0)$ for $v_{\max}(0)^T$, we get

$$\begin{aligned} v_{\max}(0)^T\dot{y}(0) &= v_{\max}(0)^T([x(0)]A(x(0),y(0))-\gamma)y(0) \\ &= \gamma(R(0)-1)v_{\max}(0)^Ty(0)\,, \end{aligned}$$

where the last equality follows from the fact that $v_{max}(\tau)$ is the left dominant eigenvector of $[x(\tau)]A(x(\tau),y(\tau))$ and from definition of $R(t)$. Since $R(0)>1$, it follows that there exists $t_1>0$ such that

$$\frac{d}{dt}\left(v_{\max}(0)^Ty(t)\right)>0\,,\quad \forall t\in[0,t_1]\,.$$

Suppose now by contradiction that $R(t)>1$ for every time t. This would imply,

$$R(t^*)=\lambda_{\max}([x^*]A(x^*,\mathbf{0}))/\gamma>1\,,$$

which means that the equilibrium $(x^*,\mathbf{0})$ would be unstable from Theorem 3.1(i) and this would contradict Proposition 3.1(iii). Then, there exists $\tau>0$ such that $R(\tau)\leq 1$.

Following similar steps as before, by multiplying $\dot{y}(\tau)$ for $v_{\max}(\tau)^T$, we get

$$\begin{aligned} v_{\max}(\tau)^T\dot{y}(\tau) &= v_{\max}(\tau)^T([x(\tau)]A(x(\tau),y(\tau))-\gamma)y(\tau) \\ &= \gamma(R(\tau)-1)v_{\max}(\tau)^Ty(\tau)\leq 0\,. \end{aligned}$$

Then there exists a time interval after τ for which $t\to v_{\max}(\tau)^Ty(t)$ is decreasing. If $t\to v_{\max}(\tau)^Ty(t)$ is not monotonically decreasing for all $t\geq\tau$, then there would exist a time instant t^* such that $v_{\max}(\tau)^T\dot{y}(t^*)=0$ and $v_{\max}(\tau)^T\dot{y}(t)<0$ for all $\tau\leq t<t^*$. We now compute the time derivative of $v_{\max}(\tau)^T\dot{y}(t)$ at $t=t^*$, that is

$$\begin{aligned} &\frac{d}{dt}\left(v_{\max}(\tau)^T\dot{y}(t)\right)\Big|_{t=t^*} \\ &= v_{\max}(\tau)^T\left([\dot{x}]A(x,y)y+[x]\frac{d}{dt}\left(A(x,y)\right)y+[x]A(x,y)\dot{y}-\gamma\dot{y}\right) \\ &= v_{\max}(\tau)^T\left([\dot{x}]A(x,y)y+[x]\frac{\partial A(x,y)}{\partial x}[\dot{x}]y+[x]\frac{\partial A(x,y)}{\partial y}[\dot{y}]y+[x]A(x,y)\dot{y}\right)-\gamma v_{\max}(\tau)^T\dot{y}(t^*) \\ &= v_{\max}(\tau)^T\left([\dot{x}]A(x,y)y+[x]\frac{\partial A(x,y)}{\partial x}[\dot{x}]y-[x]\frac{\partial A(x,y)}{\partial y}[\dot{x}]y-\gamma[x]\frac{\partial A(x,y)}{\partial y}[y]y\right)+ \\ &\quad+v_{\max}(\tau)^T\left([x]A(x,y)[x]A(x,y)y-\gamma[x]A(x,y)y\right) \\ &= -v_{\max}(\tau)^T[x]\left([A(x,y)y]A(x,y)+\frac{\partial A(x,y)}{\partial x}[x][A(x,y)y]\right)y+ \\ &+v_{\max}(\tau)^T[x]\left(\frac{\partial A(x,y)}{\partial y}[x][A(x,y)y]+A(x,y)[x]A(x,y)\right)y+ \\ &-\gamma v_{\max}(\tau)^T[x]\left(A(x,y)+\frac{\partial A(x,y)}{\partial y}[y]\right)y\,, \end{aligned}$$

where the equalities follow from (3.4). From the assumptions (4.66)-(4.67)-(4.68), we get

$$\frac{d}{dt}\left(v_{\max}(\tau)^T \dot{y}(t)\right)\Big|_{t=t^*} < 0\,,$$

By continuity, we can state that $\frac{d}{dt}\left(v_{\max}(\tau)^T \dot{y}(t)\right) < 0$ in an interval $[t^* - \varepsilon, t^*]$ for some $\varepsilon > 0$. Since $v_{\max}(\tau)^T \dot{y}(t)$ is decreasing in $[t^* - \varepsilon, t^*]$ and stays strictly below 0 for all $t < t^*$ for the assumption made, it follows that also $v_{\max}(\tau)^T \dot{y}(t) < 0$ contrarily to what we had assumed. Then $t \to v_{\max}(\tau)^T y(t)$ is monotonically decreasing for all $t \geq \tau$. □

Remark 4.7. *Note that the conditions* (4.58), (4.59), (4.60) *are not a special case of the set of conditions* (4.66), (4.67), (4.68) *stated in Proposition 4.3, nor does the converse hold, even if* (4.59),(4.60) *correspond to* (4.68),(4.66), *respectively.*

Remark 4.8. *Notice that, as already mentioned, the quantity $v_{\max}(0)^T y(t)$, which exhibits an initial growth phase, represents a weighted average of the infected fractions that depends on the initial conditions. On the other hand $v_{\max}(\tau)^T y(t)$, which explicitly depends on the state variables $x(\tau)$ and $y(\tau)$, eventually decreases over time. Consequently, this result does not provide a globally unimodal quantity that characterizes the entire epidemic trajectory. Nevertheless, in certain specific settings, discussed in this section above, it is possible to identify an aggregate infection quantity that is globally unimodal.*

Remark 4.9. *Note that assumption* (4.66) *generalizes the condition* (2.15) *for the unimodality of the infection curve in the scalar BF-SIR epidemic model* (2.5). *It expresses that the interaction induced by susceptible individuals increases with their proportion in the population: a higher proportion of susceptibles can be associated with a lower perceived risk, which can lead individuals to engage in more frequent or riskier social interactions, thereby increasing the potential for transmission. Condition* (4.67) *captures the behavioral adaptation of individuals, who tend to reduce their interaction levels in response to the spread of infection, introducing a form of negative feedback into the transmission dynamics. At the same time, condition* (4.68) *ensures that this feedback is not excessively strong: although individuals react to increasing infection levels by limiting their contacts, the effect is not so pronounced as to completely suppress epidemic propagation. Instead, these conditions jointly maintain a balance between behavioral responses and the persistence of the epidemic dynamics.*

This chapter focused on the transient dynamics of the network-based behavioral-feedback SIR model. In Section 4.1, we began by analyzing the case of constant interaction matrices. In particular, we showed in Subsection 4.1 that even very simple settings, such as a two-node network, can already give rise to multimodal infection curves, thereby illustrating the nontrivial role of heterogeneity in shaping epidemic trajectories. Building

on this, in Subsection 4.1.1 we restricted attention to rank-1 interaction matrices. Within this simplified yet insightful framework, we proved that a weighted aggregate infection index remains unimodal over time, and we established that the infection curve of each individual node can change monotonicity at most twice during the course of the epidemic. Moving beyond rank-1, in Subsection 4.1.2 we conducted numerical experiments with higher-rank interaction matrices. These simulations revealed richer dynamics at the node level, with multiple infection peaks and more complex transient patterns emerging from the network structure. Finally, in Section 4.2, we extended our analysis to state-dependent interaction matrices, capturing the impact of behavioral feedback. This generalization highlighted how different feedback mechanisms qualitatively alter the transient epidemic dynamics, underscoring the interplay between network topology, adaptive behavior, and epidemic progression.

5

Optimal Control on Behavioral-Feedback SIR Epidemic Model

In this chapter, we address an optimal control problem for the behavioral-feedback SIR model, whose uncontrolled version was introduced and analyzed in Chapter 2. It describes the disease spread within an homogeneous population with a transmission rate dynamically depends on both the susceptible and infected populations. Such dependence captures behavioral responses of individuals to the perceived epidemic risk, e.g. increased caution as infection levels rise, thus extending the classical SIR framework to a more realistic setting.

The optimal control of epidemic dynamics has become a major focus of recent research, especially following the COVID-19 pandemic. Various studies have explored strategies for minimizing both health and economic costs under various constraints, including ICU capacity limits. In these models, control signals, such as lockdown intensity, are chosen to prevent overwhelming the healthcare system while minimizing socio-economic disruption. A commonly recurring outcome in this context is the so-called *filling-the-box strategy*, which prescribes a sharp intervention only when necessary, maintaining the infection level just below the critical threshold.

Building on this line of research, we consider an optimal control problem in which the behavioral-feedback SIR epidemic model is constrained by a fixed threshold on the infected fraction, modeling, for instance, the ICU saturation limit. We formulate a socio-economic cost functional that penalizes both the level of intervention and the duration of restrictions. Our main goal is to identify policies that minimize this cost while ensuring that the infection curve never exceeds the given threshold. The optimal control framework we adopt is similar to that in Miclo et al. (2022), with the key distinction that the epidemic dynamics are governed by the behavioral-feedback SIR model.

To tackle this problem, we adopt a dynamic programming perspective based on the Hamilton-Jacobi-Bellman (HJB) framework (Soner, 2009; Liberzon, 2011). The central part of our analysis involves a geometric study of the state space associated with the uncontrolled dynamics, presented in Section 5.2. In this setting, the system evolves in

a simplex with a threshold for the fraction of infected, reflecting the saturation threshold of ICU capacity. After examining the structure of this constrained region and how trajectories evolve within it, we define a candidate value function representing the minimum cumulative cost required to keep the infection below the threshold starting from any given state. Under certain monotonicity conditions, in Section 5.3 we rigorously prove that the filling-the-box strategy remains optimal: it involves initially allowing the disease to spread uncontrolled, followed by an abrupt lockdown and then a gradual reopening until a time, after which the spread is no longer regulated. In Section 5.4, we consider a special functional form of the transmission rate and refine our previous analysis in this particular case, illustrating how the structure of the optimal policy adapts to the model's parametrization. Finally, in Section 5.5 we provide an analytical counterexample illustrating that the optimality of the filling-the-box strategy fundamentally relies on the monotonicity assumptions of the behavioral transmission rate. If these conditions are not satisfied, the filling-the-box approach may no longer be optimal, and more complex or adaptive intervention strategies may be required to minimize the overall cost.

This chapter contributes to the expanding literature on epidemic control by extending classical optimal intervention strategies to a broader class of models that explicitly account for behavioral dynamics. In doing so, it offers both new theoretical insights and practical guidance for designing more effective and realistic responses to future epidemics.

5.1 Problem Statement

We build this analysis on the behavioral-feedback SIR model, introduced and studied in Chapter 2, which describes the spread of an infectious disease within a homogeneous population, while accounting for a behavioral feedback mechanism. To incorporate external interventions, we introduce an exogenous control input $u : \mathbb{R}_+ \to [0, 1]$, representing a policy level available to a social planner. This control signal modulates the intensity of social interactions, thereby mitigating the transmission of the disease. The resulting controlled epidemic dynamics are described by the following system of ordinary differential equations:

$$\begin{cases} \dot{x} = -(1-u)\beta(x,y)xy\,, \\ \dot{y} = (1-u)\beta(x,y)xy - \gamma y\,, \\ \dot{z} = \gamma y\,, \end{cases} \tag{5.1}$$

where, $\beta : [0, 1]^2 \to (0, +\infty)$ models, as in Chapter 2, an endogenous behavioral reaction to the epidemic through changes in the effective transmission rate. We shall refer to (5.1) as the controlled behavioral-feedback SIR (BF-SIR) epidemic model.

The following result establishes well-posedness of the initial value problems for the controlled BF-SIR epidemic model (5.1) in the compact state space

$$\Delta = \left\{(x, y, z) \in \mathbb{R}^3_+ : x + y + z = 1\right\}\,.$$

Lemma 5.1. *For every initial state (x_0, y_0, z_0) in Δ and every piecewise continuous control signal $u(t)$, the controlled BF-SIR epidemic model (5.1) admits a unique solution $(x(t), y(t), z(t))$ for $t \geq 0$, such that*

$$x(0) = x_0\,, \qquad y(0) = y_0\,, \qquad z(0) = z_0\,. \tag{5.2}$$

Such solution is a piecewise-$\mathcal{C}^1$ function of t and is such that $(x(t), y(t), z(t))$ in Δ for $t \geq 0$.

Proof. The right-hand side of of (5.1) is locally Lipschitz with respect to (x, y, z). On any time interval on which u is continuous, local existence and uniqueness of a solution for the corresponding Cauchy problem is a consequence of the Picard-Lindelöf theorem Hale, 2009, p. I.3). If u admits jump discontinuities at times $0 < t_1 < t_2 < \cdots$, we define $u^k : [t_k, t_{k+1}] \to \mathbb{R}$ for $k \geq 0$ (letting $t_0 = 0$) to be the unique continuous function that coincides with u on $[t_k, t_{k+1}]$. Given an initial condition (x_0, y_0, z_0), we iteratively solve the Cauchy problem relative to (5.1) with such initial condition as follows. On every interval $[t_k, t_{k+1}]$ we use the control u^k and solve for initial conditions (x_k, y_k, z_k). We call $(x^k(t), y^k(t), z^k(t))$ the corresponding solution. We then recursively impose that $(x_{k+1}, y_{k+1}, z_{k+1}) = (x^k(t_{k+1}), y^k(t_{k+1}), z^k(t_{k+1}))$. This yields, by construction, piecewise $\mathcal{C}^1$ maximal solution $(x(t), y(t), z(t))$ that concides with $(x^k(t), y^k(t), z^k(t))$ on $[t_k, t_{k+1}]$.

By integrating equations in (5.1), assuming initial condition (x_0, y_0, z_0) in Δ, we get

$$x(t) = x_0 \exp\left(\int_0^t (-(1 - u(\tau))\beta(x(\tau), y(\tau))y(\tau))\, d\tau\right), \tag{5.3}$$

$$y(t) = y_0 \exp\left(\int_0^t ((1 - u(\tau))\beta(x(\tau), y(\tau))x(\tau) - \gamma)\, d\tau\right), \tag{5.4}$$

$$z(t) = z_0 + \gamma \int_0^t y(\tau)\, d\tau\,. \tag{5.5}$$

Moreover, the sum of the equations in (5.1) gives $\dot{x}(t) + \dot{y}(t) + \dot{z}(t) = 0$. All this implies that, as long as the solution $(x(t), y(t), z(t))$ exists, we must have that $x(t) \geq 0$, $y(t) \geq 0$, $z(t) \geq 0$, and $x(t) + y(t) + z(t) = 1$. In other terms, as long as the solution exists, it lives in Δ. In particular, this implies that the solution is globally defined (Knauf, 2018, Section 3.3). □

To facilitate our analysis, we recall the following compact set

$$\mathcal{S} = \left\{(x, y) \in \mathbb{R}_+^2 : x + y \leq 1\right\}.$$

Throughout this part, we will assume the following regularity conditions. The control signal $u : \mathbb{R}_+ \to [0, 1]$ is assumed to be a piecewise continuous function. The transmission rate function β is assumed to be of class $\mathcal{C}^2$ and satisfies the following conditions for all $(x, y) \in \mathcal{S}$,

$$x\beta_x(x, y) + \beta(x, y) > 0\,, \tag{5.6}$$

and

$$\beta_y(x, y) \leq 0\,. \tag{5.7}$$

Under condition (5.6), the uncontrolled dynamics has been analyzed in Chapter 2, where it was shown that the infection curve $y(t)$ exhibits unimodal behavior. This property will be essential for the analysis of the optimal control problem addressed in this chapter. This assumption captures how the transmission rate varies with the number of susceptibles: a higher fraction of susceptibles may lead to a lower perceived risk, encouraging social interactions and riskier behaviors that facilitate contagion. While, condition (5.7) captures the tendency of individuals to reduce their interaction levels in response to the spread of infection within the population. This second assumption has also been considered in previous works, such as (Baker, 2020; Franco, 2020). It is important to note that the constant transmission rate, along with the class of functions defined in Example 2.1, satisfies both of these conditions.

Notice that the first two equations in (5.1) can be rewritten in $\mathcal{S}$ in terms of the *behavioral reproduction number* $R(x, y)$, defined in (2.13), as follows

$$\begin{cases} \dot{x} = -(1-u)\gamma R(x, y)y, \\ \dot{y} = \gamma[(1-u)R(x, y) - 1]y. \end{cases} \tag{5.8}$$

Observe now that (5.6) and (5.7) imply that the reproduction number is increasing with respect to the fraction of susceptible individuals while non-increasing with respect to the infected individuals, i.e.,

$$R_x(x, y) > 0\,, \tag{5.9}$$

$$R_y(x, y) \leq 0\,, \tag{5.10}$$

for every point (x, y) in $\mathcal{S}$.

We consider the control problem of an external planner whose objective is to keep the fraction of infected individuals below a specified threshold $\bar{y} \leq 1$, representing, for example, the capacity of the healthcare system. The planner can intervene only through a control function $u(t)$ that modifies the rate of infection transmission, modeling possible lockdown or social distancing measures. The implementation of this intervention incurs an economic cost that we want to minimize. To formalize this constraint, we define

$$\mathcal{D}_{\bar{y}} = \{(x, y) \in \mathcal{S} : 0 < y \leq \overline{y}\}\,, \tag{5.11}$$

that is the portion of state space below this threshold. For a given initial condition (x_0, y_0) in $\mathcal{D}_{\overline{y}}$, we then consider the set $\mathcal{U}_{(x_0,y_0,\bar{y})}$ of piecewise continuous control signals $u : \mathbb{R}_+ \to [0, 1]$ such that the solution $(x(t), y(t))$ of the controlled BF-SIR epidemic model

(5.8) with initial state (x_0, y_0) satisfies

$$(x(t), y(t)) \in \mathcal{D}_{\overline{y}}\,, \qquad \forall t \geq 0\,. \tag{5.12}$$

Notice that the set $\mathcal{U}_{(x_0,y_0,\bar{y})}$ is never empty since it contains the trivial control $u \equiv 1$, which keeps the fraction of infected individuals always below the threshold by enforcing a complete lockdown and reduction of the interactions. We model the cost through a functional $J : \mathcal{U}_{(x_0,y_0,\bar{y})} \to [0, +\infty]$ defined by

$$J(u) = \int_0^{+\infty} u(t)\, dt\,,$$

and we consider the optimal control problem

$$V^*(x_0, y_0) = \min_{u \in \mathcal{U}_{(x_0,y_0,\bar{y})}} J(u)\,. \tag{5.13}$$

Remember the definition of ρ, given in (2.22), as

$$\rho(x, y) = \frac{R(x, y) - 1}{R(x, y)} = 1 - \frac{\gamma}{x\beta(x, y)}\,. \tag{5.14}$$

Building on the previous discussion, we can now formulate the main theoretical result of this chapter. A detailed proof will follow in Section 5.3.

Theorem 5.1. *Assume that β is a $\mathcal{C}^2$ function satisfying conditions (5.6) and (5.7). Fix a threshold $\overline{y} \leq 1$ and consider $\mathcal{D}_{\overline{y}}$ as defined in (5.11). Then, for any initial condition $(x_0, y_0) \in \mathcal{D}_{\overline{y}}$, the optimal control problem (5.13) admits solutions. Moreover, there exists an optimal control $u^* \in \mathcal{U}_{(s_0,\bar{y})}$ such that, if $(x^*(t), y^*(t))$ is the corresponding solution to the ODE (5.8), the control can be expressed as*

$$u^*(t) = \mu(x^*(t), y^*(t)), \quad t \geq 0\,, \tag{5.15}$$

where $\mu : \mathcal{S} \to [0, 1]$ is defined as

$$\mu(x, y) = \begin{cases} 0 & \text{if } y < \bar{y} \\ [\rho(x, \overline{y})]_+ & \text{if } y = \bar{y}\,. \end{cases} \tag{5.16}$$

Proof. See Section 5.3. □

A numerical simulation of the controlled BF-SIR (5.1) model, with $\beta(x, y) = \frac{0.35x}{1+1.5y}$ is presented in Figure 5.1. The optimal control problem (5.13) considers an infection threshold of $\bar{y} = 0.2$. The top plot shows in green the solution $y^*(t)$ corresponding to the optimal feedback policy $u^*(t)$, described by (5.15)-(5.16) and reported in the bottom plot. While the dashed blue curve is the corresponding uncontrolled solution, i.e. the solution of the BF-SIR epidemic model (5.1) with $u \equiv 0$.

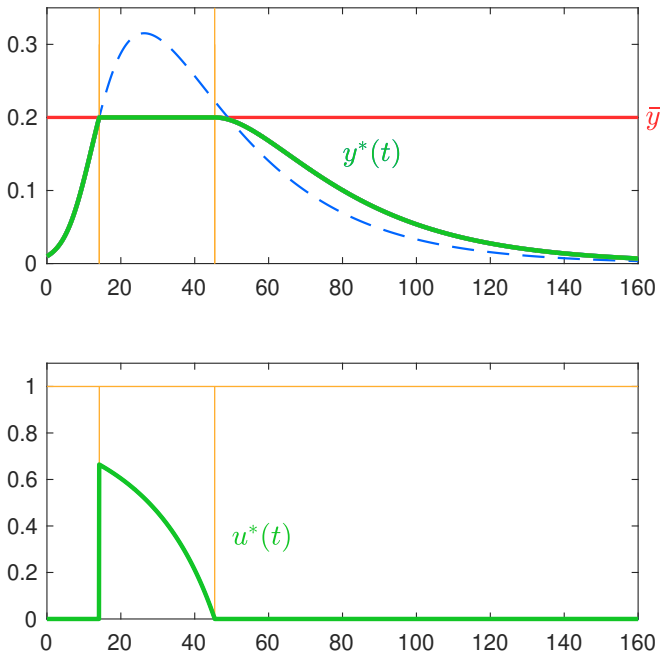

FIGURE 5.1: Numerical simulation of the controlled BF-SIR model with $\beta(x,y) = \frac{0.35x}{1+1.5y}$. The top plot shows in green the solution $y^*(t)$ corresponding to the optimal feedback policy $u^*(t)$ reported in the bottom plot. While the dashed blue curve is the corresponding uncontrolled solution.

The optimal feedback policy $u^*(t)$ consists in allowing the disease to spread without control until the fraction of infected individuals reaches the threshold $\bar{y}$. Indicated with $t^* \geq 0$ the time this happens, the system then evolves as follows,

$$\dot{x}^* = -(1-u^*)\beta(x^*,\bar{y})x^*\bar{y} = -\gamma\bar{y}, \qquad \dot{y}^* = 0\,. \tag{5.17}$$

The fraction of susceptibles $x^*(t)$ has the explicit solution $x^*(t) = -\gamma\bar{y}(t-t^*)+x^*(t^*)$. At time $\hat{t}$ such that $R(x^*(\hat{t}),\bar{y}) = 1$ (or equivalently, $\rho(x^*(\hat{t}),\bar{y}) = 0$), the control is released and the trajectory follows the uncontrolled dynamics and the infection curve declines from there on. The corresponding control signal $u^*(t)$ starts abruptly above 0 at time t^* and subsequently is adjusted in time to maintain the fraction of infected exactly at the threshold $\bar{y}$ until $\hat{t}$. At that point, the control is deactivated. The economic rationale behind this optimal policy is to avoid unnecessary societal shutdowns while ICU resources remain unused. Therefore, whenever the natural spread of the disease does not pose a threat to ICU capacity, the spread should proceed without intervention. This policy, known in the literature as *filling-the-box* strategy, was proven to be optimal also in the classical controlled SIR model, in (Miclo et al., 2022).

The proof of Theorem 5.1 will come after some geometric considerations in the state space for the dynamics with a threshold for the infected fraction of individuals, discussed in Section 5.2.

Before proceeding to the analysis, the next result ensures that the problem (5.13) is well-defined and studies the asymptotic behaviour of the solution of (5.8).

Proposition 5.1. *For any initial condition $(x_0, y_0, z_0) \in \mathcal{S}$ and any piecewise continuous control $u(t)$, the system (5.8) admits a unique piecewise $\mathcal{C}^1$ solution on $\mathbb{R}_+$, denoted by $(x(t), y(t))$ in $\mathcal{S}$. Moreover, the following statements hold:*

(i) $t \to x(t)$ is monotonically non-increasing for all $t \geq 0$;

(ii) there exists $x_\infty \in \mathbb{R}$ such that

$$\lim_{t \to +\infty} (x(t), y(t)) = (x_\infty, 0)\,.$$

Proof. (i) and (ii) follow similar steps as in the proof of Proposition 2.3(i)-(iii). □

5.2 Geometric considerations on the state space

In this section, we analyze the dynamics of the uncontrolled BF-SIR epidemic model (2.5) in the presence of a fixed infection threshold $\bar{y} \in (0, 1]$. Our goal is to determine which trajectories naturally remain below this threshold without requiring external intervention. We start with a remark.

Remark 5.1. *From the standard local existence and uniqueness results, cited in Lemma 5.1, it also follows that for the uncontrolled model there exists a map $\phi : \mathbb{R}_+ \times \mathcal{S} \to \mathcal{S}$ such that $(x_0, y_0) \mapsto \phi(t, x_0, y_0)$ and $t \mapsto \phi(t, x_0, y_0)$ are both of class $\mathcal{C}^2$ and $t \mapsto \phi(t, x_0, y_0)$ is the unique solution on $\mathbb{R}_+$ with $\phi(0; x_0, y_0) = (x_0, y_0) \in \mathcal{S}$.*

Furthermore, it is useful for the subsequent analysis to define the uncontrolled positive semi-orbit associated to an initial condition $(x_0, y_0) \in \mathcal{S}$:

$$\Gamma(x_0, y_0) = \{\phi(t, x_0, y_0) \,|\, t \geq 0\}\,.$$

In certain occasions, we also need to consider the solution backward for $t < 0$. Indicating such a solution with the same symbol $\phi(t, x_0, y_0)$ with $t \in (T, 0]$ where $T < 0$ is the maximal existence time in the past (possibly $-\infty$), we also define the uncontrolled negative semi-orbit

$$\Gamma^-(x_0, y_0) = \{\phi(t, x_0, y_0) \,|\, t \in (T, 0]\}\,.$$

The first part of our analysis leads to a decomposition of $\mathcal{D}_{\overline{y}}$ into two sets $\mathcal{D}_{\overline{y}}^-$ and $\mathcal{D}_{\overline{y}}^+$. From every initial condition in $\mathcal{D}_{\overline{y}}^-$, the solution stays below $\overline{y}$ without the need of a control, while for any initial condition in $\mathcal{D}_{\overline{y}}^+$, the uncontrolled solution always hits the line $y = \overline{y}$ and goes above it for a certain time interval. In this case the control must be active for some time. We will visualize the results in the bi-dimensional phase space Δ,

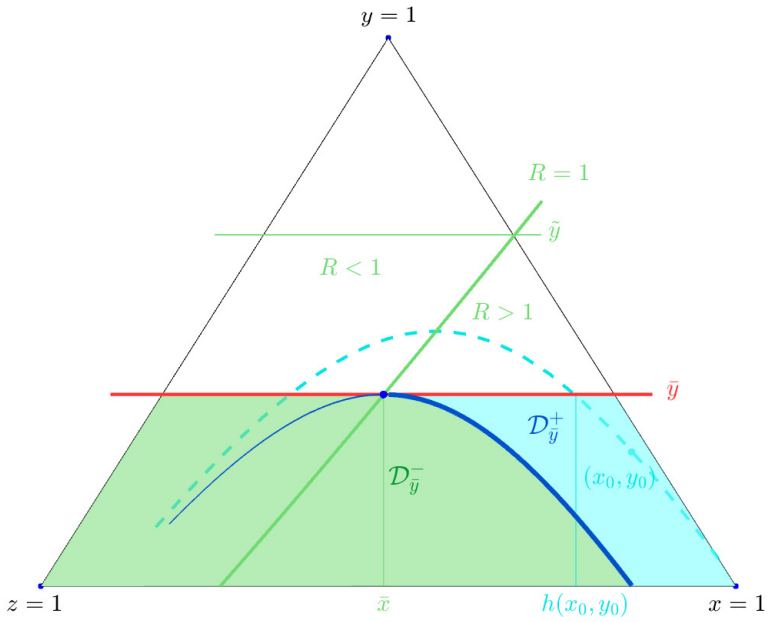

FIGURE 5.2: Phase portrait of the uncontrolled BF-SIR model (5.1) on the simplex Δ, with a transmission rate given by Example 2.1, using parameters $b(x) = 0.75x$, $c = 1.5$, and $\gamma = 0.05$. The vertices of the simplex represent states where the entire population is concentrated in one compartment (susceptible, infected, or recovered), while the boundary segments correspond to configurations in which one compartment is absent. The curve $R(x, y) = 1$ is shown in green, and the infection threshold $y = \bar{y}$ is shown in red. Two representative trajectories starting from different initial conditions are displayed in blue and light blue.

represented in Figure 5.2. Vertices correspond to scenarios in which the entire population belongs to one of the compartments (susceptible, infected, or recovered). Similarly, the boundary segments represent configurations in which one compartment is absent from the population.

The following result shows that the set of states where $R(x, y) = 1$ can be represented as the graphical of a function of y.

Lemma 5.2. *Let β satisfy conditions (5.6) and (5.7). If*

$$\beta(1, 0) > \gamma\,, \tag{5.18}$$

then there exist $\tilde{y} > 0$ and a $\mathcal{C}^1$ function $\kappa : [0, \tilde{y}] \to [0, 1]$ such that

$$\{(x, y) \in \mathcal{S} : R(x, y) = 1\} = \{(\kappa(y), y) : y \in [0, \tilde{y}]\}\,.$$

Proof. Notice first that $R(0, 1) = 0$ while $R(1, 0) > 1$ thanks to condition (5.18). Therefore, since $y \mapsto R(1 - y, y)$ is continuous on $[0, 1]$, there exists $\tilde{y}$ in $(0, 1)$ such that $R(1 - \tilde{y}, \tilde{y}) = 1$. It follows from the assumptions (5.9) and (5.10) that $R(1 - y, y) > 1$ for every $0 \leq y < \tilde{y}$. For any such y, since $R(0, y) = 0$, we have that there exists $x = k(y)$, unique because of (5.9), such that $R(k(y), y) = 1$. The fact that k is of class C^1 comes

from a direct application of the Implicit Function Theorem (Canuto and Tabacco, 2015, Theorem 7.1) given that $R_x(x,y) \neq 0$ in every (x,y) because of (5.9). □

Figure 5.2 shows the curve $R(x,y) = 1$ colored in green and the splitting of the simplex into two areas: the left-hand one with $R(x,y) < 1$ and the right-hand one with $R(x,y) > 1$.

Remark 5.2. *The function κ maps every $y \in [0, \tilde{y}]$ into the fraction of susceptibles $\kappa(y) \in [0, 1-y]$ such that $R(\kappa(y), y) = 1$. In classic SIR model, this function is a constant, i.e. $\kappa(y) = \gamma/\beta$ for all $y \in [0, 1-\gamma/\beta]$.*

We first notice that if condition (5.18) is not satisfied, $R(x,y) \leq 1$ for every $(x,y) \in \mathcal{S}$. Similarly, if condition (5.18) is satisfied and it holds $\overline{y} \geq \tilde{y}$, then, for every $x \in [0, 1-\overline{y}]$, $R(x,\overline{y}) \leq 1$. In both cases, this implies that, by item (i) of Proposition 2.4, the solution will never cross the line $y = \overline{y}$ from below. Consequently, in both cases, the control set to 0 is a feasible and optimal one.

From now on, we assume that condition (5.18) is satisfied, that $\overline{y} < \tilde{y}$, and we focus on the set $\mathcal{D}_{\overline{y}}$. It is useful in our analysis to consider the negative semi-orbit $\Gamma^-(\overline{x},\overline{y})$ of the uncontrolled system (5.1) with initial condition $(\overline{x},\overline{y})$ where $\overline{x} = k(\overline{y})$. The following result gives information on this set.

Lemma 5.3. *There exists $y^* \in (0,\overline{y})$ and a $\mathcal{C}^1$ decreasing function $\lambda : [y^*,\overline{y}] \to [0,\bar{x}]$ such that*

$$\overline{\Gamma^-(\overline{x},\overline{y})} \cap \mathcal{S} = \{(\lambda(y), y) : y^* \leq y \leq \overline{y}\}.$$

Moreover, $R(\lambda(y), y) > 1$ for every $y \in [y^*, \bar{y}]$.

Proof. We consider the backward solution $(x(t), y(t)) = \phi(t, \overline{x}, \overline{y})$ with $t < 0$ and we put $R(t) = R(x(t), y(t))$. Notice that (2.17) and the fact that by construction $R(0) = 1$ yield $\dot{R}(0) < 0$. This implies that the solution $(x(t), y(t))$ enters in the set $R(t) > 1$ for $t < 0$ and the same argument shows that such set can not be exited. In other terms $R(t) > 1$ as long as the solution exists. Since such a condition implies that $y(t)$ is strictly increasing, while $x(t)$ is always strictly decreasing, we conclude that the backward evolution $(x(t), y(t))$ has interval of existence $(-\infty, 0]$. Either $(x(t), y(t))$ converges to a point in the boundary of $\mathcal{S}$, for $t \to -\infty$, or the solution hits the boundary of $\mathcal{S}$ at some finite time. Let us indicate the convergence or hit point by (x^*, y^*). We notice that, in the first case, such point must be an equilibrium, so that necessarily $y^* = 0$. In the second case, instead, such a point must satisfy the equation $x^* + y^* = 1$ with $y^* \in (0, \overline{y})$. In both cases, considering the strict monotonicity of $y(t)$, the negative semi-orbit can be always represented as the graphical of a $\mathcal{C}^1$ strictly decreasing function of y denoted $\lambda(y)$ and defined in $[y^*, \bar{y}]$. We set $\lambda(\bar{y}) = \kappa(\bar{y}) = \bar{x}$ by construction. The fact that $R(\lambda(y), y) > 1$ for every $[y^*, \bar{y}]$ follows from (5.6) and the fact that $R(t) > 1$ as long as the solution exists. This proves the result. □

Lemma 5.3 allows for the partition of $\mathcal{D}_{\overline{y}}$ in two subsets

$$\mathcal{D}_{\overline{y}}^{+} = \{(x,y) \in \mathcal{D}_{\overline{y}} \,:\, y \in [y^*, \overline{y}],\, x > \lambda(y)\}, \qquad \mathcal{D}_{\overline{y}}^{-} = \mathcal{D}_{\overline{y}} \setminus \mathcal{D}_{\overline{y}}^{+}\,.$$

In Figure 5.2, the negative semi-orbit $\Gamma^{-}(\overline{x},\overline{y})$ is represented by the thick blue curve. The green and the light-blue area are, respectively, the sets $\mathcal{D}_{\overline{y}}^{-}$ and $\mathcal{D}_{\overline{y}}^{+}$.

The next two results discuss the behavior of the uncontrolled orbit of the system from initial conditions either in $\mathcal{D}_{\overline{y}}^{-}$ or in $\mathcal{D}_{\overline{y}}^{+}$. In the first case, the orbit remains in $\mathcal{D}_{\overline{y}}^{-}$ and thus, in particular, the number of infected never exceeds $\overline{y}$. In the second case, the orbit always crosses the line $y = \overline{y}$. We show that the ascissa of the hitting point is a regular function of the initial condition, a fact that will play a crucial role in the proof of optimality.

Lemma 5.4. *Let β satisfy (5.6) and (5.7). Then, for every $(x_0,y_0) \in \mathcal{D}_{\overline{y}}^{-}$ and for every $t \geq 0$, $\phi(t,x_0,y_0) \in \mathcal{D}_{\overline{y}}^{-}$.*

Proof. Since the negative semi-orbit $\Gamma^{-}(\overline{x},\overline{y})$ is the graphical of a $\mathcal{C}^1$ function, we have that the boundary $\mathcal{D}_{\overline{y}}^{-}$ as a subset of $\mathcal{S}$ is given by $\partial\mathcal{D}_{\overline{y}}^{-} = I \cup \Gamma^{-}(\overline{x},\overline{y})$ where $I = \{(x,\overline{y}) \,:\, x \leq \overline{x}\}$. Since the solution stays in $\mathcal{S}$ at all times, the only way it can leave $\mathcal{D}_{\overline{y}}^{-}$ is by crossing the boundary $\partial\mathcal{D}_{\overline{y}}^{-}$. Notice that $R < 1$ on every point of the segment I, consequently, $y(t)$ is decreasing and thus the solution can not cross I from below. Standard uniqueness results for ODE imply that also the negative semi-orbit can not be crossed. This completes the proof. □

Lemma 5.5. *Let β satisfy (5.6) and (5.7). Then, there exists a $\mathcal{C}^2$ map $h : \mathcal{D}_{\overline{y}}^{+} \to (\bar{x}, 1-\bar{y}]$ such that for every $(x,y) \in \mathcal{D}_{\overline{y}}^{+}$, $(h(x,y),\overline{y})$ belongs to $\Gamma(x,y)$, that is the uncontrolled positive semi-orbit of (5.8) associated to the initial condition (x,y). Moreover, for every $(x_0,y_0) \in \Gamma^{-}(\overline{x},\overline{y}) \cap \mathcal{S}$, the following limit condition holds*

$$\lim_{\substack{(x,\,y)\,\to\,(x_0,\,y_0)\\(x,\,y)\,\in\,\mathcal{D}_{\overline{y}}^{+}}} h(x,y) = \overline{x}\,. \tag{5.19}$$

Proof. We notice first that, thanks to Lemma 5.3 and condition (5.9), $R(x,y) > 1$ for every $(x,y) \in \mathcal{D}_{\overline{y}}^{+}$. This implies that the solution

$$(x(t,x_0,y_0), y(t,x_0,y_0)) = \phi(t,x_0,y_0),$$

with initial condition $(x_0,y_0) \in \mathcal{D}_{\overline{y}}^{+}$, is such that $y(t,x_0,y_0)$ is strictly increasing in t as long as the solution remains in $\mathcal{D}_{\overline{y}}^{+}$. It thus follows from Proposition 2.4 that the solution exits $\mathcal{D}_{\overline{y}}^{+}$ in finite time. Arguing as in the proof of Lemma 5.4, we have that the boundary $\mathcal{D}_{\overline{y}}^{+}$ as a subset of $\mathcal{S}$ is given by $\partial\mathcal{D}_{\overline{y}}^{+} = J \cup \Gamma^{-}(\overline{x},\overline{y})$ where

$$J = \{(x,\overline{y}) \,:\, \overline{x} < x \leq 1 - \overline{y}\}\,, \tag{5.20}$$

and that the only way the solution can leave $\mathcal{D}_{\overline{y}}^{+}$ is by crossing the segment J. Proposition 2.4 again insures that this segment is hit only once at some finite time. We call $T(x_0, y_0)$ the corresponding hitting time and we put $h(x_0, y_0) = x(T(x_0, y_0); x_0, y_0) \in (\bar{x}, 1 - \overline{y}]$. We notice now that, by construction, $y(T(x_0, y_0); x_0, y_0) = \overline{y}$ and $\dot{y}(T(x_0, y_0); x_0, y_0) > 0$ for every $(x_0, y_0) \in \mathcal{D}_{\overline{y}}^{+}$. A direct application of the Implicit Function theorem (Canuto and Tabacco, 2015, Theorem 7.1) (on all points of $\mathcal{D}_{\overline{y}}^{+}$ including the boundary segment J) together with the regularity results in Remark 5.1 yield that T is of class $\mathcal{C}^2$. By the way the function h is defined, the first part of the result follows.

We now prove the limit relation. We fix $(x_0, y_0) \in \Gamma^{-}(\overline{x}, \overline{y}) \cap \mathcal{S}$ and we let $T(x_0, y_0)$ be the time such that $x(T(x_0, y_0), x_0, y_0) = \overline{x}$. Fix now $\varepsilon > 0$ and let $0 < T < T(x_0, y_0)$ be such that $||\phi(T, x_0, y_0) - (\overline{x}, \overline{y})|| < \varepsilon/2$. Put $\bar{\varepsilon} = \min\{\varepsilon/2, \overline{y} - y(T, x_0, y_0)\}$. By the regularity results on the solution, we have that there exists $\delta > 0$ such that for every $(x, y) \in B_\delta(x_0, y_0) \cap \mathcal{D}_{\overline{y}}^{+}$, it holds $||\phi(T, x_0, y_0) - \phi(T, x, y)|| < \bar{\varepsilon}$ and $\partial y(T, x, y)/\partial t > 0$. Notice that, by construction, $\phi(T, x, y) \in \mathcal{D}_{\overline{y}}^{+}$ and the hitting time of the line $y = \overline{y}$ is above T. Since $x(t, x, y)$ is decreasing in time, we thus have that $\overline{x} < h(x, y) < \overline{x} + \bar{\varepsilon} + \varepsilon/2 \leq \overline{x} + \varepsilon$. This proves the result. □

Remark 5.3. *Note that $h(x, y)$ is the abscissa of the crossing point of the orbit with initial conditions in $\mathcal{D}_{\overline{y}}^{+}$ with the line $y = \bar{y}$, i.e. the fraction of susceptibles reached by the dynamics when the fraction of infected individuals reaches $\bar{y}$. An example of trajectory that starts in $\mathcal{D}_{\overline{y}}^{+}$ is illustrated in Figure 5.2 by the light-blue dashed curve.*

Remark 5.4. *By its definition, the function h remains constant along the uncontrolled orbits of (5.1), since all points that belong to the same orbit will hit segment $\mathcal{J}$ in the same point because of the uniqueness of the solutions. Indeed*

$$h(x(t), y(t)) = \xi\,,$$

for every $(x(t), y(t)) \in \Gamma^{-}(\xi, \overline{y}) \cap \mathcal{S}$ with $\xi \in (\bar{x}, 1 - \bar{y}]$.

Before proceeding with the analysis of the optimal control, we introduce the following technical result, which involves the behavior of the h function defined above.

Lemma 5.6. *Let β satisfy (5.6), (5.7) and (5.18). Then, the following holds*

$$0 \leq h_y(x, y) \leq \frac{1}{\rho(h(x, y), \overline{y})}\,, \tag{5.21}$$

for all $(x, y) \in \mathcal{D}_{\overline{y}}^{+}$. Moreover, the right-hand side inequality is an equality when $y = \bar{y}$.

Proof. As h is a constant of motion for the uncontrolled model (see Remark 5.4), it holds $h_x \dot{x} + h_y \dot{y} = 0$. Using (5.8) we derive the identity on $\mathcal{D}_{\overline{y}}^{+}$:

$$h_x(x, y) R(x, y) = h_y(x, y)(R(x, y) - 1)\,. \tag{5.22}$$

We now show that $h_x(x,y)$ is always non negative on $\mathcal{D}_{\overline{y}}^+$. For $(x_0,y_0)\in\mathcal{D}_{\overline{y}}^+$, choose any $\varepsilon>0$ such that $(x_0-\varepsilon,y_0)\in\mathcal{D}_{\overline{y}}^+$. Denote by $(x(t),y(t))$ and by $(x_\varepsilon(t),y_\varepsilon(t))$ the solutions associated with the initial conditions, respectively, (x_0,y_0) and $(x_0-\varepsilon,y_0)$. As long as they leave in $\mathcal{D}_{\overline{y}}^+$, such solutions are characterized by a second term that is strictly increasing in t, so that the corresponding orbits can be described as graphicals of functions say $x=f(y)$ and $x=f_\varepsilon(y)$ with $y\in[y_0,\bar{y}]$. Since orbits can not intersect and since $x_0=f(y_0)>x_0-\varepsilon=f_\varepsilon(y_0)$, it must hold that $h(x_0,y_0)=f(\bar{y})>f_\varepsilon(\bar{y})=h(x_0-\varepsilon,y_0)$. Given the arbitrariness of ε, this implies that $h_x(x_0,y_0)\geq 0$. Notice moreover that since $x\mapsto h(x,\bar{y})$ is the identity matrix on $[\bar{x},1]$, we have that $h_x(x,\bar{y})=1$. Consequently, thanks to relation (5.22) we also have that

$$h_y(x,y)\geq 0\ \forall(x,y)\in\mathcal{D}_{\overline{y}}^+,\qquad h_y(x,\bar{y})=\frac{R(x,\bar{y})}{R(x,\bar{y})-1}=\frac{1}{\rho(x,\overline{y})}\,. \tag{5.23}$$

We now analyze the behavior of $h_y(x,y)$ along the orbits, computing as follows

$$\begin{aligned}\dot{h}_y &= \dot{x}\,h_{xy}(x,y)+\dot{y}\,h_{yy}(x,y)\\ &= -R(x,y)\gamma y h_{xy}(x,y)+(R(x,y)-1)\gamma y h_{yy}(x,y)\,.\end{aligned} \tag{5.24}$$

Taking the partial derivative of expression (5.22) with respect to y and then substituting expression (5.22) inside, we get

$$\begin{aligned}h_{xy}(x,y)R(x,y) &= h_{yy}(x,y)(R(x,y)-1)+(h_y(x,y)-h_x(x,y))\,R_y(x,y)\\ &= h_{yy}(x,y)(R(x,y)-1)+R(x,y)^{-1}h_y(x,y)R_y(x,y)\,,\end{aligned}$$

and substituting in expression (5.24) we finally get

$$\dot{h_y}=-\gamma y R(x,y)^{-1}h_y(x,y)R_y(x,y)\geq 0\,, \tag{5.25}$$

where the sign follows from relation (5.10). From expression (5.25) and since $(h(x,y)\overline{y})$ belongs to the positive orbit $\Gamma(x,y)$, for all $(x,y)\in\mathcal{D}_{\overline{y}}^+$ we get that

$$h_y(x,y)\leq h_y(h(x,y),\bar{y})\,,$$

and combining with (5.23) we obtain the result. □

5.3 Proof of optimality

In this section we provide the proof of Theorem 5.1. We start by introducing a candidate value function. This is obtained by computing the cost for the candidate optimal control u^* defined in (5.15)–(5.16). The next result shows this computation and the dynamical behavior of the solution of controlled BF-SIR epidemic model (5.8).

Lemma 5.7. *Let $(x^*(t), y^*(t))$, for $t \geq 0$, be the solution of controlled BF-SIR epidemic model (5.8) with initial state (x_0, y_0) in $\mathcal{D}_{\overline{y}}$ and feedback control (5.15)-(5.16). The dynamics evolves as follows,*

(i) if $(x_0, y_0) \in \mathcal{D}_{\overline{y}}^-$ then $(x^*(t), y^*(t)) \in \mathcal{D}_{\overline{y}}$ for every $t \geq 0$ and the cost is $J(u^*) = 0$.

(ii) if $(x_0, y_0) \in \mathcal{D}_{\overline{y}}^+$ then there exist two time instants $t^*, \bar{t} \geq 0$, such that

(a) $(x^*(t), y^*(t))$ for every $t \in [0, t^*]$ coincides with the solution of the uncontrolled BF-SIR epidemic model (2.5) with initial state (x_0, y_0);

(b) $(x^*(t), y^*(t))$ for every $t \in [t^*, \bar{t}]$ evolves as (5.17) with initial state $(x^*(t^*), y^*(t^*)) = (h(x_0, y_0), \overline{y})$;

(c) $(x^*(t), y^*(t))$ for every $t \geq \bar{t}$ coincides with the solution of the uncontrolled BF-SIR epidemic model (2.5) with initial state $(\overline{x}, \overline{y})$;

and the cost is

$$J(u^*) = \frac{1}{\gamma \overline{y}} \int_{\bar{x}}^{h(x_0,y_0)} \rho(x, \bar{y}) \mathrm{d}x \,.$$

Proof. (i) Observe that $u^*(t) > 0$ if and only if $(x^*(t), y^*(t)) \in \mathcal{J} \setminus \{(\overline{x}, \overline{y})\}$, where $\mathcal{J}$ is the segment defined in (5.20). By Lemma 5.4, if $(x_0, y_0) \in \mathcal{D}_{\overline{y}}^-$, then $(x^*(t), y^*(t)) \in \mathcal{D}_{\overline{y}}$, so that $(x^*(t), y^*(t)) \notin \mathcal{J}$, for every $t \geq 0$. Hence, the cost is 0 for every state (x_0, y_0) in $\mathcal{D}_{\overline{y}}^-$.

(ii) For every state (x_0, y_0) in $\mathcal{D}_{\overline{y}}^+$, Lemma 5.5 ensures that $(x^*(t), y^*(t))$ enters the segment $\mathcal{J}$ at some time $t^* \geq 0$ in a point $(x^*(t^*), y^*(t^*)) = (h(x_0, y_0), \overline{y})$. It follows from the structure of u^* (5.15)–(5.16) that $(x^*(t), y^*(t))$ for $t \in [0, t^*]$ corresponds to a control $u^*(t) = 0$. Again from the structure of u^*, we get that the corresponding solution $(x^*(t), y^*(t))$ for $t \in [t^*, \bar{t}]$ evolves as (5.17) along the segment $\mathcal{J}$, hence keeping $y^*(t) = \overline{y}$, until reaching the point $(x^*(\bar{t}), y^*(\bar{t})) = (\overline{x}, \overline{y})$ at some time $\bar{t}$. Since $R(\overline{x}, \overline{y}) = 1$, then the control $u^*(t) = [\rho(x, \overline{y})]_+$ becomes 0, and the dynamics will evolve as (2.5). The total cost along the segment $\mathcal{J}$ is given by

$$\begin{aligned} \int_{t^*}^{\bar{t}} u^*(t) \mathrm{d}t &= \int_{t^*}^{\bar{t}} \rho(x^*(t), y^*(t)) \mathrm{d}t \\ &= \int_{t^*}^{\bar{t}} \rho(x^*(t), \overline{y}) \mathrm{d}t \\ &= \frac{1}{\gamma \overline{y}} \int_{\bar{x}}^{h(x_0,y_0)} \rho(x, \overline{y}) \mathrm{d}x \,. \end{aligned}$$

□

Motivated by Lemma 5.7, we introduce the candidate value function $V : \mathcal{D}_{\overline{y}} \to \mathbb{R}$, as

$$V(x,y) = \begin{cases} 0 & \text{if } (x,y) \in \mathcal{D}_{\overline{y}}^{-}\,, \\ \dfrac{1}{\gamma\bar{y}} \displaystyle\int_{\bar{x}}^{h(x,y)} \rho(s,\bar{y})\mathrm{d}s & \text{if } (x,y) \in \mathcal{D}_{\overline{y}}^{+}\,. \end{cases} \tag{5.26}$$

The following result characterizes technical properties of the candidate value function, which will be instrumental for the subsequent analysis.

Lemma 5.8. *Let β satisfy (5.6) and (5.7) and V defined by (5.26). Then the following facts hold:*

(i) V is continuous on $\mathcal{D}_{\overline{y}}$ and $\mathcal{C}^1$ on $\mathcal{D}_{\overline{y}}^{+}$.

(ii) Partial derivatives on $\mathcal{D}_{\overline{y}}^{+}$ are determined by the relations

$$V_y(x,y) = \frac{\rho(h(x,y),\bar{y})}{\gamma\bar{y}} h_y(x,y), \tag{5.27}$$

$$V_x(x,y) = \rho(h(x,y),\bar{y}) V_y(x,y)\,. \tag{5.28}$$

(iii) $0 \le V_y(x,y) \le \frac{1}{\gamma\bar{y}}$ for all $(x,y) \in \mathcal{D}_{\overline{y}}^{+}$.

(iv) $V_y(x,y) = \frac{1}{\gamma\bar{y}}$ for all $(x,y) \in \mathcal{J}$.

Proof. (i) is a direct consequence of the regularity of h on $\mathcal{D}_{\overline{y}}^{+}$ and the limit relation (5.19) expressed in Lemma 5.5.

(ii) It follows from a direct differentiation of the expression of V on $\mathcal{D}_{\overline{y}}^{+}$ and from (5.22).

(iii) From the previous point, Lemma 5.6 and (5.14) it follows that $V_y(x,y) \ge 0$ for all $(x,y) \in \mathcal{D}_{\overline{y}}^{+}$. Note also that, since $h(x,y) \le x$ and $g(x)$ is increasing in x then $g(h(x,y)) \le g(x)$ and $V_y(x,y) \le \frac{1}{\gamma\bar{y}}$ for all $(x,y) \in \mathcal{D}_{\overline{y}}^{+}$.

(iv) From evaluating (5.27) at $(x,\bar{y})$ and from the definition of h in Lemma 5.5, we get the result.

□

The next result shows the existence of a time instant at which the solutions, under an admissible control with finite cost, reach the region of the simplex where $R(x,y) < 1$ in finite time.

Lemma 5.9. *Let $u \in \mathcal{U}_{(x_0,y_0,\bar{y})}$ and let $(x(t),y(t))$ be the corresponding solution. Then,*

$$\int_0^{+\infty} u(t)dt < +\infty \;\Rightarrow\; \exists\, \bar{t}\ s.\ t.\ R(x(\bar{t}),y(\bar{t})) < 1\,.$$

Proof. Assume by contradiction that $R(x(t), y(t)) \geq 1$ for every time t and let $\bar{R}$ be the maximum of the function R over the compact set $\mathcal{S}$. Integrating the second equation in (5.8) and using the inequality

$$(1 - u(t))R(x(t), y(t)) - 1 \geq -u(t)R(x(t), y(t)) \geq -u(t)\bar{R}\,,$$

yields

$$\begin{aligned} y(t) &= y(0) \exp\left(\gamma \int_0^t ((1 - u(\tau))R(x(\tau), y(\tau)) - 1)\, \mathrm{d}\tau\right) \\ &\geq y(0) \exp\left(\gamma \bar{R} \int_0^t (-u(\tau))\, \mathrm{d}\tau\right)\,. \end{aligned}$$

Since $\lim_{t \to +\infty} y(t) = 0$ by Proposition 5.1(ii), we get that

$$J(u) = \lim_{t \to +\infty} \int_0^t u(\tau) d\tau = +\infty\,,$$

contradicting the assumption made. □

5.3.1 Proof of Theorem 5.1

We aim to apply the Hamilton-Jacobi-Bellman (HJB) approach (Liberzon, 2011; Kamalapurkar et al., 2018), which characterizes the optimal value function V^* as the unique solution of the HJB equation

$$\inf_{u \in \mathcal{U}_{(x_0, y_0, \bar{y})}} \{V_x(x, y)\dot{x} + V_y(x, y)\dot{y} + u\} = 0. \tag{5.29}$$

Under this framework, the candidate optimal control u^* is given by

$$u^* = \operatorname*{argmin}_{u \in \mathcal{U}_{(x_0, y_0, \bar{y})}} \{V_x(x, y)\dot{x} + V_y(x, y)\dot{y} + u\}\,. \tag{5.30}$$

The HJB theorem provides a necessary and sufficient condition for optimality, ensuring that if V is a $\mathcal{C}^1$ solution to the HJB equation, then the control u^* is optimal. However, in our setting, the function V is continuous on $\mathcal{D}_{\overline{y}}$ and $\mathcal{C}^1$ only on $\mathcal{D}_{\overline{y}}^+$. Indeed, for all $(x_0, y_0) \in \mathcal{D}_{\overline{y}}^-$, we have that $V_y(x_0, y_0) = 0$, while

$$\lim_{\substack{(x,\, y) \to (x_0,\, y_0) \\ (x,\, y) \in \mathcal{D}_{\overline{y}}^+}} V_y(x, y) = \frac{1}{\gamma y_0}\,,$$

then V is not $\mathcal{C}^1$ on all $\mathcal{D}_{\overline{y}}$. Consequently, we derive from scratch the proof of optimality.

Notice that when $R(1-\bar{y},\bar{y}) \leq 1$, we have that $R(x,y) < 1$ for every $y \geq \bar{y}$ and $x \in [0, 1-y]$, thanks to the monotonicity properties expressed in (5.9) and (5.10). Consequently, for every initial condition $(x_0, y_0) \in \mathcal{D}_{\overline{y}}$, indicated with $(x(t), y(t))$ the corresponding solution of (2.14), the peak of the function $y(t)$ is necessarily below $\bar{y}$ since, because of Proposition 2.4, it must necessarily happen at a location where $R = 1$ and $R(x,y) < 1$ for every $y \geq \bar{y}$.

We now assume that $R(1-\bar{y},\bar{y}) > 1$. Consider an initial state (x_0, y_0) in $D_{\overline{y}}$ and a admissible control signal u in $\mathcal{U}_{(x_0,y_0,\bar{y})}$ such that $J(u) < +\infty$. Let $(x(t), y(t))$, for $t \geq 0$, be the solution of (5.8) with initial state (x_0, y_0). It follows from Lemma 5.9 that necessarily there exists a finite time t° such that $(x(t^\circ), y(t^\circ)) \in \mathcal{D}_{\overline{y}}^-$. Let u° be the control signal defined as

$$u^\circ(t) = \begin{cases} u(t) & t \in [0, t^\circ), \\ 0 & t \in [t^\circ, +\infty). \end{cases}$$

Thanks to Lemma 5.4, $u^\circ \in \mathcal{U}_{(x_0,y_0,\bar{y})}$. Moreover,

$$J(u^\circ) = \int_0^{+\infty} u^*(t)\,\mathrm{d}t = \int_0^{t^\circ} u(t)\,\mathrm{d}t \leq \int_0^{+\infty} u(t)\,\mathrm{d}t = J(u)\,.$$

Let $(x^\circ(t), y^\circ(t))$, for $t \geq 0$, be the solution of (5.8) with initial state (x_0, y_0) and control u°. Notice that the function $t \mapsto V(x^\circ(t), y^\circ(t))$ is $\mathcal{C}^1$ except in a finite number of points where u° presents discontinuities and, possibly, in t°. Outside of these points, its time derivative can be computed as follows:

$$\begin{aligned} \dot{V}(x^\circ(t), y^\circ(t)) &= V_x(x^\circ, y^\circ)\dot{x}^\circ + V_y(x^\circ, y^\circ)\dot{y}^\circ \\ &= (\rho(x^\circ, y^\circ)\dot{x}^\circ + \dot{y}^\circ)V_y(x^\circ, y^\circ) \\ &= -\gamma y^\circ V_y(x^\circ, y^\circ)u^\circ\,, \end{aligned} \tag{5.31}$$

where the second equality follows from (5.28) and the last equality from (5.14), (5.8). Note that from (5.31) and Lemma 5.8(iii), it follows that for all $(x,y) \in \mathcal{D}_{\overline{y}}^+$,

$$0 \geq \dot{V}(x^\circ(t), y^\circ(t)) \geq -u^\circ(t)\,,$$

while from (5.31) and (5.26), $\dot{V} = 0$ for all $(x,y) \in \mathcal{D}_{\overline{y}}^-$. Then, $V(x^\circ(t), y^\circ(t))$ has bounded time derivative and thus it is absolutely continuous. Observe also that, by computing the time derivative of $V(x^*(t), y^*(t))$, as in (5.31), it follows from Lemma 5.8(iv) that for all $t \geq 0$ such that $y^*(t) = \overline{y}$,

$$\dot{V}(x^*(t), y^*(t)) = -u^*(t)\,,$$

while $\dot{V}(x^*(t), y^*(t)) = 0$ for all $t \geq 0$ such that $y^*(t) \leq \overline{y}$, since the candidate optimum $u^*(t)$ is 0.

For every time $T > 0$,

$$\int_0^T \dot{V}(x^\circ(t), y^\circ(t))dt + \int_0^T u^\circ(t)dt \geq \int_0^T \dot{V}(x^*(t), y^*(t))dt + \int_0^T u^*(t)dt$$

As all functions are absolutely continuous, the fundamental theorem of calculus holds and we can write

$$\int_0^T u^\circ(t)dt \geq \int_0^T u^*(t)dt + V(x^*(T), y^*(T)) - V(x^\circ(T), y^\circ(T))$$

Since both trajectories $(x^*(T), y^*(T))$ and $(x^\circ(T), y^\circ(T))$ live in $\mathcal{D}_{\overline{y}}^-$ for large T, it holds that

$$\lim_{T\to+\infty} V(x^*(T), y^*(T)) = \lim_{T\to+\infty} V(x^\circ(T), y^\circ(T)) = 0\,.$$

This yields the following inequalities

$$J(u) \geq J(u^\circ) \geq J(u^*)\,.$$

Therefore, we have shown that the functional cost resulting from the control u^* is less than or equal to the cost resulting from any other control u. In conclusion, $V(x, y)$ is the optimal cost and u^* is an optimal control.

5.4 Non-constant behavioral feedback transmission rate case

In this section, we concentrate on a special functional form of the transmission rate β, namely the one introduced in Example 2.1. Under this setting, the analysis developed in Section 2.3 allows for a substantial simplification of the optimal control problem. In particular, two key results enable this simplification: the existence of the invariant of motion described in equation (2.25), and the explicit characterization of the infection peak provided in equation (2.34).

These results permit a precise decomposition of the state space $\mathcal{D}_{\bar{y}}$ as follows:

$$\begin{aligned}\mathcal{D}_{\bar{y}}^- =& \{(x, y) \in \mathcal{D}_{\bar{y}} : R(x, y) > 1,\, \phi^{-1}(\psi(x, y)) \leq \bar{y}\} \cup \\ & \{(x, y) \in \mathcal{D}_{\bar{y}} : R(x, y) \leq 1 \text{ or } y = 0\},\\ \mathcal{D}_{\bar{y}}^+ =& \{(x, y) \in \mathcal{D}_{\bar{y}} : R(x, y) > 1, \phi^{-1}(\psi(x, y)) > \bar{y},\, y > 0\}.\end{aligned}$$

In this setting, the definition of the function h can be made explicit, thereby allowing for the direct computation of its partial derivatives and significantly simplifying the subsequent analysis. Let start by defining the function $\theta : [\overline{x}, 1 - \overline{y}] \to \mathbb{R}$ as

$$\theta(x) = \psi(x, \bar{y})\,, \qquad \forall x \in [\overline{x}, 1 - \overline{y}]\,. \tag{5.32}$$

where ψ is defined in (2.25). Since ψ is $\mathcal{C}^1$ on $\mathcal{S}_+$, so is θ on $[\overline{x}, 1-\overline{y}]$. From the second equation in (2.26) evaluated in $(x, \overline{y})$, we get

$$\theta'(x) = \psi_x(x, \overline{y}) = \rho(x, \overline{y})e^{-g(x)} > 0 \tag{5.33}$$

for every x in $(\overline{x}, 1-\overline{y}]$. Therefore, there exists a continuous inverse function $\theta^{-1} : (\psi(\overline{x}, \overline{y}), \psi(1-\overline{y}, \overline{y})] \to [\overline{x}, 1-\overline{y}]$ that is $\mathcal{C}^1$ on $(\psi(\overline{x}, \overline{y}), \psi(1-\overline{y}, \overline{y})]$. We can now define the function $h : \overline{\mathcal{D}_{\overline{y}}^+} \to [\overline{x}, 1-\overline{y}]$ as

$$h(x, y) = \theta^{-1}(\psi(x, y))\,. \tag{5.34}$$

Clearly, for every x in $[\overline{x}, 1-\overline{y}]$, we have

$$h(x, \overline{y}) = \theta^{-1}(\psi(x, \overline{y})) = x\,.$$

Moreover, since $\psi(x, y)$ is constant along the orbits of the uncontrolled dynamics by Proposition 2.5, so is $h(x, y) = \theta^{-1}(\psi(x, y))$. Notice that h is continuous on $\overline{\mathcal{D}_{\overline{y}}^+}$ since so are $\psi(x, y)$ on $\mathcal{S}_+$ and θ^{-1} on $[\psi(\overline{x}, \overline{y}), \psi(1-\overline{y}, \overline{y})]$. Similarly. h is $\mathcal{C}^1$ on $\mathcal{D}_{\overline{y}}^+$, since so are $\psi(x, y)$ on $\mathcal{S}_+$ and θ^{-1} on $(\psi(\overline{x}, \overline{y}), \psi(1-\overline{y}, \overline{y})]$. Hence, computing the partial derivatives in both sides of (5.34) yields

$$h_x(x, y) = \frac{\psi_x(x, y)}{\theta'(h(x, y))}\,, \quad h_y(x, y) = \frac{\psi_y(x, y)}{\theta'(h(x, y))}\,. \tag{5.35}$$

Substituting (2.26) and (5.33) in (5.35) we get

$$h_x(x, y) = \frac{\rho(x, y)e^{g(h(x,y))}}{\rho(h(x, y), \overline{y})e^{g(x)}}\,, \tag{5.36}$$

$$h_y(x, y) = \frac{e^{g(h(x,y))}}{\rho(h(x, y), \overline{y})e^{g(x)}}\,. \tag{5.37}$$

The explicit definition of the function h in (5.34) and its partial derivatives (5.36)-(5.37) makes it possible to simplify the analysis provided in Section 5.3 when the transmission rate β has the functional form described in Example 2.1.

5.5 Counterexample

In this subsection, we present a counterexample showing that the control strategy u^* is not always optimal. Consider the transmission rate given by

$$\beta(x, y) = \frac{1}{x}\left(\frac{y}{x} + 1\right)\,.$$

Given an initial condition $(x_0, y_0) \in \mathcal{S}_+$ with $x_0 > 0$, the corresponding Cauchy problem for the controlled system (5.1) admits a unique local solution $(x(t), y(t)) \in \mathcal{S}_+$ such that $x(t) > 0$ for all times. Note that this transmission function does not satisfy the

monotonicity conditions stated in (2.15) and (5.7), which were essential for proving the optimality of the filling-the-box strategy.

We begin by deriving the invariant of motion for the uncontrolled system under this choice of β. Then, we compare the trajectory under the control u^* with that resulting from an alternative candidate control. We will demonstrate that the value function associated with u^* is strictly larger, thus proving that u^* is not optimal in this case.

Lemma 5.10. *Let*

$$\beta(x,y) = \frac{1}{x}\left(\frac{y}{x}+1\right), \tag{5.38}$$

then the function

$$\psi(x,y) = -\frac{1}{2}\ln\left(\left(\frac{y}{x}+1\right)^2 - \gamma\right) - \ln x \tag{5.39}$$

is an invariant of motion of the uncontrolled model (2.5).

Proof. Note that equations (2.5) imply that the first time derivative of (5.39) is

$$\begin{aligned}
\dot{\psi} &= -\frac{1}{2}\frac{2\left(\frac{y}{x}+1\right)(\dot{y}x - y\dot{x})}{\left(\left(\frac{y}{x}+1\right)^2-\gamma\right)x^2} - \frac{\dot{x}}{x} \\
&= -\frac{\left(\frac{y}{x}+1\right)}{\left(\left(\frac{y}{x}+1\right)^2-\gamma\right)}\left(\frac{\left(\left(\frac{y}{x}+1\right)-\gamma\right)y}{x} + \frac{y^2\left(\frac{y}{x}+1\right)}{x^2}\right) - \frac{\dot{x}}{x} \\
&= -\frac{\left(\frac{y}{x}+1\right)}{\left(\left(\frac{y}{x}+1\right)^2-\gamma\right)}\left(\left(\frac{y}{x}+1\right) - \gamma + \frac{y}{x}\left(\frac{y}{x}+1\right)\right)\frac{y}{x} - \frac{\dot{x}}{x} \\
&= -\frac{\left(\frac{y}{x}+1\right)}{\left(\left(\frac{y}{x}+1\right)^2-\gamma\right)}\left(\left(\frac{y}{x}+1\right)^2 - \gamma\right)\frac{y}{x} - \frac{\dot{x}}{x} \\
&= -\frac{y}{x}\left(\frac{y}{x}+1\right) + \frac{\left(\frac{y}{x}+1\right)y}{x} = 0
\end{aligned}$$

which proves that (5.39) is an invariant of motion of (2.5) with $\beta(x,y)$ as in (5.38). □

Let us now consider a first policy for which the control is applied once the infection curve reaches a threshold $\bar{y}_1 < \tilde{y}$ and it is released when the fraction of susceptible individuals reaches $\bar{x}_1$, chosen so that the effective reproduction number satisfies $R(\bar{x}_1, \bar{y}_1) = 1$. The control function is defined as follows:

$$u_1(t) = \begin{cases} 0 & \text{if } y(t) < \bar{y}_1 \\ 1 - \frac{\gamma}{\beta(x(t),\bar{y}_1)x(t)} & \text{if } y(t) = \bar{y}_1 \end{cases} \tag{5.40}$$

The functional cost will be

$$\begin{aligned} J(u_1) &= \int_0^{\infty} u_1(t)dt \\ &= -\frac{1}{\gamma\bar{y}_1}\int_{x(t_1)}^{\bar{x}_1}\left(1-\frac{\gamma}{\frac{\bar{y}_1}{x}+1}\right)dx \\ &= -\frac{1}{\gamma\bar{y}_1}\Big[(1-\gamma)x+\gamma\bar{y}_1\ln(x+\bar{y}_1)\Big]_{x(t_1)}^{\bar{x}_1} \end{aligned}$$

where t_1 is the first time instant at which $y(t)=\bar{y}_1$.

We now consider a second control policy, analogous to the first one, but with an earlier intervention. In this case, the control is applied once the infection curve reaches the threshold $\bar{y}_2<\bar{y}_1$ and it is released when the fraction of susceptible individuals reaches $\bar{x}_2$, such that $R(\bar{x}_2,\bar{y}_2)=1$. The control strategy is defined as:

$$u_2(t)=\begin{cases}0 & \text{if } y<\bar{y}_2\\ 1-\frac{\gamma}{\beta(x(t),\bar{y}_2)x(t)} & \text{if } y(t)=\bar{y}_2\end{cases} \tag{5.41}$$

The functional cost in this case will be

$$\begin{aligned} J(u_2) &= \int_0^{\infty} u_2(t)dt \\ &= -\frac{1}{\gamma\bar{y}_2}\int_{x(t_2)}^{\bar{x}_2}\left(1-\frac{\gamma}{\frac{\bar{y}_2}{x}+1}\right)dx \\ &= -\frac{1}{\gamma\bar{y}_2}\Big[(1-\gamma)x+\gamma\bar{y}_2\ln(x+\bar{y}_2)\Big]_{x(t_2)}^{\bar{x}_2} \end{aligned}$$

where t_2 is the first time instant at which $y(t)=\bar{y}_2$. By comparing $J(u_1)$ and $J(u_2)$, we will show that the second policy results in a lower total cost, thereby demonstrating that u_1 (which corresponds to the filling-the-box strategy) is not optimal for this choice of β.

Observe that

$$\bar{x}_1=\frac{\bar{y}_1}{\gamma-1}\,,\qquad \bar{x}_2=\frac{\bar{y}_2}{\gamma-1}$$

therefore $\bar{x}_1>\bar{x}_2$ and after some calculations we can rewrite J_1 as

$$J_1=\frac{1}{\gamma}+\ln\left(\frac{\gamma-1}{\gamma}\frac{x(t_1)}{\bar{y}_1}+\frac{\gamma-1}{\gamma}\right)-\frac{\gamma-1}{\gamma}\frac{x(t_1)}{\bar{y}_1}\,.$$

Analogously, we can rewrite J_2 as

$$J_2=\frac{1}{\gamma}+\ln\left(\frac{\gamma-1}{\gamma}\frac{x(t_2)}{\bar{y}_2}+\frac{\gamma-1}{\gamma}\right)-\frac{\gamma-1}{\gamma}\frac{x(t_2)}{\bar{y}_2}\,.$$

From Lemma 5.10, (5.39) must be constant along the solutions. In order to find $x(t_1)$, impose now $\psi(x(t_1),\bar{y}_1)=\psi(x(0),y(0))$. We solve the resulting equation in terms of $x(t_1)$, by assuming an initial condition such that there are no recovered individuals, i.e.

$x(0) + y(0) = 1$. Then the steps follow as

$$\begin{aligned} -\ln\left(y_1^2 + 2y_1x(t_1) + x(t_1)^2 - \gamma x(t_1)^2\right) &= -\ln\left(1 - \gamma x_0^2\right) \\ y_1^2 + 2y_1x(t_1) + x(t_1)^2 - \gamma x(t_1)^2 &= 1 - \gamma x_0^2 \\ x(t_1)^2 - \frac{2}{\gamma - 1}\bar{y}_1 x(t_1) - \frac{\bar{y}_1^2 - 1 + \gamma x_0^2}{\gamma - 1} &= 0 \end{aligned}$$

Therefore,

$$x(t_1) = \frac{\bar{y}_1}{\gamma - 1} + \sqrt{\left(\frac{\bar{y}_1}{\gamma - 1}\right)^2 - \frac{\bar{y}_1^2 - 1 + \gamma x_0^2}{\gamma - 1}}$$

and then by dividing for $\bar{y}_1$ we obtain

$$\frac{x(t_1)}{\bar{y}_1} = \frac{1}{\gamma - 1} + \sqrt{\left(\frac{1}{\gamma - 1}\right)^2 - \frac{\bar{y}_1^2 - 1 + \gamma x_0^2}{(\gamma - 1)\bar{y}_1^2}} > \frac{1}{\gamma - 1}\,.$$

Since $\bar{y}_2 < \bar{y}_1$, then $x(t_2) > x(t_1)$. It follows that

$$\frac{x(t_1)}{\bar{y}_1} < \frac{x(t_2)}{\bar{y}_2}\,.$$

Consider the function $f(s) = \frac{1}{\gamma} + \ln\left(\frac{\gamma-1}{\gamma}s + \frac{\gamma-1}{\gamma}\right) - \frac{\gamma-1}{\gamma}s$, which is non-increasing for $s > \frac{1}{\gamma-1}$. It follows that

$$f\left(\frac{x(t_1)}{\bar{y}_1}\right) > f\left(\frac{x(t_2)}{\bar{y}_2}\right)$$

and this implies $J_1 > J_2$.

Therefore, we have provided an analytical counterexample showing that relaxing the monotonicity assumptions on the transmission rate may render the filling-the-box strategy suboptimal.

5.6 Generalizations

5.6.1 Alternative costs

In the optimal control problem analyzed above, the cost functional was defined as the time integral of the control $u(t)$, implicitly assuming that the social and economic cost of interventions is directly proportional to a reduction in the infection rate. While mathematically convenient, this assumption may be too simplistic. In practice, when infection levels are high, moderate measures can significantly reduce transmission at relatively low cost. Conversely, when infections are already rare, further reductions require more intrusive and costly interventions, leading to a steeper marginal cost. This motivates considering alternative formulations where the cost is weighted relative to the natural

transmission rate or to the perceived difficulty of further reducing infections. Such models better capture the diminishing returns of strict measures in low-risk contexts and encourage efficient resource allocation, while also altering the structure of the optimal control and leading to more state-dependent intervention strategies.

We still consider an exogenous control input, representing a policy level available to a social planner, which modulates the intensity of social interactions and thus mitigates disease transmission. The controlled epidemic dynamics are now described by:

$$\begin{cases} \dot{x} = -(\beta(x,y) - u)xy, \\ \dot{y} = (\beta(x,y) - u)xy - \gamma y. \end{cases} \tag{5.42}$$

where $\beta : [0,1]^2 \to (0, +\infty)$, defined as in previous sections, models the endogenous behavioral response to the epidemic through variations in the effective transmission rate, satisfying (5.6)–(5.7). The control $u : \mathbb{R}_+ \to [0, \beta(x,y)]$ represents the level of intervention (e.g., lockdown or social distancing) implemented by the planner, with the maximum admissible intensity directly determined by the current transmission rate $\beta(x,y)$. We focus on the scenario where the planner's goal is to keep the fraction of infected individuals $y(t)$ below a fixed threshold $\bar{y} \leq 1$. For an initial condition (x_0, y_0) in the domain $\mathcal{D}_{\bar{y}}$, defined in (5.11) that is the portion of state space below this threshold, we then consider the set $\mathcal{U}_{(x_0,y_0,\bar{y})}$ as the set of admissible control functions ensuring that $y(t) \leq \bar{y}$ for all $t \geq 0$. This set is never empty, since it contains the control $u \equiv \beta(x,y)$, corresponding to a complete lockdown.

To model the economic impact of interventions, we define the cost functional $J : \mathcal{U}_{(x_0,y_0,\bar{y})} \to [0, +\infty]$ defined by

$$J(u) = \int_0^{+\infty} \frac{u(t)}{\beta(x(t), y(t))}\, dt\,,$$

which measures the relative intensity of the control compared to the natural transmission rate. The optimal control problem can then be stated as:

$$V^*(x_0, y_0) = \min_{u \in \mathcal{U}_{(x_0,y_0,\bar{y})}} J(u)\,. \tag{5.43}$$

As before, we can rewrite the first two equations in (5.42) in $\mathcal{S}$ in terms of the behavioral reproduction number $R(x,y)$, defined in (2.13), as follows

$$\begin{cases} \dot{x} = -\gamma(R(x,y) - u\frac{x}{\gamma})y, \\ \dot{y} = \gamma[(R(x,y) - u\frac{x}{\gamma}) - 1]y. \end{cases} \tag{5.44}$$

Under these assumptions, the qualitative properties of the uncontrolled dynamics, as well as the geometric considerations on the state space, can be recovered with minimal modifications. Moreover, it can be shown that there exists an optimal control $u^* \in \mathcal{U}_{(x_0,y_0,\bar{y})}$ such that, if $(x^*(t), y^*(t))$ is the corresponding optimal trajectory for (5.44),

then u^* can be expressed in feedback form as:

$$u^*(t) = \mu\big(x^*(t), y^*(t)\big), \quad t \geq 0, \tag{5.45}$$

where the feedback law $\mu : \mathcal{S} \to [0,1]$ is now given by:

$$\mu(x,y) = \begin{cases} 0, & \text{if } y < \bar{y}, \\ \beta(x,\bar{y}) - \dfrac{\gamma}{x}, & \text{if } y = \bar{y}. \end{cases} \tag{5.46}$$

This new formulation normalizes the control cost with respect to the natural transmission rate, reflecting that the marginal effort to further reduce infections increases as the transmission rate decreases. The core idea of the optimal control policy remains to minimize intervention efforts while keeping the infection level below the prescribed threshold. Consequently, the optimal policy tends to avoid excessive measures in low-risk scenarios and applies stronger controls only when the infection level approaches the threshold $\bar{y}$.
In this setting, we can rely on the same candidate value function $V : \mathcal{D}_{\bar{y}} \to \mathbb{R}$ introduced in (5.26), and adapt the optimality proof previously established to the present formulation. Consider an initial state $(x_0, y_0) \in \mathcal{D}_{\bar{y}}$ and an admissible control signal $u \in \mathcal{U}_{(x_0,y_0,\bar{y})}$ such that $J(u) < +\infty$. Let $(x(t), y(t))$, for $t \geq 0$, be the trajectory of (5.44) starting from (x_0, y_0). From Lemma 5.9, there exists a finite time t° such that $(x(t^\circ), y(t^\circ)) \in \mathcal{D}_{\bar{y}}^-$. As in the previous analysis, we define a truncated control signal

$$u^\circ(t) = \begin{cases} u(t) & t \in [0, t^\circ), \\ 0 & t \in [t^\circ, +\infty)\,. \end{cases}$$

which, by Lemma 5.4, still belongs to $\mathcal{U}_{(x_0,y_0,\bar{y})}$. Moreover,

$$J(u^\circ) = \int_0^{+\infty} u^*(t)\,\mathrm{d}t = \int_0^{t^\circ} u(t)\,\mathrm{d}t \leq \int_0^{+\infty} u(t)\,\mathrm{d}t = J(u)\,.$$

Let again $(x^\circ(t), y^\circ(t))$, for $t \geq 0$, be the solution of (5.8) with initial state (x_0, y_0) and control u°. Where the function $t \mapsto V(x^\circ(t), y^\circ(t))$ is differentiable, we can compute the derivative exactly as in the previous analysis, but with the modified analysis. From relations (5.28), (5.14), (5.44) we obtain

$$\begin{aligned} \dot{V}(x^\circ(t), y^\circ(t)) &= V_x(x^\circ, y^\circ)\dot{x}^\circ + V_y(x^\circ, y^\circ)\dot{y}^\circ \\ &= (\rho(x^\circ, y^\circ)\dot{x}^\circ + \dot{y}^\circ)V_y(x^\circ, y^\circ) \\ &= -\gamma y^\circ V_y(x^\circ, y^\circ)\frac{u^\circ}{\beta(x^\circ, y^\circ)} \\ &\geq -\frac{y^\circ}{\bar{y}}\frac{u^\circ}{\beta(x^\circ, y^\circ)}\,. \end{aligned} \tag{5.47}$$

Note that from (5.47) and Lemma 5.8(iii), it follows that for all $(x, y) \in \mathcal{D}_{\overline{y}}^{+}$,

$$0 \geq \dot{V}(x^{\circ}(t), y^{\circ}(t)) \geq -\frac{u^{\circ}(t)}{\beta(x^{\circ}(t), y^{\circ}(t))}\,.$$

Since $\dot{V} = 0$ for $(x, y) \in \mathcal{D}_{\overline{y}}^{-}$, we again conclude that $V(x^{\circ}(t), y^{\circ}(t))$ has bounded derivative and is absolutely continuous. For the candidate optimal control $u^{(}t)$, Lemma 5.8(iv) implies that whenever $y^{*}(t) = \overline{y}$ we have

$$\dot{V}(x^{*}(t), y^{*}(t)) = -\frac{u^{*}(t)}{\beta(x^{*}(t), y^{*}(t))}\,,$$

while $\dot{V}(x^{*}(t), y^{*}(t)) = 0$ for all $t \geq 0$ such that $y^{*}(t) \leq \overline{y}$, since $u^{*}(t)$ is 0. Repeating the comparison argument from the previous proof, we obtain

$$J(u) \geq J(u^{\circ}) \geq J(u^{*})\,.$$

Thus, the cost achieved by u^{*} is minimal among all admissible controls, and $V(x, y)$ coincides with the optimal cost function also in this setting.

5.6.2 Partial compliance to control measures

In the previous sections, the control input was assumed to mitigate social interactions for the entire population. However, in real-world settings, interventions such as mobility restrictions or mask mandates are often subject to partial compliance: only a fraction of individuals adopt the recommended behaviors, due to factors like personal beliefs, economic constraints, and enforcement challenges. From a modeling perspective, this heterogeneity has two key implications. First, the effective reduction in the transmission is generally lower than in the idealized full-compliance case, even for the same nominal control intensity. Second, the epidemic dynamics now depend on the interactions between two distinct subpopulations: a compliant group, whose contacts are attenuated by the intervention and a non-compliant group, whose interactions remain largely unaffected. To capture this phenomenon, we introduce an explicit partition of the population into compliant and non-compliant individuals, each with their own susceptible and infected compartments. Let $\rho_c \in [0, 1]$ be the fixed fraction of the population that is compliant and subject to control, while the remaining fraction $1 - \rho_c$ is non-compliant and does not modify their behavior regardless of $u(t)$. Hence, the state variables satisfy

$$x_c(t) + y_c(t) = \rho_c, \quad x_u(t) + y_u(t) = 1 - \rho_c, \tag{5.48}$$

where (x_u, y_u) denote the fraction of susceptibles and infected individuals who behave uncontrolled, while (x_c, y_c) denote the corresponding fractions for those who comply with the policy. We denote the control function by $u : \mathbb{R}_{+} \to [0, 1]$, which represents the fraction by which the transmission rate is reduced for compliant individuals (e.g., $u = 0$ means no intervention, $u = 1$ means complete suppression of contacts for the compliant

group). Given a constant interaction matrix $A : [0,1]^2 \to \mathbb{R}^{2\times 2}$, the dynamics can be formulated as:

$$\begin{cases} \dot{x}_u = -x_u \sum_{j\in\{u,c\}} A_{uj}\, y_j, \\ \dot{x}_c = -(1-u)x_c \sum_{j\in\{u,c\}} A_{cj}\, y_j, \\ \dot{y}_u = x_u \sum_{j\in\{u,c\}} A_{uj}\, y_j - \gamma y_u, \\ \dot{y}_c = (1-u)x_c \sum_{j\in\{u,c\}} A_{cj}\, y_j - \gamma y_c. \end{cases} \tag{5.49}$$

We now formulate the associated optimal control problem. The planner's objective is to keep the total fraction of infected individuals $y_u(t) + y_c(t)$ below a specified threshold $\bar{y} \leq 1$, while minimizing the economic cost of interventions. We define

$$\mathcal{D}_{\bar{y}} = \{(x_u, x_c, y_u, y_c) \in \mathcal{S} : 0 < y_u + y_c \leq \bar{y}\} \tag{5.50}$$

the admissible set of states. For a given initial condition $s_0 = (x_u(0), x_c(0), y_u(0), y_c(0)) \in \mathcal{D}_{\bar{y}}$, we denote by $\mathcal{U}_{(s_0,\bar{y})}$ the set of piecewise continuous control functions $u : \mathbb{R}_+ \to [0,1]$ such that the solution of (5.49) satisfies

$$(x_u(t), x_c(t), y_u(t), y_c(t)) \in \mathcal{D}_{\bar{y}}, \quad \forall t \geq 0 \tag{5.51}$$

The cost functional is given by

$$J(u) = \int_0^{+\infty} u(t)\, dt \tag{5.52}$$

and the optimal control problem reads

$$V^*(s_0) = \min_{u\in\mathcal{U}_{(s_0,\bar{y})}} J(u) \tag{5.53}$$

It is important to observe that, in this setting, we cannot guarantee a priori that the admissible set $\mathcal{D}_{\bar{y}}$ is non-empty. Indeed, the control $u(t)$ acts only on the compliant fraction of the population, while the non-compliant individuals continue to follow the uncontrolled dynamics. If the compliant group is too small, the uncontrolled infections in the remaining population may prevent the threshold $\bar{y}$ from being satisfied for all time, regardless of the control intensity applied to the compliant group. It is crucial to emphasize the role of the initial condition of the non-compliant subpopulation in determining whether the epidemic can be effectively controlled. In particular, if the non-compliant group, evolving in isolation (i.e., without any control intervention), exhibits an infection peak strictly below the threshold $\bar{y}$, then applying maximal control $u \equiv 1$ to the compliant subpopulation can completely suppress the epidemic within that group. In this case, the admissible set is non-empty, meaning that it is possible to keep the total infected fraction below the threshold with a suitable control policy. To illustrate this, we consider two simulation

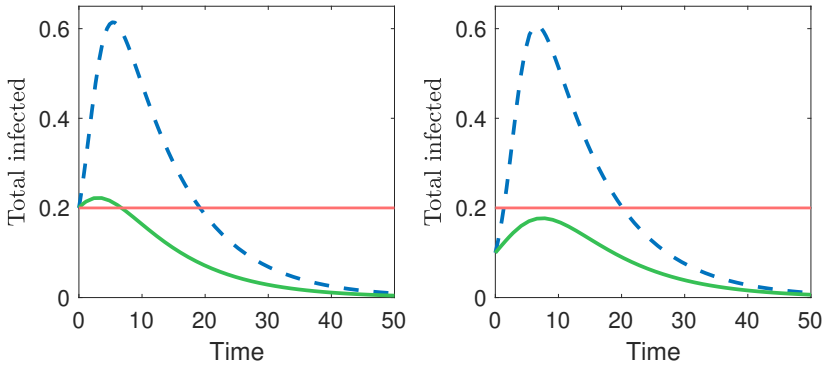

FIGURE 5.3: Comparison of two scenarios with different initial infections in the non-compliant group and a total lockdown is applied ($u \equiv 1$). On the left, the controlled total infected curve remains below the threshold $\bar{y} = 0.2$, illustrating a non-empty admissible set $\mathcal{D}_{\bar{y}}$. While on the right plot, the initial infection in the non-compliant group is high, causing the controlled total infection to exceed the threshold. In both plots, the green curve represents the controlled dynamics with maximal control $u \equiv 1$, the red horizontal line indicates the threshold $\bar{y}$, and the blue dashed curve shows the uncontrolled infection dynamics.

scenarios, illustrated in Figure 5.3. In the left plot, the initial conditions satisfy the above property, so that maximal control on the compliant group ensures that the total infected fraction remains below $\bar{y}$, corresponding to $\mathcal{D}_{\bar{y}} \neq \emptyset$. In the right plot, the initial infected fraction in the non-compliant group is sufficiently large to produce a peak exceeding the threshold $\bar{y}$, regardless of the control applied to the compliant group. These simulations highlight that the feasibility of keeping infections below the threshold crucially depends on the initial conditions of the non-compliant group. Building on this observation, one could extend the analysis in previous sections to a two-node network setting, where the two subpopulations represent the compliant and non-compliant groups and investigate whether the optimal control strategies derived in the previous sections remain effective when starting from feasible initial conditions. A natural extension of this work would be to explore time-varying compliance rates, allowing individuals to switch between compliant and non-compliant states in response to the epidemic evolution or external incentives. Another promising direction is the characterization of $\mathcal{D}_{\bar{y}}$ under stochastic infection dynamics or network-based contact structures, to assess robustness of the control policy in more realistic heterogeneous settings.

In this chapter, we investigated an optimal control problem for the behavioral-feedback SIR model, with the goal of containing infection levels below a prescribed threshold while minimizing the associated socio-economic costs of interventions. We began in Section 5.2 with a geometric analysis of the state space associated with the uncontrolled dynamics. This allowed us to characterize the structure of the admissible region, to describe how epidemic trajectories evolve within it, and to introduce a candidate value function quantifying the minimum cumulative cost required to keep the infection below the threshold from any initial condition. Building on this foundation, in Section 5.3 we showed that, under mild monotonicity assumptions, the optimal control strategy follows the *filling-the-box* pattern: interventions are delayed until they become strictly necessary, then a sharp reduction of the transmission rate is applied to prevent the infection from exceeding

the threshold, followed by a gradual relaxation of control as the epidemic subsides. This pattern captures in a simple and intuitive way the trade-off between public health protection and socio-economic burden. In Section 5.4, we focused on a special non-constant functional form of the transmission rate, which made it possible to refine the previous analysis and to provide a more explicit characterization of the optimal control strategy. This case study highlighted how the precise structure of optimal policies is shaped by the parametrization of behavioral feedback. However, as shown in Section 5.5, the *filling-the-box* strategy is not universally valid: when behavioral feedback mechanisms do not satisfy the required monotonicity conditions, the structure of the optimal solution may break down. This result underscores the importance of adaptive control designs that can accommodate richer behavioral responses. Finally, in Section 5.6 we outlined possible extensions of this framework, such as considering alternative cost structures, or partial compliance to control measures. These directions open a broader line of research aimed at capturing the complexity of epidemic–behavior interactions and at designing intervention strategies that are not only effective in controlling disease spread but also sustainable in the long run.

6 Conclusion

6.1 Summary

This thesis investigates the dynamics of the SIR epidemic model under the influence of both behavioral feedback and network effects, with the overarching goal of understanding how these two factors shape the progression of an epidemic and how such dynamics can be controlled more effectively. By incorporating these elements into the traditional epidemic framework, we provide a more nuanced understanding of disease spread and its potential mitigation.

We began in Chapter 2 by revisiting the classical scalar SIR model and introducing an extended formulation in which the transmission rate depends dynamically on both the susceptible and infected individuals. This extension captures endogenous behavioral adaptations in response to the epidemic, such as voluntary distancing or changes in risk perception. Within this framework, we derived a generalized reproduction number and showed that, under a broad monotonicity condition, the infection curve is guaranteed to be unimodal, meaning it can show at most one peak. We also identified an invariant of motion that allows for a closed-form characterization of both the peak and final size of the epidemic. A key insight from this analysis is the explicit determination of the maximum number of infected individuals, which is of central importance for public health decision-making. Indeed, policymakers often aim to ensure that this peak remains below a predefined threshold representing the healthcare system's capacity to deliver effective care without being overwhelmed. In Chapter 5, we addressed this issue by formulating an optimal control problem that incorporates the healthcare capacity constraint, with the goal of keeping infection levels below critical thresholds while minimizing the associated socio-economic costs. Through a geometric analysis of the constrained state space, we characterize the structure of optimal control policies and identify a "filling-the-box" strategy as optimal under general monotonicity assumptions. However, we also demonstrated through counterexamples that this strategy may fail in certain cases, emphasizing the importance of incorporating adaptive behavioral responses in the design of effective mitigation policies. These findings underscore the necessity of considering both public health and economic factors when formulating control strategies during an epidemic.

Building on this previous analysis, Chapter 3 introduces a network-based formulation

of the behavioral-feedback SIR model, in which individuals are grouped into subpopulations, each represented as a node in the network, with distinct behavioral and epidemiological characteristics. Interactions across subpopulations are described by a time-varying interaction matrix, which may adapt dynamically in response to the evolving epidemic state. This network perspective allows us to explore how local adaptations, contact heterogeneity, and varying risk perceptions across subpopulations influence both the global and local dynamics of disease spread. In particular, we examine the system's equilibrium stability under behavioral feedback and we derive invariants of motion and final epidemic states for specific interaction structures, such as constant rank-1 matrices.

Chapter 4 shifts focus to the transient phase of the epidemic, where we present new theoretical results under the assumption of constant rank-1 interaction matrices. Specifically, we show that a weighted aggregate of infected individuals exhibits unimodal behavior over time, thereby generalizing the classical results of the scalar SIR epidemic model. We also explore the dynamics at the single node level, proving that the infection curve for each subpopulation can undergo at most two changes in monotonicity. Complementing the theoretical analysis, numerical simulations illustrate that interaction matrices of higher rank can give rise to more complex and even multimodal transient dynamics. Building on these findings, we extend the analysis to more general behavioral-feedback models, identifying conditions under which unimodality at the aggregate level can still be preserved.

Overall, this thesis contributes to a deeper theoretical understanding of epidemic dynamics in networked and adaptive populations. By integrating behavioral feedback and network-based heterogeneity, we offer new modeling frameworks and analytical tools to study the spread and control of infectious diseases in realistic settings where human behavior and contact patterns are intrinsically coupled.

6.2 Future research lines

This work lays the foundation for several promising directions of future research, aimed at improving the way we model behavioral responses and networked interactions in epidemic dynamics. Although our current framework incorporates feedback through a state-dependent transmission rate, several open challenges remain in capturing how individuals and groups adapt their behavior in response to perceived risk.

A natural next step is to refine how people perceive epidemic risk and how this perception shapes their behavioral choices. In real-world situations, individuals rarely respond to the actual real-time number of infected individuals. Instead, their behavior is often influenced by delayed or aggregated information, which may be shaped by media coverage, public communication, or social networks. Inspired by the works of (Funk et al., 2010; Bizyaeva et al., 2024; Zhou et al., 2020), a valuable extension would be to model the transmission rate as a function of an *observed* fraction of infected individuals, possibly incorporating delays or smoothing effects. This would allow us to capture realistic response delays and study their impact on epidemic dynamics, such as the emergence of

oscillatory behaviors or secondary waves of infection, beyond what network heterogeneity alone can explain. Explicitly introducing time delays in the behavioral feedback could provide a principled way to study cycles of resurgence and control, often observed in real-world outbreaks.

Another fruitful direction is to couple epidemic dynamics with models of opinion formation and information spread. Individual decisions are influenced not only by epidemiological data, but also by beliefs, trust, peer influence, and exposure to (mis)information. Integrating epidemic models with opinion dynamics frameworks (e.g., DeGroot, Friedkin–Johnsen, Altafini) could enable a richer analysis of how public sentiment, social learning, or misinformation affect vaccination uptake, compliance with public health measures, or resistance to interventions. Such integrated models could also inform optimal strategies for information-based control, including awareness campaigns and trust-building measures.

A further promising avenue is the extension to more complex and realistic compartmental models. In particular, the SIRS model, where immunity wanes and recovered individuals may become susceptible again, offers a natural generalization of our analysis. The inclusion of reinfection dynamics would allow us to explore persistent or recurrent outbreaks and their interplay with behavioral adaptation. Preliminary studies such as Zhang and Pan (2021) and Li et al. (2014) have examined SIRS epidemic models on complex networks, showing how layered structure and heterogeneity affect epidemic persistence. Building on these works, future research could investigate how behavioral feedback modifies the long-term behavior and stability properties of SIRS models, and whether analytical techniques developed here for the classical SIR case can be extended or adapted to this richer setting.

Finally, exploring behavioral feedback in multilayer networks is a critical step toward more realistic modeling. Real-world contact structures are layered across multiple domains (e.g., households, workplaces, transportation systems, and online networks), each with distinct behavioral and epidemiological dynamics. Understanding how local behavioral adaptations interact across layers, and how these shape global epidemic outcomes, could lead to improved strategies for targeted, context-sensitive interventions.

Together, these future directions aim to bridge the gap between theoretical models and the complex, adaptive behaviors observed in real societies. By incorporating more realistic behavioral assumptions and network structures, we aim to develop more accurate and useful tools for forecasting, managing, and ultimately controlling infectious disease outbreaks.

Bibliography

Abbey, H. (1952). "An examination of the Reed-Frost theory of epidemics". In: *Human biology* 24.3, p. 201 (cit. on p. 3).

Acemoglu, D., V. Chernozhukov, I. Werning, and M. D Whinston (2021). "Optimal targeted lockdowns in a multigroup SIR model". In: *American Economic Review: Insights* 3.4, pp. 487–502 (cit. on pp. 10, 39, 44, 63).

Acemoglu, D., A. Fallah, A. Giometto, D. Huttenlocher, A. Ozdaglar, F. Parise, and S. Pattathil (2024). "Optimal adaptive testing for epidemic control: Combining molecular and serology tests". In: *Automatica* 160, p. 111391. ISSN: 0005-1098. DOI: https://doi.org/10.1016/j.automatica.2023.111391 (cit. on p. 11).

Ahn, H. J. and B. Hassibi (2013). "Global dynamics of epidemic spread over complex networks". In: *52nd IEEE Conference on Decision and Control (CDC)*. IEEE, pp. 4579–4585 (cit. on p. 5).

Allen, L. J. (1994). "Some discrete-time SI, SIR, and SIS epidemic models". In: *Mathematical biosciences* 124.1, pp. 83–105 (cit. on p. 5).

Alutto, M., L. Cianfanelli, G. Como, and F. Fagnani (2025a). "Behavioral-Feedback Network SIR Model". In preparation (cit. on p. 13).

Alutto, M., L. Cianfanelli, G. Como, F. Fagnani, and F. Parise (2025b). "Behavioral-Feedback SIR Epidemic Model: Analysis and Control". Submitted (cit. on pp. 12, 14).

— (2025c). "Optimal Control for Behavioral-Feedback SIR Epidemic Model". In preparation (cit. on p. 14).

Alutto, M., L. Cianfanelli, G. Como, and F. Fagnani (2024). "On the Dynamic Behavior of the Network SIR Epidemic Model". In: *IEEE Transactions on Control of Network Systems*, pp. 1–12. DOI: 10.1109/TCNS.2024.3448136 (cit. on p. 13).

Alutto, M., G. Como, and F. Fagnani (2021). "On SIR epidemic models with feedback-controlled interactions and network effects". In: *60th IEEE Conference on Decision and Control (CDC)*, pp. 5562–5567 (cit. on p. 12).

Alvarez, F. E., D. Argente, and F. Lippi (2021). *A Simple Planning Problem for COVID-19 Lock-down, Testing, and Tracing.* Tech. rep. 3. American Economic Review: Insights, pp. 367–82 (cit. on p. 10).

Amaral, M. A., M. M. de Oliveira, and M. A. Javarone (2021). "An epidemiological model with voluntary quarantine strategies governed by evolutionary game dynamics". In: *Chaos, Solitons & Fractals* 143, p. 110616 (cit. on p. 7).

Anderson, R. M. and R. M. May (1991). *Infectious diseases of humans: dynamics and control*. Oxford university press (cit. on p. 5).

Andersson, H. and T. Britton (2012). *Stochastic epidemic models and their statistical analysis*. Vol. 151. Springer Science & Business Media (cit. on p. 4).

Bacciotti, A. (2006). *Analisi della stabilità*. Ed. by P. Editrice (cit. on p. 36).

Bailey, N. T. (1975). *The mathematical theory of infectious diseases and its applications.* (Cit. on p. 4).

Baker, R. (2020). "Reactive Social Distancing in a SIR Model of Epidemics such as COVID-19". In: *arXiv preprint arXiv:2003.08285* (cit. on pp. 8, 20, 78).

Behncke, H. (2000). "Optimal control of deterministic epidemics". In: *Optimal control applications and methods* 21.6, pp. 269–285 (cit. on p. 10).

Bernoulli, D (1760). "Essai d'une nouvelle analyse de la mortalite causee par la petite verole, et des avantages de l'inoculation pour la prevenir". In: *Histoire de l'Acad., Roy. Sci.(Paris) avec Mem*, pp. 1–45 (cit. on p. 3).

Birge, J. R., O. Candogan, and Y. Feng (2020). "Controlling epidemic spread: reducing economic losses with targeted closures". In: *University of Chicago, Becker Friedman Institute for Economics Working Paper* 2020-57 (cit. on p. 10).

Bizyaeva, A., M. O. Arango, Y. Zhou, S. Levin, and N. E. Leonard (2024). "Active risk aversion in SIS epidemics on networks". In: *2024 American Control Conference (ACC)*. IEEE, pp. 4428–4433 (cit. on pp. 9, 45, 104).

Blanchini, F. and S. Miani (Jan. 2007). *Set-Theoretic Methods in Control*. ISBN: 9780817632557. DOI: 10.1007/978-0-8176-4606-6 (cit. on p. 33).

Boatto, S., C. Bonnet, B. Cazelles, and F. Mazenc (2018). *SIR model with time dependent infectivity parameter: approximating the epidemic attractor and the importance of the initial phase*. Working Paper hal-01677886. HAL Open Science, version 1. CNRS. URL: https://hal.science/hal-01677886 (cit. on p. 9).

Bootsma, M. C. and N. M. Ferguson (2007). "The effect of public health measures on the 1918 influenza pandemic in US cities". In: *Proceedings of the National Academy of Sciences* 104.18, pp. 7588–7593 (cit. on p. 7).

Brauer, F., C. Castillo-Chavez, and Z. Feng (2019). "Mathematical Models in Epidemiology". In: *Texts in Applied Mathematics* (cit. on pp. 5, 15–18).

Britton, T. (2010). "Stochastic epidemic models: a survey". In: *Mathematical biosciences* 225.1, pp. 24–35 (cit. on p. 3).

Canuto, C. and A. Tabacco (2015). *Mathematical Analysis II*. Vol. 85. Springer (cit. on pp. 83, 85).

Capasso, V. and G. Serio (1978). "A generalization of the Kermack-McKendrick deterministic epidemic model". In: *Mathematical Biosciences* 42.1, pp. 43–61. ISSN: 0025-5564. DOI: https://doi.org/10.1016/0025-5564(78)90006-8 (cit. on p. 8).

Castellano, C., S. Fortunato, and V. Loreto (2009). "Statistical physics of social dynamics". In: *Reviews of Modern Physics* 81.2, p. 591 (cit. on p. 7).

Certório, J., N. C. Martins, and R. J. La (2022). "Epidemic Population Games With Nonnegligible Disease Death Rate". In: *IEEE Control Systems Letters* 6, pp. 3229–3234. DOI: 10.1109/LCSYS.2022.3183477 (cit. on p. 7).

Cianfanelli, L., F. Parise, D. Acemoglu, G. Como, and A. Ozdaglar (2021a). "Lockdown Interventions in the SIR Model: Is the Reproduction Number the Right Control Variable?" In: *60th IEEE Conference on Decision and Control (CDC)*, pp. 4254–4259 (cit. on p. 43).

Cianfanelli, L., F. Parise, D. Acemoglu, G. Como, and A. Ozdaglar (2021b). "Lockdown interventions in SIR models: Is the reproduction number the right control variable?" In: *60th IEEE Conference on Decision and Control (CDC)*. IEEE, pp. 4254–4259 (cit. on pp. 10, 45).

Crosby, A. W. (2003). *America's Forgotten Pandemic: The Influenza of 1918*. Cambridge University Press (cit. on p. 7).

Daley, D. J. and J. M. Gani (2001). *Epidemic modelling: an introduction*. 15. Cambridge university press (cit. on p. 3).

Das, H. K. and L. M. Stolerman (2024). "Epidemic Thresholds and Disease Dynamics in Metapopulations: The Role of Network Structure and Human Mobility". In: *SIAM Journal on Applied Dynamical Systems* 23.2, pp. 1579–1609 (cit. on p. 6).

Di Lauro, F., I. Z. Kiss, D. Rus, and C. Della Santina (2020). "Covid-19 and flattening the curve: A feedback control perspective". In: *IEEE Control Systems Letters* 5.4, pp. 1435–1440 (cit. on p. 11).

Diekmann, O. and J. A. P. Heesterbeek (2000). *Mathematical Epidemiology of Infectious Diseases: Model Building, Analysis and Interpretation*. Wiley (cit. on p. 15).

Diekmann, O., J. Heesterbeek, and J. Metz (Jan. 1995). "The Legacy of Kermack and McKendrick". In: *Epidemic Models: Their Structure and Relation to Data* (cit. on p. 4).

Diekmann, O., J. A. P. Heesterbeek, and M. G. Roberts (2010). "The construction of next-generation matrices for compartmental epidemic models". In: *Journal of the royal society interface* 7.47, pp. 873–885 (cit. on p. 15).

Djidjou-Demasse, R., Y. Michalakis, M. Choisy, M. T. Sofonea, and S. Alizon (2020). "Optimal COVID-19 epidemic control until vaccine deployment". In: *MedRxiv*, pp. 2020–04 (cit. on p. 11).

Ellison, G. (2020). *Implications of Heterogeneous SIR Models for Analyses of COVID-19*. Working Paper 27373. National Bureau of Economic Research (cit. on pp. 6, 39, 43, 45).

Elokda, E., S. Bolognani, and A. R. Hota (2021). "A dynamic population model of strategic interaction and migration under epidemic risk". In: *2021 60th IEEE Conference on Decision and Control (CDC)*. IEEE, pp. 2085–2091 (cit. on p. 8).

En'ko, P. D. (1989). "On the course of epidemics of some infectious diseases." In: 18 (4), 749–755. ISSN: 1464-3685 0300-5771. DOI: 10.1093/ije/18.4.749 (cit. on p. 3).

Ethier, S. N. and T. G. Kurtz (2009). *Markov processes: characterization and convergence*. John Wiley & Sons (cit. on p. 4).

Fall, A., A. Iggidr, G. Sallet, and J. J. Tewa (2007). "Epidemiological Models and Lyapunov Functions". In: *Math. Model. Nat. Phenom.* 2.1, pp. 62–83. DOI: 10.1051/mmnp:2008011. URL: https://doi.org/10.1051/mmnp:2008011 (cit. on pp. 5, 6).

Feng, Z. (2007). "Final and peak epidemic sizes for SEIR models with quarantine and isolation". In: *Mathematical Biosciences & Engineering* 4.4, pp. 675–686 (cit. on pp. 19, 42).

Feng, Z. and H. R. Thieme (2000). "Endemic models with arbitrarily distributed periods of infection I: fundamental properties of the model". In: *SIAM Journal on Applied Mathematics* 61.3, pp. 803–833 (cit. on p. 8).

Ferguson, N. (2007). "Capturing human behaviour". In: *Nature* 446.7137, pp. 733–733 (cit. on p. 7).

Ferguson, N., D. Laydon, G. Nedjati-Gilani, N. Imai, K. Ainslie, M. Baguelin, S. Bhatia, A. Boonyasiri, Z. Cucunubá, G. Cuomo-Dannenburg, et al. (2020). "Report 9: Impact of non-pharmaceutical interventions (NPIs) to reduce COVID19 mortality and healthcare demand". In: *Imperial College London* 10.77482, pp. 491–497 (cit. on p. 10).

Flaxman, S., S. Mishra, A. Gandy, H. J. T. Unwin, T. A. Mellan, H. Coupland, C. Whittaker, H. Zhu, T. Berah, J. W. Eaton, et al. (2020). "Estimating the effects of non-pharmaceutical interventions on COVID-19 in Europe". In: *Nature* 584.7820, pp. 257–261 (cit. on p. 9).

Franco, E. (2020). "A feedback SIR (fSIR) model highlights advantages and limitations of infection-dependent mitigation strategies". In: *arXiv preprint arXiv:2004.13216* (cit. on pp. 8, 20, 78).

Frieswijk, K., L. Zino, M. Ye, M. Cao, and A. Rizzo (2022). "A mean-field analysis of a network behavioural-epidemic model". In: *IEEE Control Systems Letters* 6, pp. 2533–2538 (cit. on pp. 7, 8).

Funk, S., M. Salathé, and V. A. Jansen (2010). "Modelling the influence of human behaviour on the spread of infectious diseases: a review". In: *Journal of the Royal Society Interface* 7.50, pp. 1247–1256. DOI: 10.1098/rsif.2010.0142 (cit. on pp. 8, 104).

Gao, W., Y. Wang, J. Cao, and Y. Liu (2024). "Final epidemic size and critical times for susceptible-infectious-recovered models with a generalized contact rate". In: *Chaos* 34.1, p. 013152. DOI: 10.1063/5.0185707 (cit. on p. 8).

Giordano, G., F. Blanchini, R. Bruno, P. Colaneri, A. D. Filippo, A. D. Matteo, and M. Colaneri (2020). "Modelling the COVID-19 epidemic and implementation of population-wide interventions in Italy". In: *Nature Medicine* 26.6, pp. 855–860 (cit. on p. 5).

Guckenheimer, J. and P. Holmes (1983). *Nonlinear Oscillations, Dynamical Systems, and Bifurcations of Vector Fields*. Vol. 42. Applied Mathematical Sciences. New York, NY: Springer. ISBN: 978-0-387-90819-9 (cit. on p. 36).

Guo, H., M. Li, and Z. Shuai (2008). "A graph-theoretic approach to the method of global Lyapunov functions". In: *Proceedings of the American Mathematical Society* 136.8, pp. 2793–2802 (cit. on p. 6).

Hale, J. K. (2009). *Ordinary differential equations*. Courier Corporation (cit. on pp. 20, 33, 77).

Han, Z., Y. Wang, S. Gao, G. Sun, and H. Wang (2024). "Final epidemic size of a two-community SIR model with asymmetric coupling". In: *Journal of Mathematical Biology* 88.5, p. 51 (cit. on p. 6).

Hansen, E. and T. Day (2011). "Optimal control of epidemics with limited resources". In: *Journal of mathematical biology* 62, pp. 423–451 (cit. on p. 10).

Harko, T., F. S. N. Lobo, and M. K. Mak (2014). "Exact analytical solutions of the Susceptible-Infected-Recovered (SIR) epidemic model and of the SIR model with equal death and birth rates". In: *Applied Mathematics and Computation* 236, pp. 184–194 (cit. on pp. 18, 42).

Hethcote, H. W (1978). "An immunization model for a heterogeneous population". In: *Theoretical population biology* 14.3, pp. 338–349 (cit. on pp. 5, 6).

Hethcote, H. W. (2000). "The Mathematics of Infectious Diseases". In: *SIAM review* 42.4, pp. 599–653 (cit. on pp. 4, 5).

Hethcote, H. W. and S. A. Levin (1989). "Periodicity in epidemiological models". In: *Applied mathematical ecology*. Springer, pp. 193–211 (cit. on p. 4).

Hota, A. R. and S. Sundaram (2019). "Game-theoretic vaccination against networked SIS epidemics and impacts of human decision-making". In: *IEEE Transactions on Control of Network Systems* 6.4, pp. 1461–1472 (cit. on p. 8).

Hsiang, S., D. Allen, S. Annan-Phan, K. Bell, I. Bolliger, T. Chong, H. Druckenmiller, L. Y. Huang, A. Hultgren, E. Krasovich, et al. (2020). "The effect of large-scale anti-contagion policies on the COVID-19 pandemic". In: *Nature* 584.7820, pp. 262–267 (cit. on p. 7).

Huang, Y. and Q. Zhu (2022). "Game-theoretic frameworks for epidemic spreading and human decision-making: A review". In: *Dynamic Games and Applications* 12.1, pp. 7–48 (cit. on p. 8).

Kabir, K. A. and J. Tanimoto (2020). "Evolutionary game theory modeling to represent the behavioural dynamics of economic shutdowns and shield immunity in the COVID-19 pandemic". In: *Royal Society Open Science* 7.9, p. 201095.
DOI: 10.1098/rsos.201095 (cit. on p. 7).

Kamalapurkar, R., P. Walters, J. A. Rosenfeld, and W. E. Dixon (2018). *Reinforcement learning for optimal feedback control: A Lyapunov-based approach*. Communications and Control Engineering. Springer International Publishing.
DOI: 10.1007/978-3-319-78384-0 (cit. on p. 89).

Kantner, M. and T. Koprucki (2020). "Beyond just "flattening the curve": Optimal control of epidemics with purely non-pharmaceutical interventions". In: *Journal of Mathematics in Industry* 10.1, p. 23 (cit. on p. 11).

Kemper, J. T. (1978). "The effects of asymptomatic attacks on the spread of infectious disease: a deterministic model". In: *Bulletin of mathematical biology* 40.6, pp. 707–718 (cit. on p. 5).

Kermack, W. O. and A. G. McKendrick (1927). "A contribution to the mathematical theory of epidemics". In: *Proceedings of the Royal Society of London. Series A, Containing papers of a mathematical and physical character* 115.772, pp. 700–721 (cit. on pp. 1, 4, 15, 16).

— (1932). "Contributions to the mathematical theory of epidemics II. The problem of endemicity". In: *Proceedings of the Royal Society of London. Series A, containing papers of a mathematical and physical character* 138.834, pp. 55–83 (cit. on p. 4).

Khanafer, A., T. Başar, and B. Gharesifard (2016). "Stability of epidemic models over directed graphs: A positive systems approach". In: *Automatica* 74, pp. 126–134 (cit. on p. 6).

Khazaei, H., K. Paarporn, A. Garcia, and C. Eksin (2021). "Disease spread coupled with evolutionary social distancing dynamics can lead to growing oscillations". In: *60th IEEE Conference on Decision and Control (CDC)*. IEEE, pp. 4280–4286 (cit. on p. 8).

Knauf, A. (2018). "Ordinary Differential Equations". In: *Mathematical Physics: Classical Mechanics*. Vol. 109. UNITEXT. Berlin, Heidelberg: Springer, pp. 31–60. DOI: 10.1007/978-3-662-55774-7_3 (cit. on pp. 20, 33, 77).

Korobeinikov, A. (2006). "Lyapunov functions and global stability for SIR and SIRS epidemiological models with non-linear transmission". In: *Bulletin of Mathematical biology* 68, pp. 615–626 (cit. on p. 8).

Kruse, T. and P. Strack (2020). "Optimal control of an epidemic through social distancing". In: *SSRN Electronic Journal*. DOI: 10.2139/ssrn.3583186 (cit. on p. 10).

Lajmanovich, A. and J. A. Yorke (1976). "A deterministic model for gonorrhea in a nonhomogeneous population". In: *Mathematical Biosciences* 28.3-4, pp. 221–236 (cit. on p. 5).

Lau, J. T., X. Yang, E. Pang, H. Tsui, E. Wong, and Y. K. Wing (2005). "SARS-related perceptions in Hong Kong". In: *Emerging infectious diseases* 11.3, p. 417 (cit. on p. 7).

Li, C.-H., C.-C. Tsai, and S.-Y. Yang (2014). "Analysis of epidemic spreading of an SIRS model in complex heterogeneous networks". In: *Communications in Nonlinear Science and Numerical Simulation* 19.4, pp. 1042–1054 (cit. on p. 105).

Liberzon, D. (2011). *Calculus of Variations and Optimal Control Theory: A Concise Introduction*. USA: Princeton University Press. ISBN: 0691151873 (cit. on pp. 75, 89).

Liu, W.-m., H. W. Hethcote, and S. A. Levin (1987). "Dynamical behavior of epidemiological models with nonlinear incidence rates". In: *Journal of mathematical biology* 25, pp. 359–380 (cit. on p. 8).

Martcheva, M. (2015). *An introduction to mathematical epidemiology*. Vol. 61. Springer (cit. on p. 15).

Martins, N. C., J. Certório, and R. J. La (2023). "Epidemic population games and evolutionary dynamics". In: *Automatica* 153, p. 111016. ISSN: 0005-1098. DOI: https://doi.org/10.1016/j.automatica.2023.111016 (cit. on p. 7).

Mei, W., S. Mohagheghi, S. Zampieri, and F. Bullo (2017). "On the dynamics of deterministic epidemic propagation over networks". In: *Annual Reviews in Control* 44, pp. 116–128 (cit. on pp. 5, 6, 33, 50, 56, 71).

Meyer, C. D. (2000). *Matrix Analysis and Applied Linear Algebra*. Philadelphia, PA: SIAM. ISBN: 978-0-89871-454-8 (cit. on p. 37).

Miclo, L., D. Spiro, and J. Weibull (2022). "Optimal epidemic suppression under an ICU constraint: An analytical solution". In: *Journal of Mathematical Economics* 101, p. 102669. ISSN: 0304-4068.
DOI: https://doi.org/10.1016/j.jmateco.2022.102669 (cit. on pp. 10, 75, 80).

Morton, R. and K. H. Wickwire (1974). "On the Optimal Control of a Deterministic Epidemic". In: *Advances in Applied Probability* 6.4, pp. 622–635.
DOI: 10.2307/1426183 (cit. on p. 10).

Newman, M. E. (2002). "Spread of epidemic disease on networks". In: *Physical review E* 66.1, p. 016128 (cit. on p. 5).

Nguyen, M. M. (2024). "Upper bounds on overshoot in SIR models with nonlinear incidence". In: *npj Complexity* 1.1, p. 11 (cit. on p. 8).

Nowzari, C., V. M. Preciado, and G. J. Pappas (2016). "Analysis and Control of Epidemics: A Survey of Spreading Processes on Complex Networks". In: *IEEE Control Systems Magazine* 36.1, pp. 26–46 (cit. on pp. 3, 5, 50).

Ogura, M. and V. M. Preciado (2016). "Stability of Spreading Processes over Time-Varying Large-Scale Networks". In: *IEEE Transactions on Network Science and Engineering* 3, pp. 44–57 (cit. on p. 5).

Our World in Data (2024). *COVID-19 Cases*. Online. Accessed: 2025-04-07. URL: https://ourworldindata.org/covid-cases (cit. on pp. 1, 68).

Paarporn, K. and C. Eksin (2023). "SIS epidemics coupled with evolutionary social distancing dynamics". In: *2023 American Control Conference (ACC)*. IEEE, pp. 2023–2028 (cit. on p. 7).

Paré, P. E., C. L. Beck, and T. Başar (2020). "Modeling, Estimation, and Analysis of Epidemics over Networks: An Overview". In: *Annual Reviews in Control* 50, pp. 345–360 (cit. on pp. 5, 31).

Parino, F., L. Zino, and A. Rizzo (2024). "Optimal Control of Endemic Epidemic Diseases With Behavioral Response". In: *IEEE Open Journal of Control Systems* (cit. on p. 11).

Pastor-Satorras, R., C. Castellano, P. Van Mieghem, and A. Vespignani (2015). "Epidemic Processes in Complex Networks". In: *Reviews of Modern Physics* 87, pp. 925–979 (cit. on pp. 5, 31).

Ruhi, N. A. and B. Hassibi (2015). "SIRS epidemics on complex networks: Concurrence of exact Markov chain and approximated models". In: *54th IEEE Conference on Decision and Control (CDC)*. IEEE, pp. 2919–2926 (cit. on p. 5).

Sahneh, F. D., C. Scoglio, and P. Van Mieghem (2013). "Generalized epidemic mean-field model for spreading processes over multilayer complex networks". In: *IEEE/ACM Transactions on Networking* 21.5, pp. 1609–1620 (cit. on p. 6).

Sandholm, W. H. (2010). *Population games and evolutionary dynamics*. MIT Press (cit. on p. 7).

Satapathi, A., N. K. Dhar, A. R. Hota, and V. Srivastava (2022). "Epidemic propagation under evolutionary behavioral dynamics: Stability and bifurcation analysis". In: *American Control Conference (ACC)*. IEEE, pp. 3662–3667 (cit. on p. 7).

She, B., J. Liu, S. Sundaram, and P. E. Paré (2022). "On a networked SIS epidemic model with cooperative and antagonistic opinion dynamics". In: *IEEE Transactions on Control of Network Systems* 9.3, pp. 1154–1165 (cit. on p. 9).

Soner, H. M. (2009). *Lecture Notes on Stochastic Optimal Control* (cit. on p. 75).

Sontag, E. D. (2023). "An Explicit Formula for Minimizing the Infected Peak in an SIR Epidemic Model When Using a Fixed Number of Complete Lockdowns". In: *International Journal of Robust and Nonlinear Control* 33.9, pp. 4708–4731 (cit. on pp. 19, 42).

Srivastava, A., T. Das, and P. K. Srivastava (2024). "Nonlinear dynamics of an SIRS model with ratio-dependent incidence and saturated treatment function". In: *Journal of Applied Mathematics and Computing* 70.5, pp. 4537–4561 (cit. on p. 8).

Stolerman, L. M., D. Coombs, and S. Boatto (2015). "SIR-network model and its application to dengue fever". In: *SIAM Journal on Applied Mathematics* 75.6, pp. 2581–2609 (cit. on p. 6).

Taubenberger, J. K. and D. M. Morens (2006). "1918 Influenza: the mother of all pandemics". In: *Revista Biomedica* 17.1, pp. 69–79 (cit. on p. 1).

Thieme, H. R. (2003). *Mathematics in Population Biology*. Princeton University Press. DOI: 10.2307/j.ctv301f9v (cit. on p. 1).

Van Mieghem, P., J. Omic, and R. Kooij (2008). "Virus spread in networks". In: *IEEE/ACM Transactions On Networking* 17.1, pp. 1–14 (cit. on p. 5).

Verelst, F., L. Willem, and P. Beutels (Dec. 2016). "Behavioural change models for infectious disease transmission: A systematic review (2010-2015)". In: *Journal of The Royal Society Interface* 13. DOI: 10.1098/rsif.2016.0820 (cit. on p. 8).

Wang, F., J. Zhang, and M. Liu (2024). "Dynamical analysis of a network-based SIR model with saturated incidence rate and nonlinear recovery rate: an edge-compartmental approach". In: *Mathematical Biosciences and Engineering* 21.4, pp. 5430–5445. DOI: 10.3934/mbe.2024239 (cit. on p. 9).

Wang, Y., D. Chakrabarti, C. Wang, and C. Faloutsos (2003). "Epidemic spreading in real networks: An eigenvalue viewpoint". In: *22nd International Symposium on Reliable Distributed Systems, 2003. Proceedings.* IEEE, pp. 25–34 (cit. on p. 5).

Wilson, E. B. and M. H. Burke (1943). "The epidemic curve: II". In: *Proceedings of the National Academy of Sciences* 29.1, pp. 43–48 (cit. on p. 3).

World Health Organization (2024). *COVID-19 Dashboard*. Accessed: 2025-04-07. URL: https://covid19.who.int/ (cit. on p. 1).

Xu, Q. and H. Ishii (2024). "On a Discrete-Time Networked SIV Epidemic Model with Polar Opinion Dynamics". In: *IEEE Transactions on Network Science and Engineering* PP, pp. 1–16 (cit. on p. 9).

Xu, Q., T. Masada, and H. Ishii (2025). "Stability Analysis and Intervention Strategies on a Coupled SIS Epidemic Model with Polar Opinion Dynamics". In: *arXiv preprint arXiv:2503.01285* (cit. on p. 9).

Yang, J. (2024). "Some novel results of a two-community SIR model with asymmetric structure". In: *Applied Mathematics Letters* 157, p. 109168 (cit. on p. 6).

Ye, M., L. Zino, A. Rizzo, and M. Cao (2021). "Game-theoretic modeling of collective decision making during epidemics". In: *Physical Review E* 104.2, p. 024314 (cit. on pp. 7, 8).

Yi, Y., L. Shan, P. E. Paré, and K. H. Johansson (2022). "Edge deletion algorithms for minimizing spread in SIR epidemic models". In: *SIAM Journal on Control and Optimization* 60.2, S246–S273 (cit. on p. 11).

Youssef, M. and C. Scoglio (2011). "An individual-based approach to SIR epidemics in contact networks". In: *Journal of theoretical biology* 283.1, pp. 136–144 (cit. on p. 6).

Zhang, Y. and D. Pan (2021). "Layered SIRS model of information spread in complex networks". In: *Applied Mathematics and Computation* 411, p. 126524 (cit. on p. 105).

Zhou, Y., S. Levin, and N. Leonard (Jan. 2020). "Active Control and Sustained Oscillations in actSIS Epidemic Dynamics". In: *IFAC-PapersOnLine* 53, pp. 807–812. DOI: 10.1016/j.ifacol.2021.04.175 (cit. on pp. 9, 45, 104).

Zino, L. and M. Cao (2021). "Analysis, prediction, and control of epidemics: A survey from scalar to dynamic network models". In: *IEEE Circuits and Systems Magazine* 21.4, pp. 4–23 (cit. on pp. 5, 10, 31).